Link between Ciliogenesis and Disorders of the Proximal Tubule of the Kidney

---

Dissertation

zur

Erlangung der naturwissenschaftlichen Doktorwürde
(Dr. sc. nat.)

vorgelegt der

Mathematisch-naturwissenschaftlichen Fakultät

der

Universität Zürich

von

Alkaly Gassama

aus

Frankreich

Promotionskommission

Prof. Dr. Olivier Devuyst (Vorsitz)

Prof. Dr. Carsten Wagner
Prof. Dr. Andrew Hall
Prof. Rudolf Wüthrich
Dr. Stéphane Lourdel

Zürich, 2018

Acknowledgments

Firstly, I would like to thank my family, particularly my parents and my brothers for their unwavering support throughout this thesis and in my life in general.

Second, I would like to express my sincere gratitude to my supervisor Prof. Olivier Devuyst for the continuous support of my Ph.D. study and related research, for his patience, motivation, and immense knowledge. His guidance helped me in all the time of research and writing of this thesis.

Besides my advisor, I would like to thank the rest of my thesis committee: Prof. Carsten Wagner, Prof. Andrew Hall, Prof. Rudolf Wüthrich and Dr. Stéphane Lourdel, for their insightful comments and encouragement, but also for the hard questions which incented me to widen my research from various perspectives.

Last but not the least, I thank my fellow labmates in for the stimulating discussions, for the sleepless nights we were working together, and for all the fun we have had in the last years. Also, I thank my friends in the institute of physiology who made the time during my Ph.D. a much more enjoyable experience.

Zusammenfassung

Der Nierenproximale Tubulus spielt eine fundamentale homöostatische Rolle, indem er eine große Menge an Stoffen resorbiert, einschließlich Proteine mit niedrigem Molekulargewicht, Glucose, Phosphat, Wasser und Vitamine, die sonst im Urin verloren gehen würden. Diese Kapazität beruht auf einem sehr effizienten Transportsystem, das der Rezeptor-vermittelten Endozytose einschließt, die die Aufnahme von essentiellen Nährstoffen in den Epithelzellen, die den proximalen Tubulus auskleiden, sowie deren korrekte Verarbeitung entlang des endolysosomalen Wegs sicherstellt. Das endolysosomale Kompartiment ist auch entscheidend für den Abbau von beschädigten Organellen und intrazellulären Materialien durch Autophagie, ein hoch konservierter Qualitätskontrollsystem, das die Aufrechterhaltung der Zellen sicherstellt. Angeborene Erkrankungen der Multi-Liganden-Endozytose-Rezeptoren (z.B. Donnai-Barrow oder Imerslund-Gräsbeck-Syndrom) oder der endolysosomalen Signalwege (z.B. Dent-Krankheit oder nephropathische Cystinose) sind mit einer niedermolekularen Molekulargewicht Proteinurie und einem Verlust von verschiedener gelösten Stoffen über den Urin verbunden, was oft zu multisystemischen Komplikationen und zur Progression einer chronischen Niereninsuffizienz führt.

Im Laufe der Jahre wurde ein großes Interesse hinsichtlich der mutmaßlichen Rolle des primären Ziliums in den proximalen Tubulus geweckt. Diese Organelle sticht aus den meisten Säugerzellen heraus und wurde ausführlich auf ihre Fähigkeit hin beschrieben, extrazelluläre Stimuli wie den luminalen Fluss zu transduzieren, wodurch ein zellulärer Eintritt von Calcium Ionen ausgelöst wird, der dann mehrere zelluläre Prozesse reguliert. Interessanterweise wurden spezialisierte Strukturen, angereichert mit Clathrin-beschichteten Grübchen, die für die Initiierung der Endozytose entscheidend sind, an der Basis des primären Ziliens identifiziert. Jüngste Studien, die in immortalisierten Nierenzellen durchgeführt wurden, zeigten eine spezifische Zunahme der endozytischen Aktivität bei der Flussschubspannungsstimulation des primären Ziliums, eine Wirkung, die durch chemische Entfernung der primären Zilien aufgehoben wurde. Auch deuten mehrere Indizien darauf hin, dass Patienten mit einer autosomal-dominanten polyzystischen Nierenkrankung (ADPKD), einem Prototyp der Ziliopathie, eine proximale tubuläre Dysfunktion aufweisen. ADPKD ist die häufigste ererbte Nierenerkrankung die bis zu 1: 1000 Menschen betrifft. Diese Krankheit ist durch die bilaterale Entwicklung von Zysten gekennzeichnet, die allmählich das normale Parenchym ersetzen und schließlich zu einer

terminalen Nierenerkrankung führen. Bei Patienten wurde in einem frühen Stadium der Erkrankung im Urin eine abnormale Ausscheidung der Marker für Schäden des proximalen Tubulus darunter KIM-1, β2-Mikroglobulin und β-Hexosaminidase nachgewiesen. Zusammengefasst legen diese Daten eine fundamentale Rolle des primären Ziliums in der endozytischen Funktion der Epithelzellen des proximalen Tubulus nahe.

In dieser Arbeit untersuchte ich die zugrunde liegenden Mechanismen, die proximale tubuläre Dysfunktionen und Ciliogenese miteinander verbinden, mit genetischen Modellen von Ziliopathien sowie Modellen endolysosomaler Störungen (Dent-Krankheit und nephropathische Cystinose). Die klinische Relevanz unserer Studien wurde in einer Kohorte von Patienten mit ADPKD untersucht.

Bei vielen Störungen der endolysosomalen Signalwege, wie der Dent-Krankheit, fehlt es an kurativen Therapien und die derzeitigen Bemühungen konzentrieren sich auf die Linderung der Symptome und Komplikationen, verursacht durch die Entwicklung der chronischen Nierenerkrankung. Kürzlich wurde gezeigt, dass Knochenmark- und hämatopoetische Stammzelltransplantation bei der nephropathischen Cystinose von Vorteil sind, indem die Nierenfunktion erhalten und der Cystingehalt in den Zellen gesenkt wird. Diese Ergebnisse werfen die Frage auf, ob eine Knochenmarktransplantation die Funktionsstörungen der proximalen Tubuli bei einer reinen endosomalen Störung wie der Dent-Krankheit korrigieren könnte. Im zweiten Teil der Arbeit untersuchen wir, ob eine Knochenmarktransplantation in dem etablierten *Clcn5*-Knockout-Mausmodell der Dent-Krankheit von Nutzen ist. Wir untersuchten die assoziierten Mechanismen mit Hilfe eines In-vitro-Systems von Knochenmarks Zellen co-kultiviert mit primären proximalen Tubulus Zellen der Maus.

Die hier beschriebenen Studien identifizieren eine neue Rolle des primären Ziliums in der Endocytose-Funktion der proximalen Tubulus Epithelzellen und liefern zellbasierte Therapieansätze zur Verbesserung der Nierenfunktion.

Summary

The proximal tubule of the kidney plays a fundamental homeostatic role by reabsorbing large amount of solutes including low molecular weight proteins, glucose, phosphate, water and vitamins which would otherwise be lost in the urine. This capacity relies on a very efficient transport system including receptor-mediated endocytosis, which ensures the uptake of essential nutrients and solutes in the epithelial cells lining the proximal tubule as well as their correct processing along the endolysosomal pathway. The endolysosomal compartment is also crucial for the removal of damaged organelles and intracellular materials through autophagy, a highly conserved quality control system that sustains cellular maintenance. Congenital diseases affecting the multi-ligand endocytic receptors (e.g. Donnai-Barrow or Imerslund-Gräsbeck syndromes) or the endolysosomal pathway (e.g. Dent disease or nephropathic cystinosis) are associated with low molecular weight proteinuria and the loss of various solutes in urine, which often leads to multi-systemic complications and progression to chronic kidney disease.

Over the years, a lot of interest has been gained regarding the putative role of the primary cilium in the proximal tubule. This organelle protrudes from most mammalian cells and has been extensively characterized for its ability to transduce extracellular stimuli such as the luminal flow into a cellular entry of calcium ions which then regulates multiple cellular processes. Interestingly, specialized structures enriched in clathrin-coated pits, which are crucial to initiate endocytosis, have been identified at the base of the primary cilium. Recent studies performed in immortalized tubular cells demonstrated a specific increase of the endocytic activity upon flow shear stress stimulation of the primary cilium, an effect abrogated by chemical removal of the cilia. Also, several lines of evidence suggest that patients affected by autosomal dominant polycystic kidney disease (ADPKD), a prototype of ciliopathy, exhibit proximal tubular dysfunction. ADPKD is the most common inherited kidney disorder, affecting up to 1:1000 people. This disease is characterized by the bilateral development of cysts, progressively replacing the normal parenchyma and ultimately leading to end-stage renal disease. Patients with ADPKD have been shown to display abnormal urinary excretion of proximal tubule damage markers including KIM-1, β2-microglobulin, β-hexosaminidase at an early stage of the disease. Taken together, these data suggest a fundamental role of the primary cilium in the endocytic function of the epithelial cells of the proximal tubule.

In this thesis, I investigated the underlying mechanisms linking proximal tubular dysfunction and ciliogenesis using genetic models of ciliopathies and models of endolysosomal disorders (Dent disease and nephropathic cystinosis). The clinical relevance of our studies was evaluated in a cohort of patients suffering from ADPKD.

For many endolysosomal disorders such as Dent disease, there is a lack of curative therapies with current efforts focused on alleviating the symptoms and complications due to the development of chronic kidney disease. Recently, bone marrow and hematopoietic stem cell transplantation have been shown to be beneficial in nephropathic cystinosis by preserving the kidney function and lowering the cystine content in the cells. These results raised the question of whether bone marrow transplantation would correct manifestations of proximal tubule dysfunction in an endosomal disorder such as Dent disease. In the second part of the thesis, we evaluated the effect of bone marrow transplantation in the well-established *Clcn5* knock-out mouse model of Dent disease. We investigated the associated mechanisms using a co-culture *in vitro* system of bone marrow derived cells and primary mouse proximal tubular cells.

The studies described here identify a novel role of the primary cilium in the endocytosis function of proximal tubule cells and provide a proof-of-concept for cell-based therapies to improve proximal tubule dysfunction

List of abbreviations

AC6	Adenylate cyclase 6
ADPKD	Autosomal polycystic kidney disease
AVP2R	Arginine vasopressin receptor 2
BM	Bone marrow
cAMP	Cyclic adenyl-monophosphate
CCP	Clathrin-coated pit
CCV	Clathrin-coated vesicles
CKD	Chronic kidney disease
ClC-5	Chloride-proton exchanger
DAV	Distal appendage vesicle
ESRD	End stage renal disease
GFR	Glomerular filtration rate
GvHD	Graft versus host disease
HLA	Human leukocyte antigen
HSC	Hematopoietic stem cell
IFT	Intraflagellar transport
LDL	Low density lipoprotein
LMWP	Low molecular weight proteins
LSD	Lysosomal storage diseases
MDCK	Madin Darby canine kidney
mPTC	Mouse primary proximal tubule cell
MT	Microtubules
mTOR	Mammalian target of rapamycin
NHE3	Sodium–hydrogen exchanger 3

PC	Polycystin
PDE	Phosphodiesterase
PKA	Protein kinase A
PT	Proximal tubule
RFS	Renal Fanconi syndrome
RME	Receptor-mediated endocytosis
rPTC	Rat primary proximal tubule cells
SNARE	Soluble N-ethylmaleimide-sensitive factor Attachment Protein receptorTZ Transition zone
ULK	UNC51-like kinase
V-ATPase	Vacuolar ATPase

Table of Contents

I- Introduction

I- Introduction

1. Kidney proximal tubule

The kidney plays a fundamental homeostatic role by controlling the body fluid composition and regulating essential parameters such as the blood pressure, intercellular pH and the electrolyte equilibrium. From the 180 liters of primary urine that are daily filtered by the kidney, only 1.5 L of final urine is excreted, almost entirely devoid of low molecular weight (LMW) proteins and essential solutes, demonstrating the impressive ability of this organ to concentrate urine and reabsorbing essential metabolites, thus tightly controlling various homeostatic processes. To ensure its function, the kidney is composed of one million functional units, the nephrons. The latter contain a filtration unit, the glomerulus, followed by a long tubule structured in different segments made of highly specialized epithelial cells (Fig. 1.1). The glomerulus forms a very complex filtration barrier defined by podocytes with foot processes surrounding the fenestrated glomerular capillaries and separated by a filtration slit permeable to water, electrolytes and LMW proteins (Haraldsson, Nystrom et al. 2008). After passing through the glomerulus, the ultrafiltrate is then heavily modified along the nephron to form the final urine. One of the largest contributors to this process is the first segment of the kidney tubule, the proximal tubule (PT).

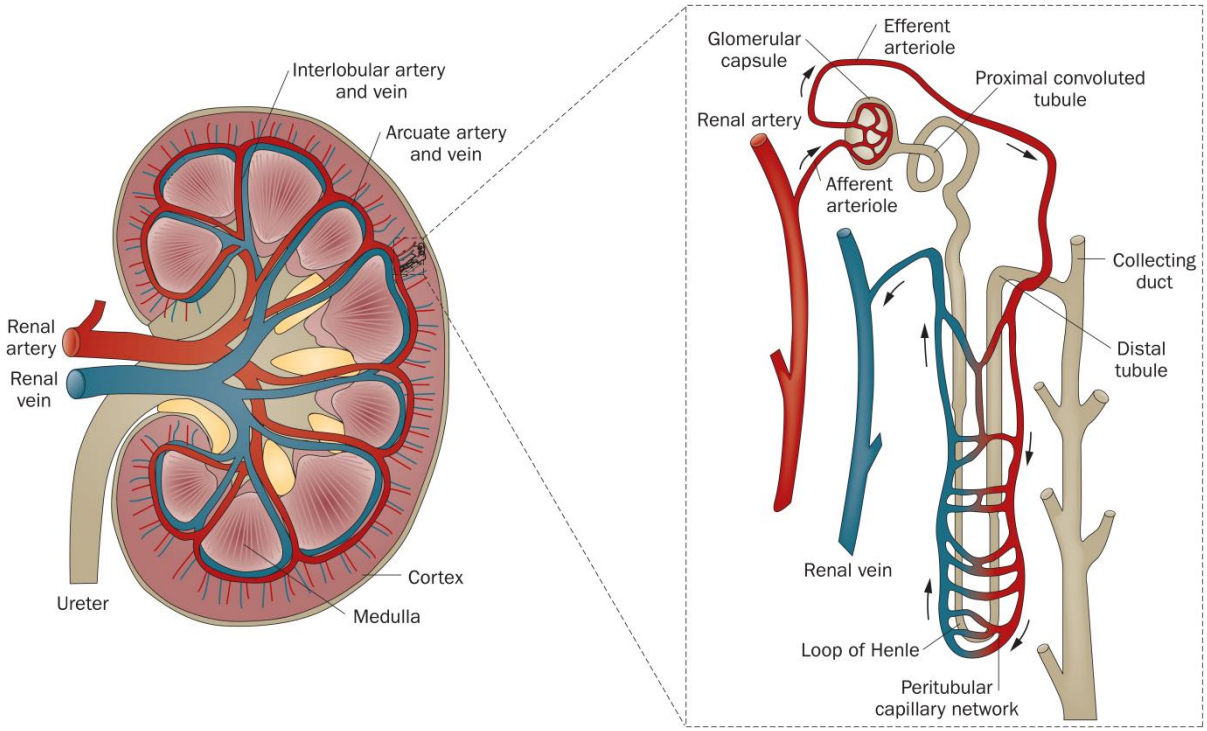

Figure 1.1: Structure of the nephron, functional unit of the kidney (adapted from (Mimura and Nangaku 2010)

1.1. Proximal tubular epithelial cells

1.1.1. Structure and function

The epithelial cells lining the PT are highly differentiated allowing an efficient directional transport of many molecules from the primary urine to the blood circulation. The apical side of these cells is covered with densely packed microvilli forming the apical brush border, which effectively increases the luminal surface area and facilitates the reabsorption process. Morphologically the proximal tubule is subdivided in the convoluted part composed of S1 and S2 segments and the straight part with S3 segment. The PT cells of the convoluted segment are characterized by a more developed brush border compared to the cells lining the straight segment and by the presence of numerous mitochondria, which provide the energy required by the high transport activity (Fig. 1.2) (Jacobson and Kokko 1976).

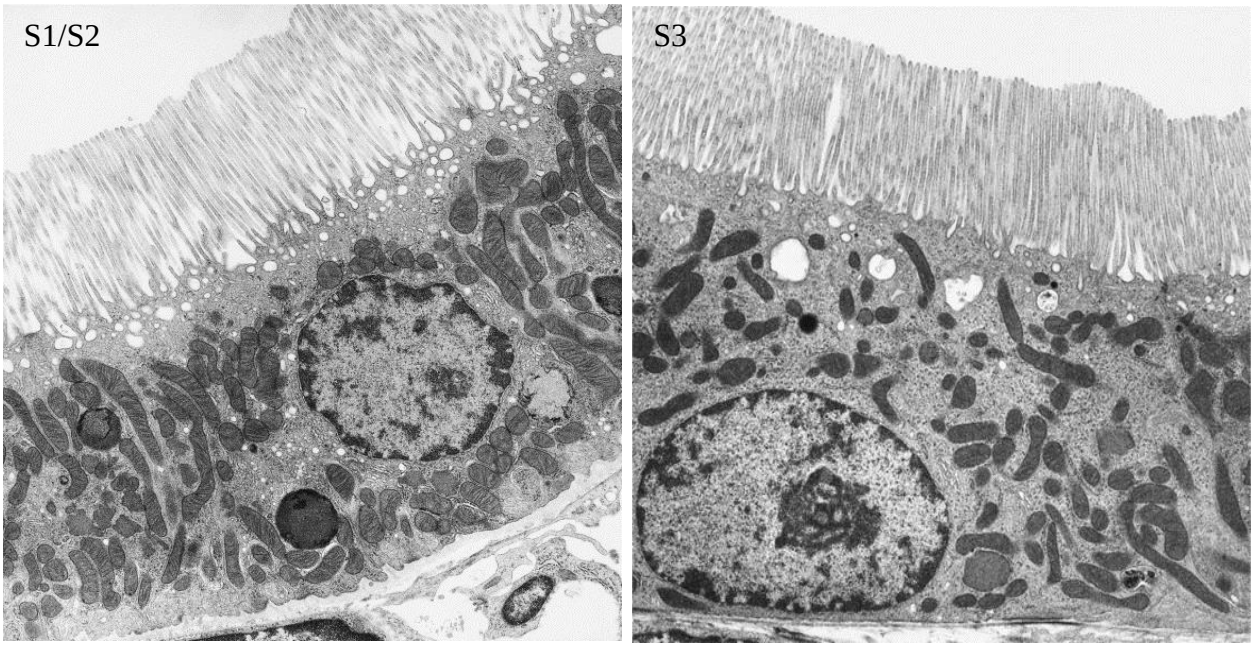

Figure 1.2: Ultrastructure of the proximal tubule (adapted from (Maunsbach 1966)

Without a functional PT, a substantial amount of ions, glucose and many other filtered elements including amino acids would be lost in the urine resulting in serious clinical manifestations (Camargo, Bockenhauer et al. 2008). The reabsorption of many solutes is possible due to the asymmetry of transport systems operating in the apical and the basolateral membrane of PT cells. Indeed, various cotransporters are expressed at the apical membrane allowing the coupling of the

uptake of solutes such as glucose, amino acids and phosphate to the uptake of Na^+. These transports are driven by the Na^+ gradient generated by the Na^+-K^+-ATPase pump expressed at the basolateral membrane. The importance of this process can be illustrated by the pivotal role of PT cells in regulating plasmatic pH by secreting protons H^+ via the electroneutral Na^+/H^+ exchanger NHE3 and the reclamation of the buffer $HCO3^-$ in parallel (Amemiya, Loffing et al. 1995).

1.2. Receptor-mediated endocytosis and vesicular trafficking

Most LMW proteins filtered through the glomeruli are reabsorbed in PT cells through receptor-mediated endocytosis (RME) (Fig 1.3). This process is extremely efficient since the normal urine is virtually devoid of proteins. During the RME, filtered proteins bind the multi-ligands receptors megalin and cubilin which trigger their internalization in clathrin-coated vesicles. These vesicles are delivered to the endosomes where an acidification process allows the separation between the receptor and its ligand. Subsequently the receptor is recycled to the plasma membrane whereas the ligands are delivered and processed in the lysosome. The different elements of RME will be described in the following sections

1.2.1. Endocytic receptors megalin and cubilin

A remarkable variety of ligands are filtered through the glomerulus including vitamins, essential hormones and LMW proteins with a molecular mass below 60 kDa. The reabsorption of these solutes requires a dynamic ligand binding ability of receptors expressed at the apical membrane of PT cells. Megalin, a 600 kDa transmembrane protein which belongs to the low density lipoprotein (LDL) receptor family, possess a large extracellular domain conferring its ability to binds multiple ligands (Raychowdhury, Niles et al. 1989). More specifically, the extracellular domain of megalin is composed of numerous complement-type repeats which are essential to ligand binding (Fass, Blacklow et al. 1997, Wolf, Dancea et al. 2007). The cytoplasmic tail of megalin contains two endocytic motifs, NPXY and NQNY, which are crucial for clathrin-coated vesicles formation by interacting with AP-2 and for receptors apical sorting respectively (Collins, McCoy et al. 2002, Takeda, Yamazaki et al. 2003).

The main interacting partner of megalin is cubilin, a 460 kDa protein that do not contain a transmembrane or an intracellular segment. 27 CUB (complement C1r/C1s, Uegf (epidermal growth factor-related sea urchin protein) domains have been identified in this protein, further

increasing the ligand binding ability of the complex made by megalin and cubilin (Kristiansen, Kozyraki et al. 1999, Yammani, Seetharam et al. 2001). The correct trafficking of cubilin depend on amnionless, a 50 kDa transmembrane protein which includes two endocytic motifs in the cytoplasmic tail. Mutations in *LRP2* (megalin), *CUBN* (cubilin) and *AMN* (amnionless) have been shown to impair endocytic activity resulting in several disorders such as Imerslund-Gräsbeck or Donnai–Barrow syndrome (He, Madsen et al. 2005).

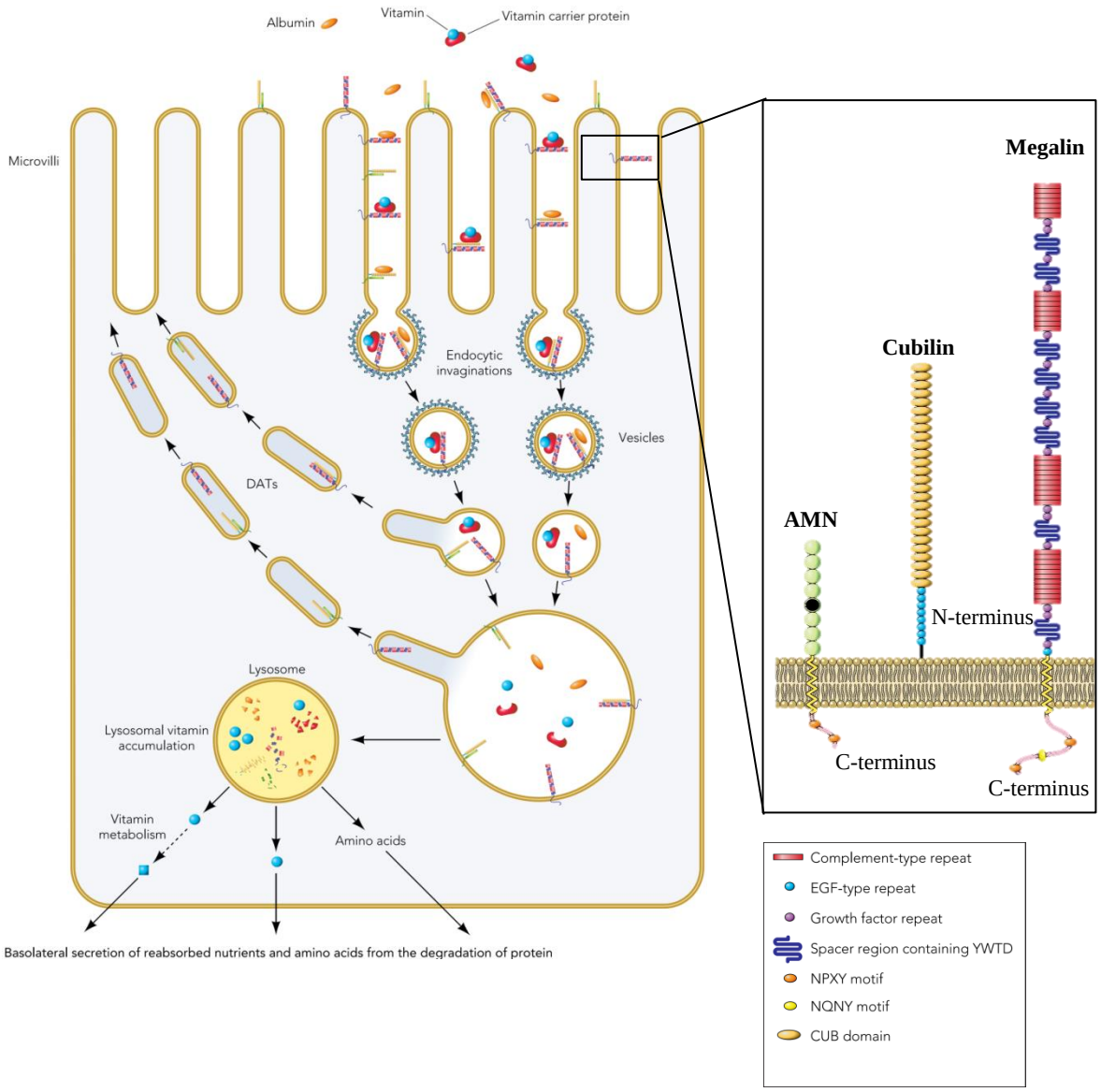

Figure 1.3: Schematic representation of receptor-mediated endocytosis (adapted from (Christensen, Birn et al. 2012)

1.2.2. Endosomes

Upon internalization, the clathrin-coated vesicles containing the complexes ligand-receptor fuses with the endosomes. This process is determined by the interaction of complementary transmembrane proteins (v-SNARE and t-SNARE) and by Rab GTP-binding proteins (Wilson, Wilcox et al. 1989, Somsel Rodman and Wandinger-Ness 2000). The dissociation of the ligand-receptor complexes occurs in the endosomes and is facilitated by a progressive acidification along the endocytic pathway, mainly driven by the influx of protons ions H^+ mediated by the vacuolar-ATPase (V-ATPase) (Herak-Kramberger, Brown et al. 1998, Brown, Paunescu et al. 2009). In absence of a compensating system, the constant proton influx would generate a transmembrane electrical potential ultimately resulting in V-ATPase inhibition. Indeed, to maintain electroneutrality, protons entry must be coupled with anion entry or cation exit. Several studies showed that chloride channels are instrumental in the dissipation of the transmembrane potential effectively defining Cl^- conductance as a major regulator of endosomal acidification (Scheel, Zdebik et al. 2005). In particular, the chloride-proton exchanger ClC-5, expressed at the endosomal membrane, establishes a countercurrent with a $2Cl^-:1H^+$ stoichiometry which is fundamental to the endosome function. Disruption of ClC-5 is typically inducing a severe endocytic defect which will be discussed in the section 1.4. After dissociation of the receptor and its ligand, the former is recycled to the plasma membrane while the latter is targeted to lysosomes for degradation.

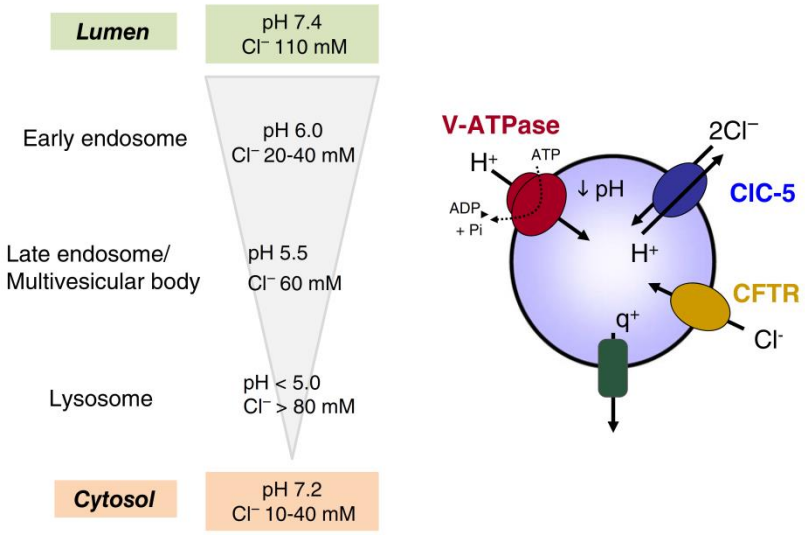

Figure 1.4: Vesicular acidification along the endolysosomal pathway (adapted from Devuyst et al., 2015)

1.2.3. Lysosomes

The lysosomes, initially described by Christian de Duve in 1963, mediate the degradation and recycling of intracellular and extracellular material (Fig. 1.5) (De Duve 1963). Structurally, these organelle are characterized by an acidic lumen containing numerous catabolic enzymes including hydrolases, sulphatases, lipases, nucleases, peptidases, glycosidases and phosphatases (Schroder, Wrocklage et al. 2010). The trafficking of these enzymes to the lysosomes, and their ability to be secreted and reabsorbed, is mediated by mannose-6-phosphate modifications in the Golgi apparatus and these properties have been used for enzymes replacement therapy for lysosomal storage diseases (LSD) (Neufeld 1980, Nielsen, Courtoy et al. 2007, Braulke and Bonifacino 2009). The lysosomal acidification (pH ~ 5) is generated by the V-ATPase with the contribution of other ion channels such as ClC-7 (Kasper, Planells-Cases et al. 2005, Marshansky and Futai 2008). Of note, the lysosomal membrane is protected from the degradative enzymes by a thick glycocalyx lining its inner surface. Additionally membrane-associated RAB GTPases and SNARE proteins are located at the lysosomal membrane and mediate the fusion between lysosomes and different cellular compartments including late endosomes (Pryor, Mullock et al. 2004, Rink, Ghigo et al. 2005).

The main function of the lysosome is to degrade extracellular material, mostly originating from endocytosis, and cellular waste through the autophagic process which is essential for cellular homeostasis.

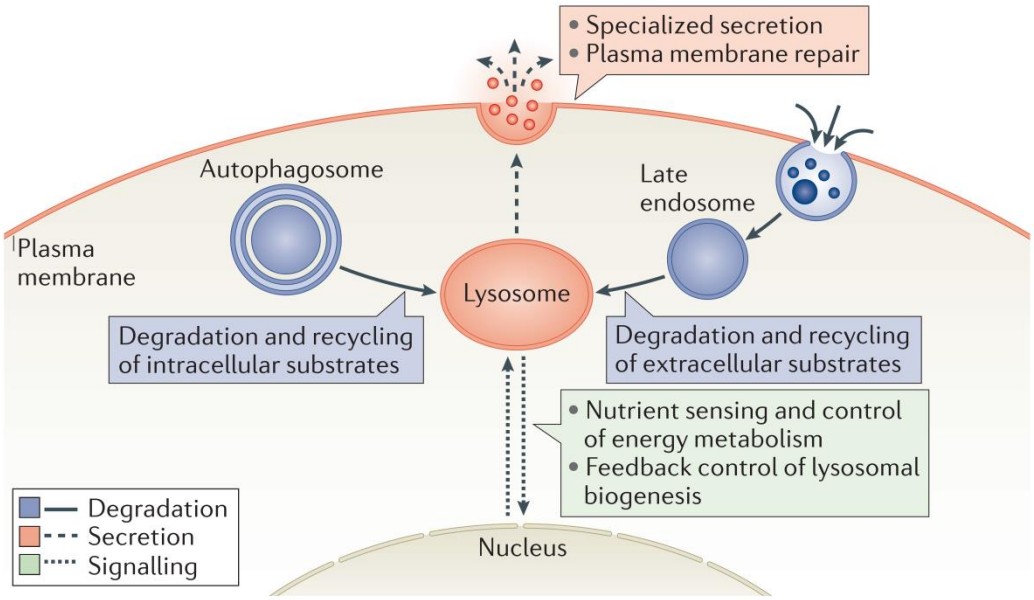

Figure 1.5: Main function of the lysosomes and their relationship with key cellular processes (adapted from (Settembre, Fraldi et al. 2013))

1.3. Autophagy

Autophagy is a highly conserved mechanism resulting in the irreversible degradation of substrates from intracellular origin into essential components (e.g. aa) that are reused by the cells(Settembre, Fraldi et al. 2013). In basal conditions, autophagy is necessary to cellular maintenance by degrading long-lived proteins and organelles as well as the damaged cellular components. Different stimuli can induce an increase of autophagy activity such as nutrients deprivation (i.e. starvation), resulting in an increase of cellular energetic demands or an increase of reactive oxygen species (ROS) caused by oxidative stress (Kirkland, Adibhatla et al. 2002, Scherz-Shouval, Shvets et al. 2007). Dysfunctions of the autophagic process have been involved in various disease including neurodegenerative disorders and cancer (reviewed here (White 2015, Zare-Shahabadi, Masliah et al. 2015) highlighting the crucial role of this process in cellular homeostasis.

The autophagic pathway can be classified in three types: chaperone-mediated autophagy, microautophagy and macroautophagy. The latter will be detailed in the current section and be

referred as autophagy. The initiation of autophagy begins with the engulfment of cytoplasmic portions by a double membrane structure called phagophore (Fig. 1.4). This mechanism is governed by the UNC51-like kinase (ULK) protein family which, in turn, activates the class III PI3K complex resulting in the formation of a pool of phosphatidylinositol specific to the phagophore compartment. Several proteins, namely ATG12-ATG5-ATG16, are recruited to the phagophore where the lipidation of microtubule-associated protein 1 light chain 3 (MAP1LC3 or LC3) with phosphatidylethanolamine is facilitated. LC3 lipidation results in the elongation of the phagophore forming an autophagosome. The autophagic vesicles subsequently fuse with endosomes creating amphisomes or directly with lysosomes forming autolysosomes where the degradation of cellular components takes place. Both autophagy and RME pathways share several cellular organelles including the lysosomes and disorders in either of these mechanisms severely impair PT function.

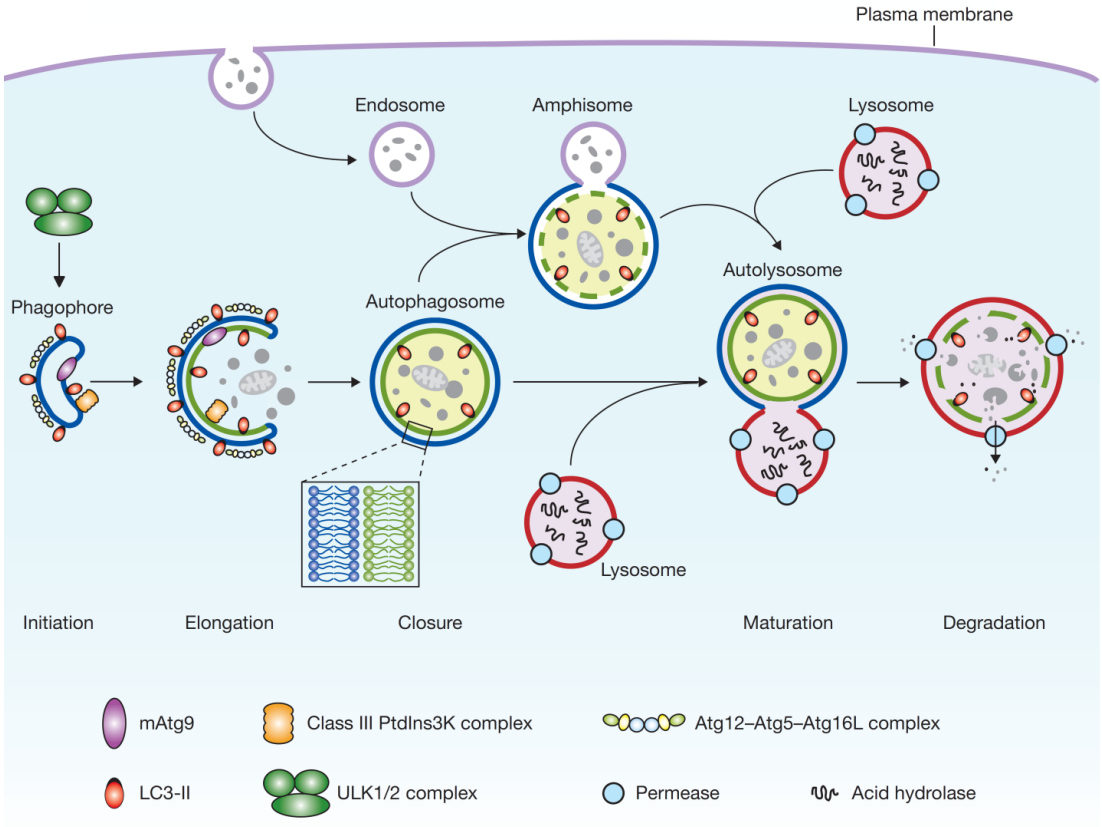

Figure 1.6: Schematic description of macroautophagy in mammalian cells (adapted from (Yang and Klionsky 2010)

1.4. Kidney proximal tubule dysfunction: Renal Fanconi syndrome

The concept of defective proximal tubule reabsorption was first proposed by the Swiss pediatrician Guido Fanconi whose patients showed rickets and fever associated to glycosuria and albuminuria, hence the name renal Fanconi syndrome (RFS) (Fanconi 1931, de Toni 1933, Debré, Marie et al. 1934). This condition is characterized by the presence of polyuria, phosphaturia, glycosuria, aminoaciduria, LMW proteinuria resulting in several clinical manifestations including electrolytes imbalance, growth retardation, dehydration, muscle weakness, rickets and progressive renal failure. RFS can be caused by congenital disorders such as Dent disease and cystinosis or acquired in disorder such as light chain monoclonal gammopathy (Raggi, Luciani et al. 2014, Luciani, Sirac et al. 2016).

1.4.1. Endosomal disorder: Dent disease

Dent disease (MIM #300009, Xp11.22) is a rare X-linked renal tubulopathy caused by inactivating mutation in the *CLCN5* gene which encode for the $2Cl^-$-H^+ exchanger ClC-5 (Lloyd, Pearce et al. 1996, Scheel, Zdebik et al. 2005). Clinical features of this disease includes RFS associated with nephrolithiasis, nephrocalcinosis, LMWP and end stage renal disease (ESRD) between the third and the fifth decades of life in 30-80% of affected males (Scheinman 1998).

These clinical manifestations highlight the importance of ClC-5 for the reabsorptive process in PT epithelial cells where this protein is markedly expressed. Studies in animal models harboring *Clcn5* mutations showed that the inactivation of ClC-5 strongly impedes cellular trafficking with the loss of the apical expression of megalin and cubilin, endolysosomal disorders and impaired internalization of NaPi-IIa and NHE3 (Piwon, Gunther et al. 2000, Wang, Devuyst et al. 2000, Christensen, Devuyst et al. 2003). Although ClC-5 has been extensively described as a facilitator of endosomal acidification, it should be noted that the mechanisms involved in PT dysfunction are more complex. Indeed, Novarino and colleagues showed that a knock-in mouse model possessing a mutated ClC-5 converted in an uncoupled Cl^- conductor exhibited similar renal phenotype than the KO mouse model despite a normal endosomal acidification (Novarino, Weinert et al. 2010).

1.4.2. Lysosomal storage disorders: nephropathic cystinosis

Lysosomes are essential to RME and dysfunctions of this organelle often result in a spectrum of diseases that are lysosomal storage disorders (LSD) often associated with manifestations of PT dysfunction. In fact, the leading hereditary cause of RFS in children is a genetic disease, nephropathic cystinosis, an autosomal recessive metabolic disorder caused by mutations in *CTNS* (MIM #219800, 17p13.2) which encode for a cystine-proton symporter, cystinosin (McDowell, Gahl et al. 1995, Gahl, Thoene et al. 2002). The loss of function of this transporter leads to the formation and accumulation of cystine crystals resulting in the impairment of the degradative ability of the lysosomes (Raggi, Luciani et al. 2014). The lysosomal impairment induces an increase of oxidative stress due to the defective autophagic clearance of damaged mitochondria ultimately resulting in the alteration of several intracellular pathways leading to PT defect (Festa, Chen et al. 2018). The patients with cystinosis rapidly develop RFS, which is invariably followed by the development of CKD and renal failure (Gahl, Thoene et al. 2002).

Both Dent disease and cystinosis demonstrates that the integrity of the endolysosomal compartment is crucial for PT homeostasis.

2. Primary cilium

The primary cilium is a highly conserved sensory organelle which protrudes from the surface of most mammalian cells. This structure was first characterized in the seminal studies of Sergei Sorokin (Sorokin 1968) who generated motile and non-motile cilia from fetal lung of rats. Motile cilia are present in specialized organs such as the Fallopian tubes and respiratory tract epithelium and differ from the non-motile cilia by their ability to generate movement (McGee, Johnson et al. 1981, Lyons, Saridogan et al. 2006). Additionally, a single cell can possess several hundred motile cilia enabling the coordinated directional beating conferring fluid clearance properties for example in the lungs (Popatia, Haver et al. 2014). Primary cilia have now extensively been described as key coordinators involved in many physiological processes such as left-right axis determination, development, chemosensation and mechanosensation. The following sections will focus on its morphological structure for a better understanding of its complex cellular function.

2.1. Morphological structure

2.1.1. Axoneme

Structurally, the primary cilium is composed of nine peripheral microtubule (MT) doublets emanating from the basal body (Fig. 2.1) with a 9+0 arrangement. Compared to the motile cilia which possess a 9+2 MT arrangement, primary cilia lack the central pair of MTs as well as molecular motors such as dynein motor proteins required for ciliary movement. The tubulin present in the axoneme has been shown to be subjected to post-transcriptional modifications such as acetylation, glutamylation and glycation (O'Hagan, Silva et al. 2017, Wloga, Joachimiak et al. 2017). These changes are essential for the stability and the function of the axoneme by regulating the interaction of the MT associated proteins namely kinesins or by ensuring the correct localization of some channels like polycystin-2 (PC-2).

2.1.2. Basal body

The basal body is a specialized structure present at the base of the primary cilium. The basal body originates from the centrosome and is required for the cilium formation. Indeed the centrosome, an organelle composed of two centrioles arranged in a cylindrical structure composed of nine triplets MT, plays an essential role in organizing the MTs network during cell division. At the exit of the mitotic cycle, vesicles originating from the Golgi apparatus as well as recycling endosomes, collective termed distal appendage vesicles (DAVs), are recruited at the distal

appendage of the mother centriole allowing its docking at the plasma membrane and initiating the centriole-to-basal body transition (Schmidt, Kuhns et al. 2012, Lu, Insinna et al. 2015). The basal body is anchored to the plasma membrane via specific structures that are the transition fibers and the distal appendages (Anderson 1972, Kobayashi and Dynlacht 2011). DAVs fuse in a ciliary vesicle triggering remodeling events which allow two of the three MT of the mother centriole to extend in the axoneme.

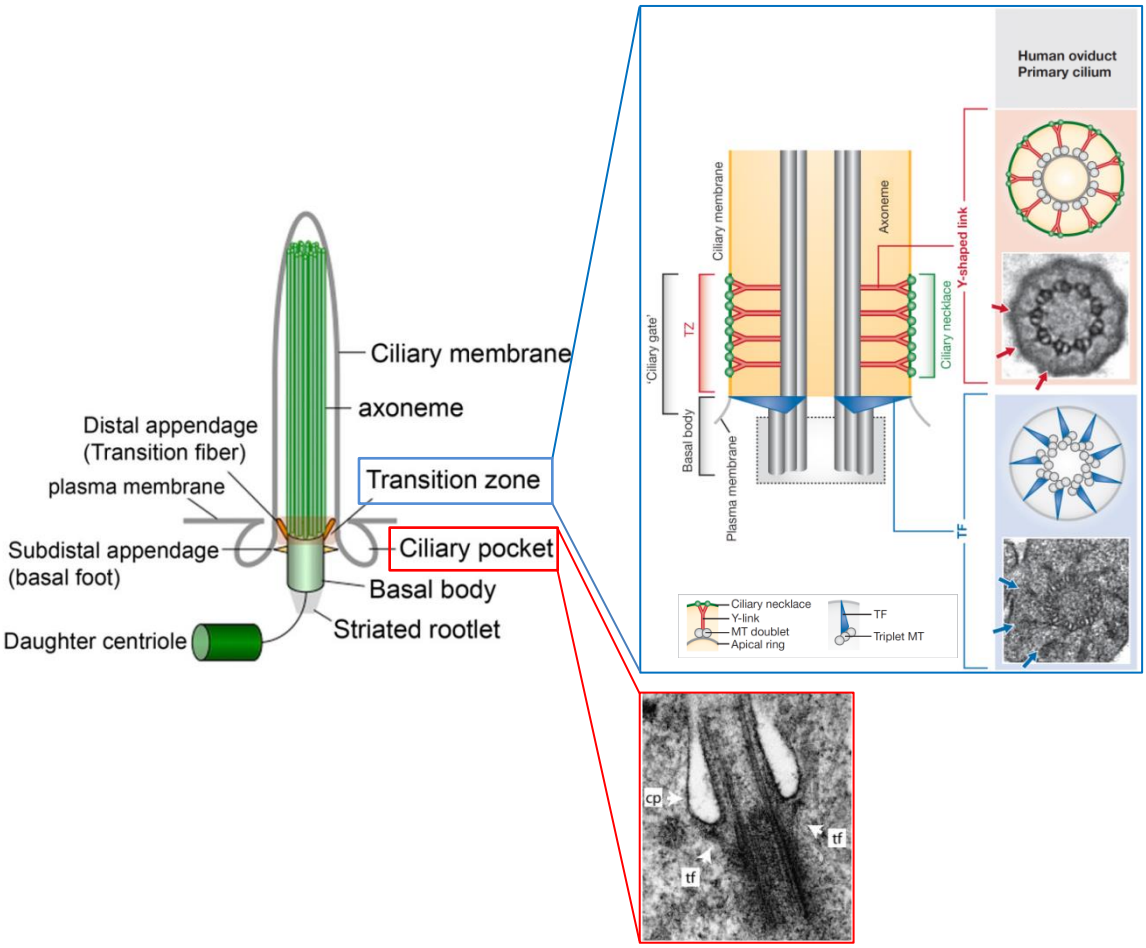

Figure 2.1: Overview of the primary cilium structure. CP: Clathrin-coated pit, TF: transition fibers, TZ: transition zone, MT: microtubules (Adapted from (Rohatgi and Snell 2010, Kobayashi and Dynlacht 2011, Reiter, Blacque et al. 2012)

2.1.3. Transition zone

The transition zone (TZ) is a specialized ciliary subdomain present at the base of the cilium and act together with the transition fibers as a "ciliary gate" that regulates the trafficking of the proteins in and out of the axoneme (Chih, Liu et al. 2011, Garcia-Gonzalo, Corbit et al. 2011).

Morphologically the TZ is characterized by the presence of "Y-shaped" linkers which bounds the axoneme MTs to a specialized region of the ciliary membrane called ciliary necklace (Fig. 2.1) (Gilula and Satir 1972). A substantial number of proteins that either localizes to or are sorted through the TZ are associated with human diseases highlighting the crucial role of this subdomain for ciliary function. Indeed, mutations in gene *BBS10* which encode for chaperonin-like proteins that localizes to the TZ causes the Bardet-Biedl syndrome (BBS), a disorder characterized by polydactyly, cognitive impairment and renal anomalies (Marion, Stoetzel et al. 2009). Similarly Joubert syndrome, a disorder of brain development, is caused by loss-of-function of Tectonic1 (Tctn1) which impairs the ciliary gate (Garcia-Gonzalo, Corbit et al. 2011).

2.1.4. Ciliary pocket

The ciliary pocket is a region at the base of the cilium characterized by an invagination of the periciliary membrane which has gain interest over the recent years for its crucial role in vesicular trafficking (Rohatgi and Snell 2010, Pedersen, Mogensen et al. 2016). Indeed, morphological analyses by microscopy methods reveal that the structure of the ciliary pocket is maintained by stable and dynamic actin filaments. Additionally, clathrin-coated pits (CCPs) are present at the ciliary pocket with a higher density than the rest of the plasma membrane and functionally active as shown by their ability to form clathrin-coated vesicles (CCVs) (Molla-Herman, Ghossoub et al. 2010). The ciliary pocket plays a major role in regulating signal transduction by coordinating the localization and the internalization of receptors essential to ciliary signaling. In fact, transforming growth factor β (TGF-β) receptors have been shown to localize to the ciliary pocket upon TGF-β stimulation and increase the activation of downstream effectors like SMAD2/3 and ERK1/2, emphasizing the crucial importance of clathrin-dependent endocytosis for cilia signal transduction (Clement, Ajbro et al. 2013).

2.2. Intraflagellar transport

The primary cilia assembly and maintenance requires materials from different cellular organelles that cannot be synthesized in the cilia due to the lack of appropriate machinery. These elements are therefore provided by a mechanism called intraflagellar transport (IFT), a bidirectional transport system of multiprotein complexes relying on motor proteins (Ishikawa and Marshall 2017, Prevo, Scholey et al. 2017). The IFT process is highly conserved in eukaryotes and was first described in the motile flagella of *Chlamydomonas reinhardtii* (Kozminski, Johnson et al.

1993) using microscopy methods. Since then, IFT has been extensively characterized and can be summarized in Fig. 2.2. To be functional, IFT requires IFT motor proteins and IFT complexes proteins.

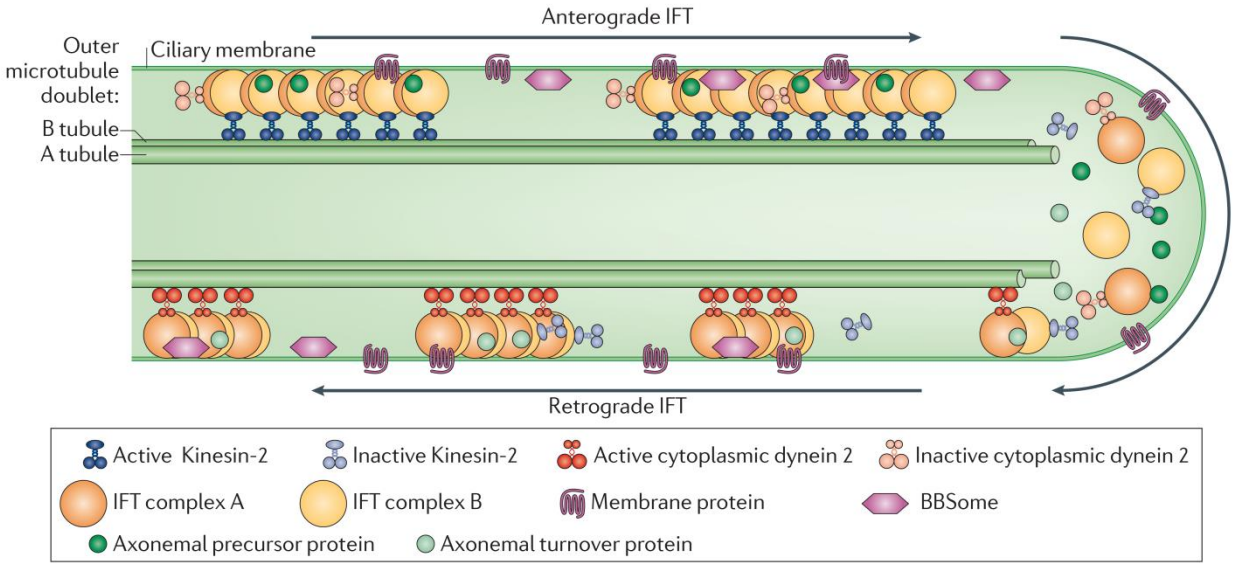

Figure 2.2: Intraflagellar transport machinery (Adapted from (Ishikawa and Marshall 2011)

2.2.1. Ciliary motor proteins

Essentially two motor proteins are involved in IFT, the heterotrimeric kinesin-2 responsible for the anterograde transport (from the ciliary base to the distal region of the axoneme) and the homodimeric dynein-2 ensuring the retrograde transport. Kinesin-2 consists of two motor subunits, KIF3A and KIF3B, and a non-motor subunit kinesin-associated protein. Kinesin-2 was originally isolated from sea urchin eggs (Cole, Chinn et al. 1993) and is vital for cilia assembly as *KIF3B* mutations were shown to severely impair cilia elongation and IFT in mice (Nonaka, Tanaka et al. 1998). Cytoplasmic dynein-2 is a complex multiprotein composed of different subunit: a heavy chain, a light intermediate chain, an intermediated chain and a light chain (Pazour, Wilkerson et al. 1998, Schafer, Haycraft et al. 2003). Dynein-2 is driving the retrograde transport and its contribution is more complex than kinesin-2. Indeed, it was shown that mutations targeting the light intermediate chain lead to a broad range of phenotype including a decrease of IFT dynein stability and a reduction of kinetic properties of retrograde IFT but not its complete loss (Reck, Schauer et al. 2016).

2.2.2. IFT complexes proteins

Two large multimeric IFT protein complexes have been isolated with classic biochemical studies where conditional mutant of *C. reinhardtii* lose their cilia in a temperature-dependent manner (Piperno and Mead 1997, Cole, Diener et al. 1998). These complexes, IFT complex A and B, move along the cilia axoneme by interacting with the ciliary motor proteins, and exert distinct functions. IFT complex A, composed of at least six proteins, is mainly involved in the retrograde transport of protein from the cilium to the cell body but its role for cilia assembly seems limited (Absalon, Blisnick et al. 2008, Tsao and Gorovsky 2008, Iomini, Li et al. 2009). By contrast, IFT complex B, a much larger complex involving at least fourteen proteins, plays a significant role in cilia assembly and mutations in this complex have been shown to lead to shorter or abrogation of cilia (Pazour, Dickert et al. 2000, Haycraft, Schafer et al. 2003, Ou, Blacque et al. 2005, Follit, Tuft et al. 2006). The IFT complex proteins are enriched in protein – protein interaction domains conferring them unique properties for transporting cargo including ciliary tubulin, ciliary membrane proteins or signal transduction proteins ensuring the maintenance and the signaling role of the cilia (Avidor-Reiss, Maer et al. 2004, Craft, Harris et al. 2015). A particularly important IFT cargo is the BBSome which consists in a multimeric proteins complex involved in the removal of G-protein coupled receptors (GPCRs) and membrane-associated proteins from the cilia (Lechtreck, Johnson et al. 2009, Xu, Zhang et al. 2015).

2.3. Regulation of ciliogenesis

Considering that both cell division and primary cilia assembly rely on the centrioles, ciliogenesis usually occurs in quiescent cells at G1/G0 phase of cell cycle. Two main mechanisms have been described for cilia assembly, depending on cell type: ciliogenesis is either initiated intracellularly (in fibroblasts) or at the cell surface (in renal polarized epithelial cells). We will focus on the latter for the following sections.

2.3.1. Assembly and disassembly of primary cilium

The ciliogenesis begins when vesicles from the Golgi and recycling endosomes dock and fuse at the distal end of the mother centriole to form the ciliary vesicle (Sorokin 1962, Lu, Insinna et al. 2015). This vesicular trafficking is tightly controlled by Rab GTPases among which Rab8a activation has been shown to regulate the elongation of the ciliary membrane (Yoshimura, Egerer et al. 2007). Subsequently, the mother centriole transitions to a basal body and docks to the

plasma membrane with the distal appendages (Tanos, Yang et al. 2013). These events involve the recruitment of different proteins such as Cep83, Cep89, Cep164, SCLT1 and FBF1 which facilitates the interaction between IFT proteins and distal appendages (Deane, Cole et al. 2001). Concomitantly, CP110, a strong inhibitor of ciliogenesis expressed at the basal body, is selectively degraded releasing the inhibition of the MT growth and the extension of the axoneme (Chen, Indjeian et al. 2002).

The mechanisms involved in cilia disassembly are generally less well understood than their assembly counterpart. A biphasic model is currently proposed for this process. First, upon mitogenic stimulation, the kinase Aurora A is activated by the scaffolding protein Human enhancer of filamentation 1 (HEF1) and phosphorylate the histone deacetylase HDAC6, which promotes the destabilization of the axonemal MTs (Pugacheva, Jablonski et al. 2007). In a second phase, the activation of two members of the kinesin-13 family, Kif2a and Kif24, triggers the MTs depolymerization with Kif24 ensuring that this process is irreversible and that ciliogenesis cannot occurs during the S phase of cell cycle (Kim, Lee et al. 2015, Miyamoto, Hosoba et al. 2015).

2.3.2. Autophagic control of ciliogenesis

In recent years, autophagy has been established as a key regulator of ciliogenesis. The primary cilium is a very dynamic structure requiring a constant supply of proteins from the cell body: it has been shown that, in starvation-induced autophagy, several key anterograde components of the IFT machinery are routed through the basal body in vesicle containing autophagy-related proteins such as ATG16L1 which are essential to the autophagosomes formation (Fig. 2.3) (Pampliega, Orhon et al. 2013). However, the regulation of ciliary growth by autophagy is complex, considering that both proteins that promote and inhibit cilia elongation are degraded via the autophagic pathway depending on the type of stimuli (Pampliega, Orhon et al. 2013, Tang, Lin et al. 2013). Adding to the complexity, autophagy itself is regulating by different cellular mechanisms like mammalian target of rapamycin (mTOR) signaling. In fact, in nutrient-rich conditions, mTORC1 is recruited at the lysosomal membrane and inhibits autophagy. However, to prevent an excessive activation of mTORC1 signaling, a feedback loop system is established and involves the activation of the negative regulator GATOR1 mediated by Skp2 E3 ligase (Jin, Lee et al. 2015). The expression levels or activity of Skp2 E3 ligase has been demonstrated to partially explain the ciliary length in various cell types in a tissue. Taken together, these studies define autophagy as a crucial regulator of ciliogenesis with basal and induced autophagy exerting

different effects on ciliary growth in response to cellular demands and the fine tuning of this process is essential to cilia homeostasis.

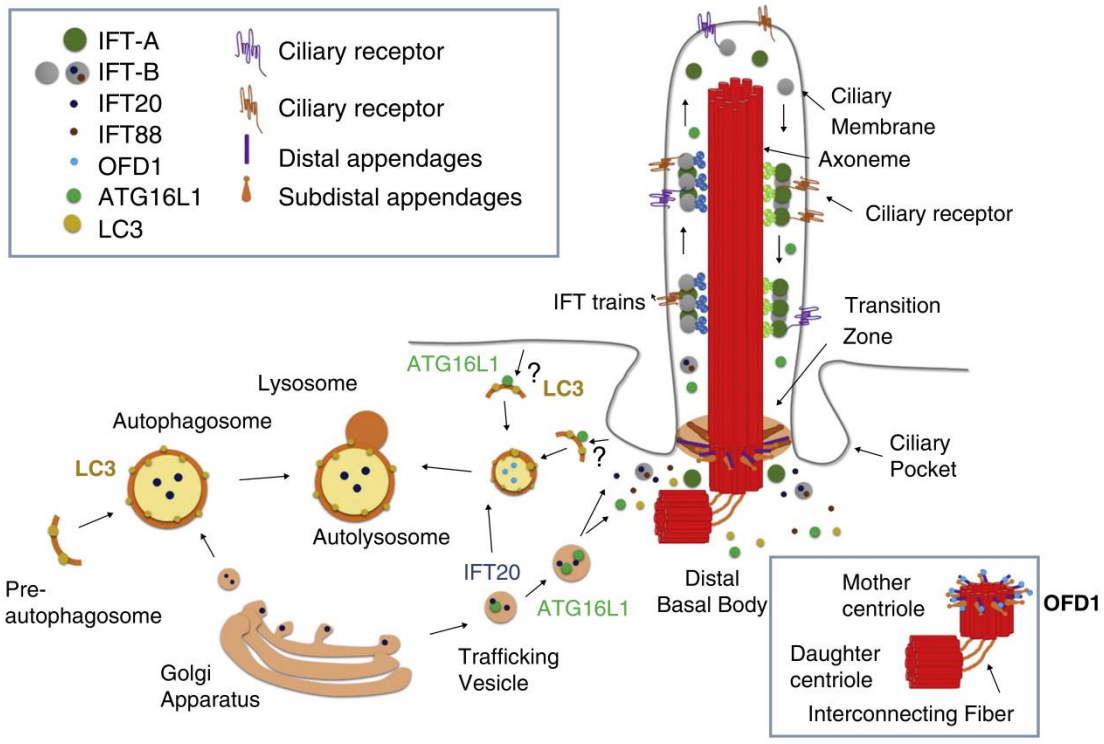

Figure 2.3: Molecular interaction between autophagy and ciliogenesis (adapted from (Pampliega and Cuervo 2016)

2.4. Role of the primary cilium in kidney

Primary cilia protrude from all the epithelial cells lining the kidney tubule, with the exception of the intercalated cells in the collecting ducts (Madsen, Clapp et al. 1988). One of the most studied functions of the cilia in the kidney tubule is the ability to transduce subtle changes in the laminar flow in cellular responses. The proposed model involves calcium entry in the cilia via specific channels, as shown in early studies using Madin Darby canine kidney (MDCK) cells where flow stimulation increases intracellular calcium (Praetorius and Spring 2001). In turn, this entry of calcium triggers the release of calcium from intracellular stores after activation of the ryanodine receptors (Jin, Mohieldin et al. 2014). Calcium ions are critical second messenger and the

increase of intracellular calcium regulates many intracellular processes including survival, differentiation or vitamin D synthesis (Cantiello 2004).

More recently, a novel role of the primary cilium in controlling the endocytosis in epithelial cells of the proximal tubule has emerged. Indeed, considering that (1) the cilia possess specialized structure, namely, the ciliary pocket highly active in endocytosis initiation and (2) this organelle possesses mechanotransduction properties, the concept that the PT could adapt its activity depending on the glomerular filtration rate (GFR) has always been attractive. The first argument supporting this hypothesis came with evidence that albumin uptake was increased in an immortalized PT cell line upon flow stimuli in a microfluidic bioreactor (Ferrell, Ricci et al. 2012). Subsequent studies showed that the increase of endocytic activity requires a functional primary cilium (Raghavan, Rbaibi et al. 2014). Nonetheless the precise intracellular pathways involved remain unclear with a putative contribution of calcium and mTOR signaling (Bhattacharyya, Jean-Alphonse et al. 2017, Long, Shipman et al. 2017).

Finally, it should be noted that the primary cilium defines a signaling hub integrating many cellular pathways including Hedgehog, Wnt, PDGFRα and these mechanisms are important for kidney physiology despite not being kidney specific *per se* (Pala, Alomari et al. 2017).

2.5. Ciliopathies

A number of genetic defects targeting both motile and non-motile cilia have been associated with a spectrum of diseases collectively termed ciliopathies. These disorders often share overlapping manifestations but differ by distinct features due to the specific function of the gene in which the mutation occurs. The most common ciliopathies include nephronophthisis (NPHP), Joubert Syndrome (JS), Meckel-Gruber syndrome (MKS), Bardet-Biedl Syndrome (BBS), Senior Løken syndrome (SLS) and Leber Congenital amaurosis (LCA) (Waters and Beales 2011). Among the different ciliopathies, we will focus on one of the most frequent inherited kidney disease, autosomal dominant polycystic kidney disease (ADPKD).

2.5.1. Autosomal polycystic kidney disease

ADPKD is one of the most common genetic causes of chronic kidney disease with a prevalence of up to 1:1000 live births (Willey, Blais et al. 2017). This disease is characterized by the development of numerous cysts which originate from all nephron segments resulting in the

enlargement of both kidneys and replacement of normal parenchyma (Wilson 2004). The glomerular filtration rate (GFR) remains preserved up to the age of 40 years in most patients because glomerular hyperfiltration in functioning nephrons compensates for the ongoing loss of renal tissue, until end-stage renal failure (ESRD) ensues in patients usually at 60 years old (Spithoven, Kramer et al. 2014). The total kidney volume (TKV) increases over time and is the strongest predictor of renal function decline in ADPKD (Grantham and Torres 2016). ADPKD diagnosis is based on imaging testing with renal ultrasound being the most common used method for cost and safety reason. Extrarenal manifestations can occur including cyst development in the liver or intracranial aneurysm.

2.5.2. Polycystins

ADPKD is associated with mutations in mainly two genes, *PKD1* (MIM#601313, 16p13.3) which accounts for approximately 78% of affected patients and *PKD2* (MIM#173910, 4q22) for 13% (Audrezet, Cornec-Le Gall et al. 2012). About 10% of the patients do not present any *PKD1* or *PKD2* mutations and these cases remains debated on whether another ADPKD locus exists. *PKD1* encodes for polycystin-1 (PC1), a membrane protein of 460 kDa (about 4303 aa) containing a large N-terminal region (3074 aa), 11 transmembrane region (1032 aa) and an intracellular C-terminal region (197 aa) (Fig. 2.4). The extracellular region of PC1 contains a considerable amount of PKD repeat domains which precise function remain unclear and could be involved in protein-protein or protein-carbohydrate interaction. Additionally, this region possess a highly conserved G-protein-coupled site, the GPS domain, located just before the first transmembrane domain and mutations in this domain has been shown to improve survival in *pkd1*-null mice model (Yu, Hackmann et al. 2007) highlighting its functional importance for PC1. Finally the C-terminal region of PC1 allows the interaction with polycystin-2 (PC2) via the coiled coil domain.

PC2, encoded by the *PKD2* gene, is a smaller protein than PC1 (110 kDa) composed of a N-terminal cytoplasmic region, 6 transmembrane domains and a short C-terminal portion. PC2 belongs to the transient receptor potential (TRP) channel family and calcium-binding motifs (EF-hand) can be found in the C-terminal region supporting a role of PC2 in calcium signaling. PC2 is located at the base of the primary cilium as well as in the endoplasmic reticulum (ER) and forms a complex with PC1 which is involved in ADPKD cystogenesis.

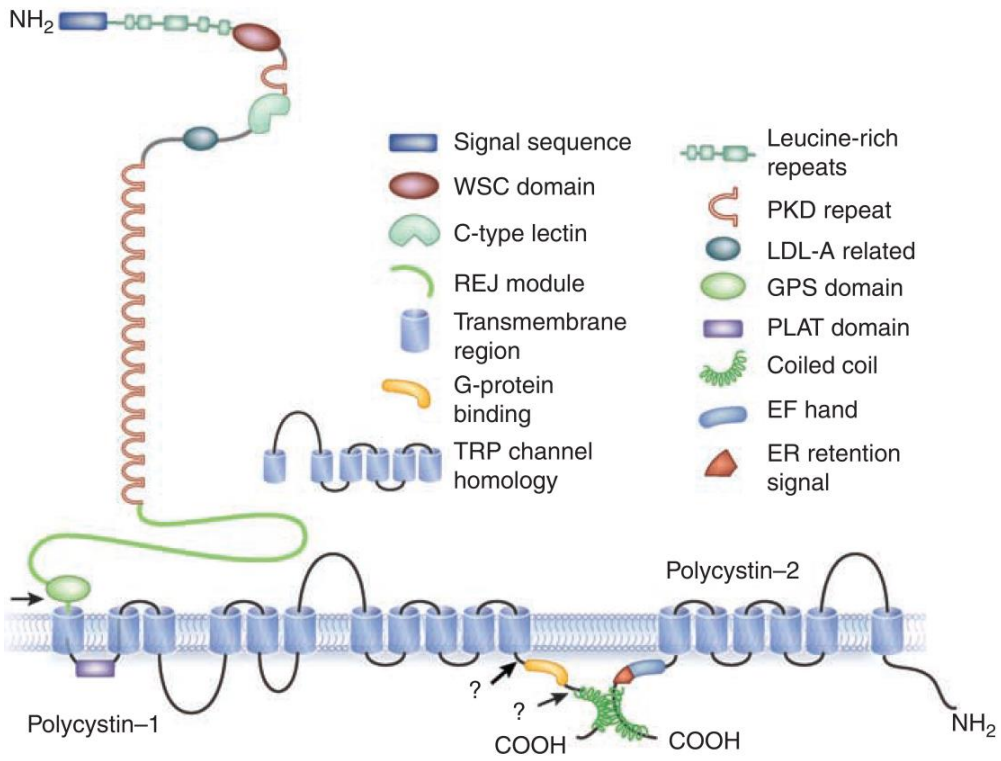

Figure 2.4: Molecular structure of polycystin-1 and polycystin-2 (adapted from (Torres and Harris 2009)

2.5.3. Pathophysiology

The cellular changes involved in ADPKD are summarized in Fig. 2.5. The precise function of the complex PC1-PC2 remains debated. The current model describes PC1 as a mechanoreceptor which induces calcium entry via PC2 in response to a flow stimulus (Nauli, Alenghat et al. 2003). This extracellular calcium would then activate PC2-ryanodine in the ER complex ultimately leading to the intracellular calcium release. Calcium controls several cell signaling pathways including the regulation of cyclic adenyl-monophosphate (cAMP) (Cooper, Mons et al. 1995). Indeed cAMP levels depends on the balance between the activity of the adenylate cyclase 6 (AC6) favoring its synthesis and phosphodiesterase (PDE) 1 and 3 responsible for its degradation and low intracellular calcium have been associated to an increase of cAMP due to AC6 activation and PDE1/PDE3 inhibition (Wang, Ward et al. 2010). The increase of the second messenger cAMP leads to the activation of several proliferative pathways through the activation of the protein kinase A (PKA) and the associated downstream effectors such as extracellular signal regulated kinase (ERK), mTOR, c-AMP binding element response (CREB) and signal transducer and activator of transcription 3 (STAT3) (Yamaguchi, Nagao et al. 2003, Talbot, Song et al. 2014). PKA is also involved in fluid secretion in the cyst via the activation of cystic fibrosis

transmembrane conductance regulator (CFTR) resulting in the excretion of chloride ions followed by sodium ions in the cyst lumen (Albaqumi, Srivastava et al. 2008).

AC6 is also regulated by the G-protein coupled receptor among which vasopressin receptor (AVP2R) expressed in the collecting duct and in the thick ascending limb plays a major role. Therefore several therapeutic strategies inhibiting AC6, thus reducing cAMP levels, have been developed and tolvaptan, an AVP2R inhibitor, has been shown particularly effective by slowing down the decline of GFR even in later stage ADPKD (Torres, Chapman et al. 2017). Recently the role of calcium signaling mediated by the primary cilia in ADPKD has been questioned for several reasons. Indeed, in a recent study, Clapham and colleagues developed a sophisticated model where genetically labelled calcium could be precisely monitored and they show that changes in ciliary calcium could not account for the overall cytoplasmic calcium variations (Delling, Indzhykulian et al. 2016). Additionally, it was shown that Ca^{2+} current can be mediated by polycystin-1L1 and polycystin-2L2 independently of the flow (DeCaen, Delling et al. 2013). These studies suggest that PC1/PC2 complex signaling involve partners yet to be discovered and the associated mechanisms could be independent from calcium.

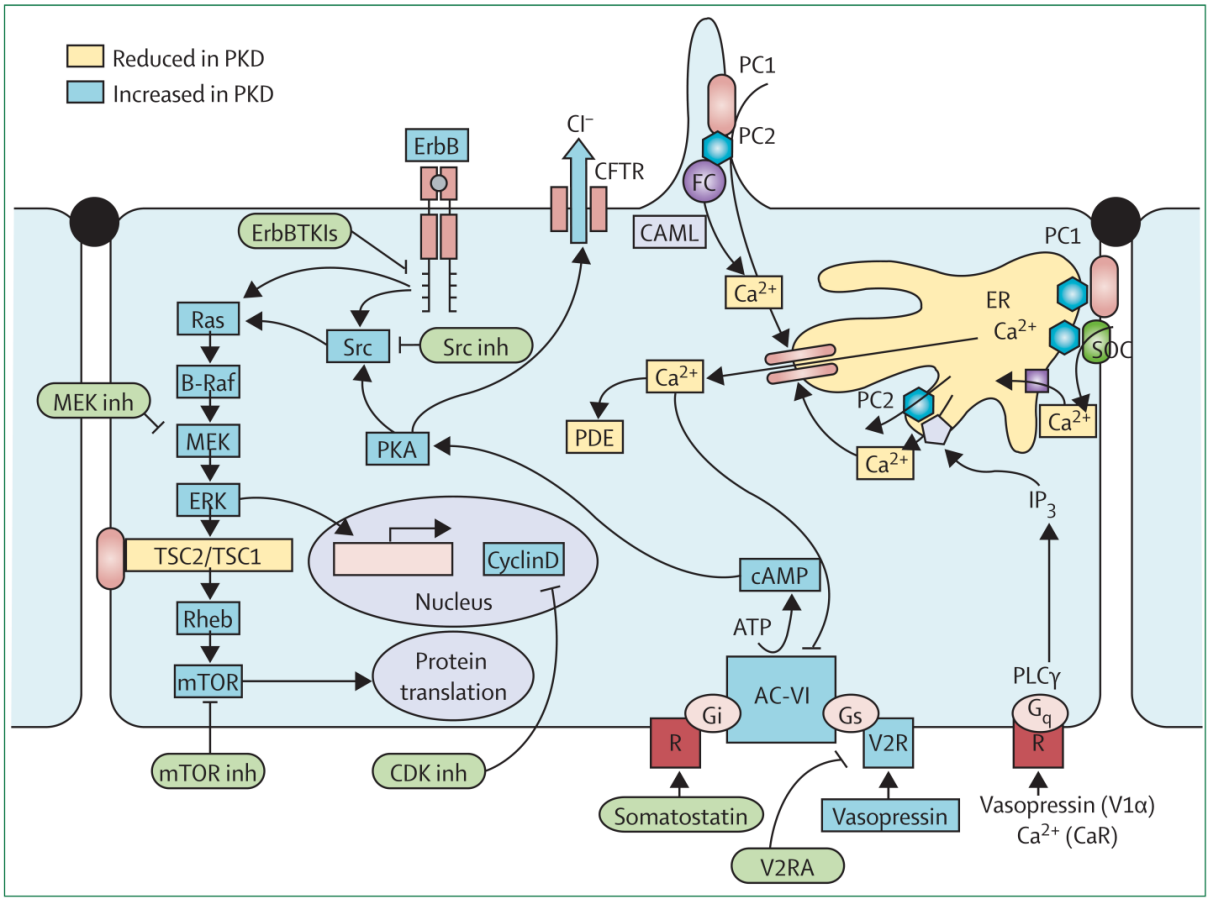

Figure 2.5: Cellular pathways affected in polycystic kidney disease. AC-VI; adenylyl cyclase 6, CDK; cyclin-dependent kinase, ER; endoplasmic reticulum, MAPK; mitogen-activated protein kinase, mTOR; mammalian target of sirolimus, PC1; polycystin-1, PC2; polycystin-2, PDE; phosphodiesterase, PKA; protein kinase A, R; receptor, TSC; tuberous sclerosis proteins tuberin (TSC2) and hamartin (TSC1), V2R; vasopressin V2 receptor, V2RA; vasopressin V2 receptor antagonists (adapted from (Torres, Harris et al. 2007)

2.5.4. Proximal tubule dysfunction in ADPKD

Several lines of evidence indicate that ADPKD could be associated with specific defects targeting the epithelial cells lining the PT. Indeed, it is well established that the cysts originates from every nephron segment including PT (Devuyst, Burrow et al. 1996). Additionally, *Pkd1* null mouse model exhibit polyhydroamnios and analyses of the amniotic fluid, a surrogate of the urine at this developmental stage, revealed increased level of solutes and proteins typically reabsorbed by PTs such as clara cell 16 (CC16) reflecting low molecular weight proteinuria (Ahrabi, Jouret et al. 2010). This phenotype is associated with defects in the expression profile of the multi ligands receptors megalin and cubilin. A second argument supporting PT disorders in ADPKD context is the fact that patients shows specific urinary loss of vitamin D binding protein and transferrin in

absence of renal failure (GFR > 90 mL.min^{-1}). Additionally, recent studies showed an association of proximal tubule markers including β2-microglobulin with GFR decline in patients with ADPKD (Messchendorp, Meijer et al. 2018). Finally, considering that PT homeostasis heavily relies on its transport ability and that the primary cilium has been recently described to play a significant role in endocytosis, one could hypothesize that there are mechanisms linking cilia dysfunction to PT disorders.

3. Bone marrow transplantation

Bone marrow (BM) or hematopoietic stem cell transplantation (HSCT) is a curative therapy which has been shown beneficial for malignant and genetic diseases of the hematopoietic system such as leukemia, sickle cell disease or severe combined immunodeficiency (SCID). This procedure involves the injection of HSC from a compatible donor to the recipient after a myeloablative treatment either by radiation or by the use of chemotherapeutic agents to allow the engraftment of the injected HSC (Ljungman, Bregni et al. 2010). In the 1950s, bone marrow transplantation was demonstrated effective in animal experiments where mice and guinea-pigs showed higher survival after irradiation and subsequent transplantation from other animals (Lorenz, Congdon et al. 1952). In humans, Dr. E. Donnell Thomas pioneered stem cells transplantation in 1957 to treat a patient from leukemia and this work was followed in 1968 by the treatment and long-term survival of two patients suffering from SCID and the Wiskott-Aldrich syndrome (Thomas, Lochte et al. 1957, Gatti, Meuwissen et al. 1968, De Koning, Van Bekkum et al. 1969). According to the worldwide network for blood and marrow transplantation (WBMT), over 50000 HSC transplants are carried out every year with about 90% success rate if a good combination donor recipient can be found. HSC are essential to this method and will be described in the following sections.

3.1 Hematopoietic stem cells

BM has been well established as the source of blood and immune cells throughout life. Seminal studies of Till and McCulloch identified the precise components of bone marrow allowing the renewal of blood cells thereby defining HSCs and their two unique core properties that are (1) the ability to self-renew and (2) to differentiate and generate a variety specialized cells (Till 1961). In fact, HSCs are the progenitor of all mature cell types of the mammalian blood system including erythrocytes, platelets, granulocytes, macrophages, dendritic cells, lymphocyte B/T cells and natural killer cells (Fig. 3.1). The main source of HSC is the bone marrow which can be isolated from the hipbone in humans for donor purposes. Alternatively, HSCs can also be found in peripheral blood but required the injection of granulocyte-colony stimulating factor (G-CSF), a glycoprotein that stimulates the production of granulocytes while hindering the mobilization of stem cells from bone marrow niches resulting in an increase of HSCs in the blood representing

then 1-2% of blood cells (Vij, Brown et al. 2000, Levesque, Hendy et al. 2003, Behfar, Faghihi-Kashani et al. 2017).

Mainly two types of HSCT are performed and will be described in the following sections: autologous and allogenic.

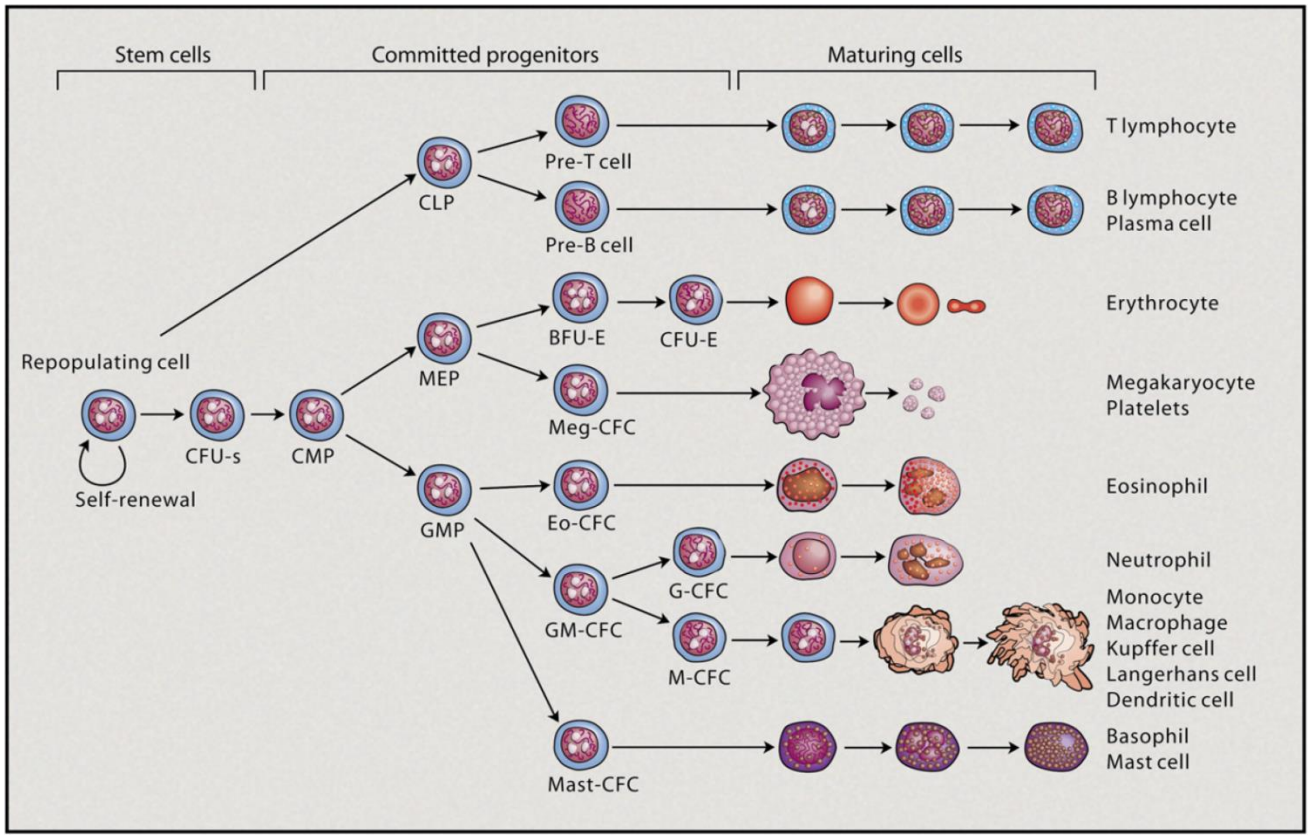

Figure 3.1: Hematopoietic family tree describing the mature cells derived from HSCs CFU-s, colony-forming unit-spleen; CMP, common myeloid progenitor; CLP, common lymphoid progenitor, MEP, megakaryocyte-erythroid progenitor; GMP, granulocyte-macrophage progenitor; BFU-E, burst-forming unit-erythroid; Meg, megakaryocyte; Eo, eosinophil; G, granulocyte; and M, macrophage. (adapted from (Metcalf 2007)

3.1.1 Autologous hematopoietic stem cell transplantation

Autologous HSCT consists in using the patient's stem cell after removal of the malignancy to reconstitute the immune system. This therapeutic approach is used for certain leukemia and multiple myeloma and presents the advantage of a decreased risk of infection and graft versus host disease (GvHD). Recently the spectrum of diseases for which autologous HSCT is applied has also been expanded to autoimmune diseases like multiple sclerosis, systemic lupus,

rheumatoid arthritis and Crohn's disease (Snowden, Passweg et al. 2004, Passweg and Tyndall 2007, Mancardi, Sormani et al. 2017). However, patient subjected to autologous HSCT present increased risk of *de novo* autoimmunity during re-emerging lymphopoiesis and also a potential increased frequency of secondary malignancies showing the need of additional prospective long-term follow-up studies to assess the risk of developing complications after autologous HSCT (Daikeler, Tichelli et al. 2012).

3.1.2 Allogenic hematopoietic stem cell transplantation

Allogenic transplant is performed for a wider range of hematological diseases using HSCs from a human leukocyte antigen (HLA) matched donor who is either a relative or a person found in a donor bank. HLA are highly polymorphic genes that encode for the major histocompatibility (MHC) complexes expressed at the cellular surface and are crucial for the success of the engraftment as mismatches in MHC are associated with an increase of graft rejection and GvHD (Imus, Blackford et al. 2017, William, Wang et al. 2017). Allogenic HSCT is mainly used as a curative therapy for malignancies as the donor HSCs are able to reconstitute the recipient immune system which then generate T cells targeting the malignant cells by a mechanisms termed graft versus tumor (GvT). Compared to the autologous HSCs, allogenic stem cells do not require a conditioning protocol and thus are obtained more easily. One major concern of this procedure is that the risk of complications including graft rejection and GvHD is much higher as the donor T cells can target and damage the host tissues leading to the need of immunosuppressive treatment for most patients.

3.2 Hematopoietic stem cell transplantation in kidney diseases

The effectiveness of HSCT in non-hematopoietic diseases has long been debated. Despite these controversies, several mechanisms have been proposed to explain tissue repair including cell replacement, cell fusion and paracrine interactions (Wang, Willenbring et al. 2003, Ratajczak, Kucia et al. 2012, Ogawa, LaRue et al. 2013). Indeed it was suggested that HSC plasticity could be higher than expected and adipocytes, chondrocyte and fibroblasts were shown to exhibit markers of HSC origin leading to the hypothesis that cells HSC could fuse and/or replace differentiated cells other than blood and immune cells. (Lang, Ebihara et al. 2006, Sera, LaRue et al. 2009, Mehrotra, Williams et al. 2013). HSCT can be investigated using the methods summarized in Fig.3.2. Numerous studies have reported that BM and HSCT could be effective in

lysosomal storage diseases including leukodystrophy and Hurler syndrome (Krivit, Aubourg et al. 1999). More recently, Cherqui and colleagues elegantly showed in *Ctns* deficient mice that HSCT provided long-term renal protection by alleviating the proteinuria due to PT defects (Harrison, Yeagy et al. 2013). In a subsequent study, the mechanisms involved were refined showing that BM derived cells were engrafted in a stable manner and they exchanges functional protein and genetic materials by specialized structure called tunneling nanotubes (Naphade, Sharma et al. 2015). The nanotubes allow the transfer of vesicles containing material (RNA and protein) between the BM transplanted cell and the kidney cells. Therefore, combining fluorescently labelled proteins and live cell imaging techniques, Cherqui and colleagues showed that functional lysosomes were transferred from the BM cells to the kidney cells therefore improving the kidney function by decreasing the amount of cystine (Naphade, Sharma et al. 2015). These seminal studies evidenced that HSCT can restore a functional transmembrane protein expressed in an intracellular compartment and raise the question of the effectiveness of HSCT in other type of endolysosomal disorders in the kidney.

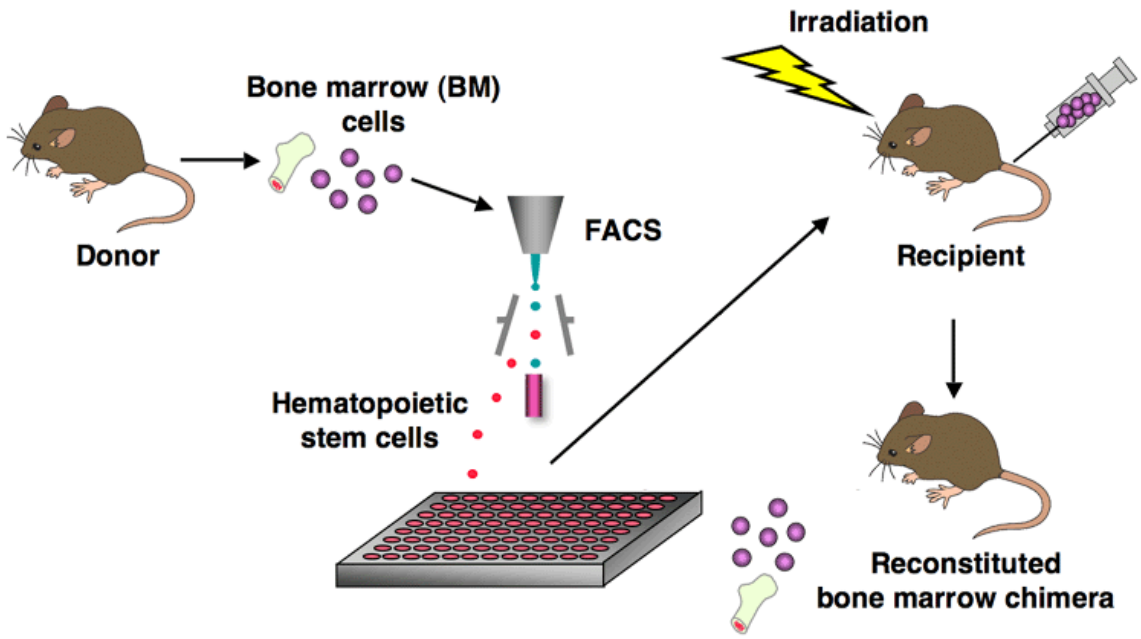

Figure 3.2: Principle of hematopoietic stem cell transplantation experiment (adapted from Dr. Miyoshi, RIKEN, BioResource Research Center)

II- Aims of the thesis

II- Aims of the thesis

The crucial role played by the PT in homeostasis relies on active transport systems that include receptor-mediated endocytosis. The latter drives the reabsorption of essential nutrients that are ultrafiltered, preventing their loss in the urine and ensuring that they are correctly processed along the endolysosomal pathway. Additionally, the endolysosomal system is essential for the degradation of intracellular materials and defective organelles through autophagy. In turn, dysfunctions in the endolysosomal system (e.g. Dent disease, cystinosis) are associated with urinary loss of solutes and LMW proteins, together with defective autophagy and accumulation of intracellular substrates including deficient mitochondria, with further consequences on the epithelial phenotype (Festa, Chen et al. 2018). Studies on the regulation of receptor-mediated endocytosis in the kidney have been largely focused on the deficiency or the trafficking of the receptors involved in this process (Nielsen, Christensen et al. 2016, De Matteis, Staiano et al. 2017).

A growing body of evidence shows that the primary cilium could regulate the endocytosis activity of the epithelial cells lining the PT. A specialized structure present at the ciliary base, the ciliary pocket, is enriched in clathrin-coated pits and is a very active site of clathrin-coated vesicles formation - the first step in receptor-mediated endocytosis (Molla-Herman, Ghossoub et al. 2010). Moreover recent studies evidenced a specific increase of endocytic activity upon mechanical stimulation of the primary cilium, an effect that is abrogated upon removal of the primary cilium (Raghavan, Rbaibi et al. 2014, Long, Shipman et al. 2017). On the other hand, autophagy, which depends on lysosomal function and also plays a preeminent role in PT function, has also been shown to be a major regulator of ciliogenesis (Pampliega, Orhon et al. 2013, Tang, Lin et al. 2013). Finally, patients suffering from ADPKD, a prototype of ciliopathy, have been shown to display an abnormal urinary excretion of PT damage markers including KIM-1, β2-microglobulin, β-hexosaminidase at an early stage of the disease. Taken together, these data suggest a possible link between ADPKD, taken as a paradigm of ciliopathy, and defective endocytosis in the cells lining the kidney PT. ***The first aim of this thesis*** **is to substantiate the evidence for PT dysfunction in ADPKD and to investigate the mechanisms linking PT dysfunction and ciliogenesis using congenital and inducible models of cystic kidney and endolysosomal disorders.**

Few therapeutic solutions are available to target congenital disorders of the endolysosomal pathway, such as Dent disease, which is usually complicated by generalized PT dysfunction. The current efforts focus mostly on the prevention of complications due to the massive loss of solutes in the urine, of the development of CKD. Recently bone marrow (BM) and hematopoietic stem cells (HSC) transplantation have been shown to efficiently preserve kidney function in nephropathic cystinosis, a lysosomal storage disorder which the most frequent cause of renal Fanconi syndrome in children. The mechanisms of the protective effect of BM transplantation without indication of target tissue differentiation and replacement of damaged PT epithelial cells remain elusive. These studies also raised the issue of whether BMT would be beneficial for a pure endolysosomal disorder such as Dent disease. ***The second aim of the thesis*** **is to assess whether bone marrow transplantation can preserve kidney function in the *Clcn5* KO mouse model of Dent disease and to study the potential mechanisms involved using a co-culture system of BM derived cells and primary mouse proximal tubular cells.**

III- Experimental studies

III-1 Lysosomal function links ciliogenesis and receptor mediated endocytosis

Alkaly Gassama[1], Nathalie Demoulin[2], Dorien J M Peters[3], Alessandro Luciani[1], Olivier Devuyst[1,2]

[1] Institute of Physiology, University of Zurich, Zurich, Switzerland

[2]Division of Nephrology, UCL Medical School, Brussels, Belgium

[3]Department of Human and Clinical Genetics, Leiden University Medical Centre

Correspondence: Prof. Dr. Olivier Devuyst**;** Institute of physiology, University of Zurich; Winterthurerstrasse, 190, 8057 Zürich, Switzerland**;** Tel.: +41(0)44 635 50 82, E-mail: olivier.devuyst@uzh.ch

Manuscript in preparation

ABSTRACT

The epithelial cells lining the proximal tubules (PT) of the kidney reabsorb large amounts of filtered solutes owing to a particularly efficient receptor–mediated endocytosis and endolysosomal pathway. A growing number of evidence suggests that receptor–mediated endocytosis could be regulated by the primary cilium and that ciliopathies could lead to PT dysfunction. The mechanisms underlying these associations remain poorly understood. Here we demonstrate, by combining *in vitro* and *in vivo* approaches, that anomalies in primary cilia are causing an epithelial phenotype switch, with proliferation and apical dedifferentiation leading to defective receptor–mediated endocytosis and PT dysfunction. These cellular abnormalities are linked to defective lysosome/autophagy–mediated elimination of intracellular flagellar protein 20 (IFT20), which is required for cilia function and growth. Restoring cilia length, induced by IFT20 depletion, rescues receptor–mediated endocytosis and PT epithelial function in a rat model of human ciliopathy. Conversely, IFT20 accumulation, which is caused by dysfunctional endolysosomal pathways, sustains cilia growth and PT dysfunction in acquired and congenital kidney disorders. These results evidence a functional interplay between ciliogenesis, receptor–mediated endocytosis and autophagy–lysosome degradation pathways, so that impaired ciliary homeostasis is a common pathway underlying PT dysfunction in various kidney diseases.

INTRODUCTION

The existence of an effective communication between the external environment and the endomembrane system is a fundamental property of epithelial cells. Such interplay between the lumen and the apical membrane domain is crucial in cells lining the intestine and the kidney, which absorb large quantities of essential nutrients through specialized transport processes. The kidney PT cells represent a paradigm for these properties, as they continuously recycle receptors and transporters at the apical membrane, ensuring the recovery of essential filtered substances that would otherwise be lost in the urine. These substances include low-molecular–weight (LMW) proteins that interact with multi–ligand receptors, megalin and cubilin, followed by internalization and subsequent delivery to endosomes and further to lysosomes for processing. This uptake accounts for ~80% of the total metabolic clearance of small proteins and peptides, playing an important role in preserving body homeostasis (Christensen & Birn, 2002). Congenital diseases targeting multi–ligand receptors (e.g. Donnai–Barrow or Imerslund–Gräsbeck syndromes) or the endolysosomal pathway (e.g. Dent disease or cystinosis) lead to massive urinary losses of solutes and LMW proteins, often complicated by multi-systemic complications and progression to end–stage renal disease (Devuyst & Luciani, 2015).

Most mammalian cells have a primary cilium, a microtubule–formed organelle that protrudes toward the lumen and transduces signals (Malicki & Johnson, 2017). An interesting characteristic of the cilium is its ability to adjust morphology in response to environmental conditions. Indeed, cilia appear to act as a self–adjusting antenna, and modify their size and shape depending on the strength of the signal that they detect (Reiter & Leroux, 2017). By functioning as a signaling hub that senses different stimuli, primary cilia might regulate the specialized function of epithelial cells that line proximal tubule of the kidney. As a result, flow–induced ciliary Ca^{2+} and signaling might promote endocytic clearance of low–molecular weight (LMW)

proteins and other ligands from the glomerular filtrate via remote activation of LRP2 located at the base of microvilli (Raghavan et al, 2014). Interestingly, recent studies reported that Lowe syndrome protein OCRL1–a congenital disorder resulting in defective receptor–mediated endocytosis and PT dysfunction– might control the vesicular trafficking of ciliary proteins and signaling molecules (Coon et al, 2012; De Matteis et al, 2017) , ensuring the maintenance of primary cilia formation and composition. As such, defective primary cilia formation has been detected in kidney cells and zebrafish depleted of OCRL1 (Luo et al, 2012; Oltrabella et al, 2015), highlighting potential interactions between primary cilium formation, receptor–mediated endocytosis and transport properties in PT epithelial cells.

The formation and maintenance of the primary cilium depends on the continuous trafficking of structural, regulatory and signaling molecules in and out of the ciliary axoneme mediated by the intraflagellar transport (IFT) system. This vesicular trafficking is interconnected with autophagy, a pathway for degradation of cellular components in lysosomes (Settembre et al, 2013). By removing specific ciliary proteins (e.g. IFT20), the autophagy–mediated degradation system – a homeostatic process particularly active in specialized epithelial cells– regulates primary cilia formation and biogenesis (Pampliega & Cuervo, 2016; Pampliega et al, 2013). Nonetheless, signaling ciliary proteins exit the cilium near the basal body, where regulatory autophagy–related proteins required for the autophagosome formation are located, suggesting that primary cilia signaling might safeguard cell homeostasis through the regulation of autophagy (Kaliszewski et al, 2015). This homeostatic process is particularly active in kidney cells, whose high reabsorptive transport activity requires an efficient autophagy-mediated clearance system to protect against acute tubular injury (Kimura et al, 2011).

The regulation of apical endocytosis and the interplay between the primary cilia, the endolysosomal function and autophagy in particular are gaining attention due to their biological

relevance for tissue homeostasis and the pathogenic mechanisms of ciliopathies. Challenges in deciphering these interactions reflect experimental issues to modulate primary cilium functions and differences in epithelial phenotype and apical differentiation (Pampliega & Cuervo, 2016; Raghavan & Weisz, 2016).

In the present study, we use the kidney proximal tubule as paradigm of epithelial differentiation to demonstrate a functional cross–talk between primary cilium, autophagy–lysosome degradation system and endocytosis within specialized epithelial cells. Taking advantage of rat (*Cy/+*) and mouse (*Pkd1*) models of human ciliopathies (autosomal dominant polycystic kidney disease, ADPKD), in combination with *in vitro* studies on primary cultured kidney PT cells, we show that ciliary alterations are associated with a severe, specific defect in receptor-mediated endocytosis, reflecting a phenotype switch associating abnormal proliferation and dedifferentiation. Mechanistically, these cellular abnormalities are linked to defective lysosome/autophagy–mediated elimination of IFT20, which is required for cilia growth. Deregulated ciliary autophagy was also observed in other disease models that affect defective receptor–mediated endocytosis (e.g. Dent disease) and endolysosomal pathway (e.g. cystinosis and light chain disease), resulting in apical dedifferentiation and epithelial dysfunction, and in patients with ADPKD. These results indicate that impaired cilia/lysosome–autophagy interplay is a common pathway underlying PT dysfunction in various kidney diseases.

RESULTS

Defective receptor-mediated endocytosis in HAN:SPRD *Cy/+ rats*

We first investigated parameters of endocytic uptake in the Han:SPRD *Cy/+* rats, an established model of ciliopathy characterized by the development of PT cysts with a slow progression of chronic kidney disease (Schafer et al, 1994). *Cy/+* rats showed a marked increase in the urinary excretion of the LMW proteins transferrin, vitamin D binding protein (VDBP) and Clara cell protein of 16 kDa (CC16) from 5 weeks of age (Fig. 1A, B) when compared to their control littermates. The LMW proteinuria in *Cy/+* rats was observed in absence of renal failure, as shown by the unchanged values of blood urea nitrogen (BUN) and serum creatinine (Table 1, Supp Fig. 1A). Consistent with the pivotal role of receptor–mediated endocytosis in handling essential nutrients, *Cy/+* rats displayed decreased expression of endocytic receptor megalin (Fig. 1C-D) contrasting the abnormal proliferation of PT cells as evidenced by a major increase in KI67 and PCNA (Fig. 1C-E). The defective megalin expression is likely due to post-transcriptional events since no significant changes were observed at the mRNA level (Suppl. Fig.1C).

To substantiate the changes observed *in vivo* and confirm the defective epithelial phenotype in PT cells, we developed a primary culture system from micro-dissected PT segments from HAN:SPRD rat kidneys (rPTC), using well-established protocols (Terryn et al, 2007) (Luciani et al, 2016). The purity of the rPTC culture was verified by enrichment in specific segmental markers such as AQP1, NaPi-IIa and megalin and exclusion of distal tubule markers (Fig. 1F, Suppl. Fig. 2A). When grown to confluence, rPTCs showed a typical endocytic activity, as quantified by the uptake of fluorescent–tagged albumin (Al488-BSA), with a dose–dependent saturation and inhibition by Dynasore (80 μM, 30 min pre-treatment) (Suppl. Fig. 2B).

The endocytosis activity of rPTCs derived from 5 week– old *Cy/+* kidneys showed a 70%-reduction of Al488-BSA uptake compared to the rPTCs derived from control littermates (Fig.

1E). The defect affected specifically receptor-mediated endocytosis, as the uptake of the fluid-phase tracer alexa488-dextran was unaffected (Fig. 1E). The defective receptor–mediated endocytosis was reflected by the decrease in the protein levels of megalin in *Cy/+* derived rPTCs compared to control rPTCs, increased expression of proliferation markers including PCNA (Fig. 1F).

These data demonstrate defective receptor-mediated endocytosis and PT cell dysfunction in a rat model of ciliopathy.

Defective ciliogenesis impairs megalin expression and endocytosis

Considering previous evidence suggesting that PT endocytosis could be regulated by the primary cilium (Long et al, 2017; Raghavan et al, 2014), we investigated whether the endocytosis defect observed in Cy/+ rats was related to primary cilium dysfunction. We tested this hypothesis by experimentally measuring ciliary growth. We observed that the ciliary length was markedly increased in *Cy/+* kidneys and their derived rPTCs when compared to their control littermates as scored by confocal microscopy analysis of acetylated (Ac)–tubulin. (Fig. 2A, B). As primary cilia functions as fluid flow sensing organelle (Kolb et al, 2004; Raghavan et al, 2014),we therefore asked whether abnormal ciliary elongation might affect the endocytosis rate in response to fluid flow induced shear stress in *Cy/+* rPTCs. The cells were subjected to fluid flow stimuli by using an orbital shaker at 1 Hz (Fig. 2B, C) for increasing amounts of time, followed by an endocytosis assay (Al647-BSA uptake). After 4h of stimuli, +/+ derived rPTCs showed a significant increase of endocytosis activity compared to the controls (Fig. 2B) paralleled by an increased expression of megalin (Fig. 2C). In contrast, fluid flow–stimulated–*Cy/+* rPTCs experiencing long cilia showed decrease in receptor–mediated endocytosis and (Fig. 2B) in

megalin levels (Fig. 2C). These data suggest that fine–tuned regulation of cilia growth maintains transport activity and function within kidney epithelial cells in response to mechanical cues.

To further understand the ciliary defects in *Cy/+* cells, we investigated regulators of ciliogenesis including intraflagellar transport (IFT) particles which are large multiprotein complexes essential for delivering ciliary proteins to the basal body and initiate cilium elongation (Follit et al, 2006). We studied two essential IFT proteins: IFT20 which shuttle between the Golgi complex and the basal body and IFT88 which localizes to the basal body and the axoneme of cilia. IFT20 expression was significantly increased in *Cy/+* derived rPTCs compared to their +/+ counterpart whereas IFT88 was unchanged (Fig. 2D). This abnormal expression occurred in absence of transcriptional changes for cilia assembly genes (Fig. 2E), implying defective turnover of ciliary proteins.

In an attempt to mechanistically connect increased IFT20 with cilium growth and endocytosis defects, we we performed loss–of function approaches in primary renal tubular cells (PTCs) derived from *Cy/+* rats. We then used an adenovirus–expressing shRNA-*Ift20* to elicit *Ift20* deletion in primary renal tubular *Cy/+* cells.

The transduction reduced IFT20 expression in Cy/+ derived rPTCs to levels comparable to +/+ rPTCs (Fig. 2F), with normalization of cilia length (Fig. 2G), recovery of megalin expression (Fig. 2F) and improved endocytosis uptake (Fig. 2G).

To further investigate the link between primary cilium and endocytosis, we treated mPTCs with cytochalasin D (100 nM, 12 h), an actin polymerization inhibitor which facilitates cilia elongation, followed by an endocytosis assay (Suppl. Fig. 3A-B). Treatment with cytochalasin D led to a significant increase in the primary cilia length, paralleled by a major decrease in Al647-BSA uptake linked to an impairment of megalin expression while dextran uptake was unchanged (Suppl. Fig. 3A-B). Additionally, when cilia were chemically removed using ammonium sulfate

(Suppl. Fig. 3D), a similar decrease of the endocytosis activity was observed associated with a progressive loss of megalin (Suppl. Fig. 3E, F).

Considering that the decrease of megalin expression in Cy/+ kidneys and derived rPTCs was observed in absence of transcriptional changes (Suppl. Fig. 1, 2) and that the primary cilium has been shown to regulate the proteasome activity (Gerhardt et al, 2015; Liu et al, 2014), we investigated whether the proteasomal degradation of megalin was affected by ciliary length. We first examined the ubiquitination rate of megalin by performing an immunoprecipitation of megalin from mPTCs treated with cytochalasin D for 12h and we observed a marked increase of megalin ubiquitination upon elongation of the cilia (Suppl. Fig 3C). Next, we treated Cy/+ derived rPTCs with MG-132, a proteasome inhibitor for 24 h and 48 h and we observed a recovery of megalin expression in Cy/+ rPTCs upon proteasome inhibition (Fig. 2H).

Taken together, these results support a fundamental role of the primary cilia in regulating transport function in PT cells.

Defective autophagy leads to an accumulation of the ciliary protein IFT20

Recent studies have established that autophagy is a major regulatorciliogenesis by controlling the trafficking and the degradations of IFTs (Lee et al, 2016; Pampliega et al, 2013; Tang et al, 2013) . In view of the above findings, we hypothesized that the increased protein level of IFT20, which leads to cilia endocytosis dysfunctions in *Cy/+* cells, might arise from alterations in autophagy pathway.

The expression levels of the polyubiquitin-binding protein p62 and the microtubule-associated protein 1A/1B-light chain 3 (LC3), reflecting the number of autophagosomes, were significantly increased in Cy/+ kidneys compared to controls, with a major increase in immunofluorescence signal in PT segments (Fig. 3A-B), suggesting an impaired autophagic flux in Cy/+ kidneys.

To substantiate this hypothesis, we analyzed the autophagy flux in rPTCs by monitoring the conversion of LC3-I to the autophagosome-bound LC3-II and its subsequent degradation in presence or absence of nutrients. In nutrient-rich media, Cy/+ derived rPTCs exhibited an increase of LC3-II compared to +/+ rPTCs, which was not further increased in absence of nutrients (Fig. 3C). In presence of BafilomycinA1 (BfnA1), an inhibitor of the proton pump V-ATPase blocking the late phase of autophagy, +/+ rPTCs cultured in nutrient-depleted medium showed as expected an increase of LC3-II and p62 compared to the nutrient-rich conditions, whereas LC3-II and p62 levels were unchanged in Cy/+ derived rPTCs (Fig. 3C). A similar profile was observed for IFT20 protein level (Fig. 3C) suggesting that the late-autophagy clearance is defective in Cy/+ derived cells. These findings were supported by electron microscopy analysis showing a marked increase of autophagic-like vacuoles containing undigested material in Cy/+ derived rPTCs (Fig. 3D).

Furthermore we determined the intracellular localization of IFT20 in +/+ and Cy/+ derived rPTCs by transducing the cells with an adenovirus expressing LC3-GFP. In nutrient rich conditions, almost no colocalization was observed between LC3-GFP and IFT20 in +/+ rPTCs whereas a high number of LC3-GFP vesicles positive for IFT20 were detected in Cy/+ cells. In absence of nutrient and in presence of BfnA1, IFT20 accumulated in LC3-GFP vesicles in +/+ derived rPTCs while no change was observed for Cy/+ rPTCs suggesting that (i) IFT20 degradation was prevented in +/+ cells in presence of BfnA1 and (ii) the clearance of IFT20 is impaired in Cy/+ PT cells (Fig. 3E).

Taken together, these data suggest that defective autophagic clearance is responsible for the accumulation of IFT20 in Cy/+ kidneys and cells.

Lysosomal dysfunction causes defective autophagic clearance and abnormal ciliogenesis. One mechanism by which the autophagic cargo clearance might be impeded is defective lysosomal degradation capacity (Festa et al, 2018). To investigate whether the defective autophagy clearance observed in *Cy/+* kidneys is due to impaired lysosomal function, *Cy/+* and +/+ rats were injected with Cy5 tagged lactoglobulin, a LMW protein typically reabsorbed and processed along the endolysosomal pathway in PT cells (Fig. 4A). At 15 min, the lactoglobulin uptake by PT cells was strongly reduced in Cy/+ compared to +/+ kidneys. At 120 min, the lactoglobulin signal was strongly reduced in +/+ kidneys compared to 15 min, indicative of efficient lysosomal degradation. In contrast, Cy/+ animals showed a significant *increase* of lactoglobulin vesicles at 120 min compared to 15 min, suggesting a profound defect in the lysosomal degradation of the tracer. The defective lysosomal activity in Cy/+ derived rPTCs was further evidenced by: (i) a striking decrease in the mature form of the lysosomal hydrolase cathepsin-D (CtsD) in presence or absence of BfnA1 (Fig. 4B); (ii) a 80% decrease in lysosomal degradation activity using Bodipy-FL PepstatinA (PepA), a fluorescent probe which specifically binds mature CtsD in acidic lysosomes (Fig. 4C); and (iii) a major reduction in the signal intensity following incubation of rPTCs with Magic-Red (MR), a substrate which fluoresces upon cleavage by the lysosomal cathepsin-B (Fig. 4C). It should be noted that Cy/+ animals presented a strong increase in the urinary excretion of CtsD, which is normally endocytosed through megalin (Nielsen et al, 2007), contributing to the lysosomal dysfunction in Cy/+ PT (data not shown).

We next investigated whether established models of primary lysosomal dysfunction are also associated with a ciliary defect. We first used a model of acquired lysosomal dysfunction caused by the abnormal accumulation of specific □ light chains (□LCs) in lysosomes (Luciani et al, 2016). Mouse primary PT cells (mPTCs) cultured for 24 h with pathogenic □LCs (κCH) showed

a significant increase of ciliary length compared to mPTCs cultured with control □LCs (κCHm) that do not cause lysosomal dysfunction (Fig. 4D). The increased cilia length was associated with increased expression of IFT20 and p62 (Fig. 4E). Similar changes were observed in a *Ctns* knock-out mouse model of nephropathic cystinosis, a lysosomal storage disease that is characterized by a lysosomal accumulation of cystine leading to defective endocytosis (Raggi et al, 2014). The cilia length and IFT20 expression level were increased in PT cells of the $Ctns^{-/-}$ compared to wild-type kidneys, as shown by immunofluorescence staining (Fig. 4F).

We assessed the primary cilia length in $Clcn5^{Y/-}$ mouse model, a faithful model of Dent disease which exhibits a severe impairment of the endocytic activity and lysosomal processing (Christensen et al, 2003; Wang et al, 2000)) (Fig. 5B). The primary cilia length was significantly increased in AQP1 positive PTs kidney and mPTCs derived from $Clcn5^{Y/-}$ (Fig. 5A-B). These changes were associated with a decreased expression of megalin and an increase of IFT20 as well as an impairment of the autophagic process shown by the increase of p62 levels (Fig. 5C). These data suggests that the integrity of endo-lysosomal compartment is fundamental to regulate the ciliogenesis.

Taken together, these data demonstrate that congenital or acquired lysosomal dysfunction causing defective autophagic clearance of IFT20 leads to defective ciliogenesis.

Autophagy regulates the primary cilia and the endocytosis activity

To substantiate the link between autophagy, primary cilia and endocytosis, we investigated the effect of starvation-induced autophagy on these parameters in mPTCs (Fig. 6A-B). Serum starvation induced a progressive increase in the primary cilia length contrasting with a progressive decrease of albumin (Al647-BSA) uptake (Fig. 6A), paralleled by a decreased in megalin protein levels (Fig. 6B) culminating after 4 to 8h of starvation.

In a reverse experiment, we tested whether autophagy dysfunction alone was sufficient to disrupt the primary cilium morphology by using the *Atg7*$^{fl/fl}$ inducible mouse model (Komatsu et al, 2005). The increase of p62 and the near absence of LC3-II and ATG7 in *Atg7*$^{fl/fl}$ derived mPTCs upon transduction with a Cre-expressing adenovirus confirmed a major autophagic dysfunction in this model (Fig. 6C). In absence of ATG7, mPTCs displayed significant increase of ciliary length associated to an increase of IFT20 and a decrease of albumin uptake (Fig. 6D).

These data confirmed that autophagy regulates the primary cilium and endocytosis activity in PT cells.

Ksp-Cre;Pkd1*$^{del2–11,lox}$ *mouse model recapitulates defective autophagy and endocytosis

To determine whether the defective autophagy and endocytosis observed in Han:SPRD Cy/+ rats is common to PKD and ciliopathies, we investigated the *Ksp-Cre;*Pkd1$^{del2–11,lox}$ orthologous mouse model which is generated by kidney-specific tamoxifen-induced deletion of *Pkd1* and a late disease onset when mice are injected at post-natal day 40 (Lantinga-van Leeuwen et al, 2006). When analyzing urinary markers of PT function, 8-week old *Pkd1*$^{del2–11,lox}$ exhibited a significantly increased excretion of the LMW proteins CC16 and transferrin – in absence of renal failure (Table 2, Fig. 7A-B).

Investigation of the endocytic machinery in mPTCs derived from *Pkd1*$^{del2–11,lox}$ kidneys showed a sizeable and specific reduction of megalin compared to controls, without general dysfunction of the endocytic machinery as shown by comparable levels of Rab5 and Rab7 (Fig. 7C), and an increased proliferation of PT cells as shown by PCNA immunostaining (Fig. 7D). The defective endocytosis was confirmed by a 60% reduction of the alexa488-albumin uptake in mPTCs derived from *Pkd1*$^{del2–11,lox}$ kidneys compared to the controls (Fig. 7E). The defective endocytosis was paralleled by a significant increase of the primary cilia length (Fig. 7F) and of the IFT20

expression (Fig. 7D) in mPTCs derived from Pkd1$^{del2–11,lox}$ kidneys. Autophagy process was impaired as shown by the increase of p62 and LC3 in PT of *Pkd1* deficient kidneys compared to the controls by immunostaining (Fig. 7G).

Early manifestations of defective endocytosis and ciliogenesis in ADPKD patients

Finally, we assessed the clinical relevance of our findings by measuring urinary markers of PT dysfunction in ADPKD patients with a normal kidney function, compared to healthy volunteers. 16 ADPKD patients displayed an increase of microalbuminuria (Fig. 8A) as well as an increased urinary excretion of the LMW proteins transferrin and DBP (Fig. 8B). Studies on 5 kidney samples revealed that a marked increase in the ciliary length in the proximal tubule segments (AQP1-positive) in ADPKD compared to control kidneys (Fig. 8C) associated with a decrease of megalin expression (Fig. 8D). These data demonstrate that some ADPKD patients shows manifestations of PT dysfunction associated with morphological alteration of the primary cilium.

DISCUSSION

The interplay between receptor-meditated endocytosis, endolysosomal processing and autophagy is critical for the capacity of PT cells to handle essential nutrients. A potential link between the primary cilium and flow-mediated regulation of endocytosis has been suggested by *in vitro* studies, but the underlying mechanisms as well as the relevance for ciliopathies or endolysosomal diseases remain unclear. Here, we used *in vivo* and *in vitro* approaches on various disease models to decipher the interplay between ciliogenesis, endocytosis, lysosomal function and autophagy in kidney PT cells taken as paradigm of specialized epithelial lineage. We show that genetic and pharmacologically-induced alterations of the primary cilium are associated with defective flow sensing and a selective defect in receptor-mediated endocytosis, causing lysosomal dysfunction, impaired autophagic degradation of IFT20, and further damage in the primary cilia and defect in endocytosis. This chain of events was recapitulated with models targeting endocytosis (*Clcn5* KO mice, dynasore), lysosomal function (*Ctns* KO mice, light chains, bafilomycin A1) and autophagy (*Atg7* KO, fasting). Defective receptor-mediated endocytosis and ciliogenesis was also verified in a cohort of patients with ADPKD.

The primary cilium has been extensively characterized for its ability to transduce external stimuli in intracellular responses (Pazour & Witman, 2003). In normal kidney tubules, primary cilia are thought to sense the luminal flow of urine and allow a rapid influx of calcium ions into the cells, which then controls multiple cellular processes (Nauli et al, 2003). Recent studies conducted on immortalized PT cells (OK, LLCPK) demonstrated that increased fluid shear stress (FSS) induces a rapid and sustained increase in both receptor-mediated (e.g. albumin uptake) and fluid-phase (e.g. dextran uptake) endocytosis, paralleled by an increase in intracellular Ca^{2+} $[Ca^{2+}]_i$, and a release of extracellular ATP that required the presence of primary cilia (Raghavan et al, 2014). The involvement of primary cilia in the endocytic response to FSS in PT cells raised

the possibility that genetic defects in ciliogenesis could impair the regulation of apical endocytosis (Raghavan & Weisz, 2016).

Our investigations substantiate the defect in receptor-mediated endocytosis in the Han:SPRD Cy/+ rat and in the *Pkd1* inducible KO mouse, two models of autosomal dominant polycystic kidney disease (ADPKD), the most common inherited ciliopathy and by far the most common genetic cause of chronic kidney disease. The inbred Cy/+ rat strain resembles human ADPKD, with slow progression of cystic disease and renal failure. The kidney cysts are caused by missense mutations in ANKS6 (also named SamCystin) – a protein localized in PT cells, explaining why cysts predominantly originate from the PT in this model (Brown et al, 2005). Recessive mutations in *ANKS6* have been identified in families with nephronophthisis, with ANKS6 playing a crucial role in an interacting module linking NEK8 to INVS and NPHP3 in the Inv compartment at the proximal part of the body of the cilium (Hoff et al, 2013; Nakajima et al, 2018). The vast majority (about 85%) of individuals with ADPKD carry mutations in *PKD1* encoding polycystin-1 (Ong, 2017). Polycystin-1 is a membrane protein localized in the ciliary membrane, where it is involved in cell signalling (Pazour & Witman, 2003). The disruption of *Pkd1* after post-natal day 12 in mouse results in a slow cystogenesis process, reflecting a state of differentiation and corresponding to the human disease (Piontek et al, 2007).

Of note, the defect in receptor-mediated endocytosis is observed at an early stage of disease - before any renal failure in these models.

The results were confirmed in ADPKD patients (*PKD1* mutation) who exhibit a loss of several LMWPs typically reabsorbed by the PT, in the early stage of disease and with normal renal function (eGFR < 90 $ml.min^{-1}$), together with increased primary cilia length on PT cells.

The changes in primary cilia and receptor-mediated endocytosis observed *in vivo* were recapitulated in primary cultured PT cells obtained from the Han:SPRD rat (rPTC) and *Pkd1* mouse (mPTC) models. These cells, which keep their differentiation and polarized transport processes, provide a particularly well suited model to investigate receptor-mediated endocytosis of apical ligands and their lysosomal processing (Festa et al, 2018; Raggi et al, 2014; Terryn et al, 2007). Our studies reveal that the primary ciliopathies induced a selective defect in RME (monitored by albumin uptake), observed both in static and flow conditions, and a consistent loss of megalin. Similar loss of megalin and decreased albumin uptake were observed upon exposure of mPTC to cytochalasin D which promotes cilia elongation and to NH_4SO_4 which deciliates mPTCs. The consistent loss of megalin, associated with increased cell proliferation, suggest an early loss of differentiation of the tubular cells - similar to what has been observed in endolysosomal disorders such as cystinosis (Festa et al, 2018) and light chain-associated tubulopathy (Luciani et al, 2016).

The robust increase in ciliary length associated with the endocytic defects in the Han:SPRD rat and *Pkd1* mouse *in vivo* and *in vitro* was associated with a specific increase in the expression of IFT20, a critical component that regulates ciliogenesis through continuous and bidirectional intraflagellar trafficking (Follit et al, 2006). Functioning of the primary cilium has been recently connected to autophagy, a pathway for degradation of cellular components in lysosomes. Autophagy regulates the length of the cilia by modulating the load of essential proteins required for ciliogenesis, a phenomenon that is molecularly different performed by basal autophagy or when autophagy is induced in response to various stressors (Pampliega & Cuervo, 2016). Interestingly, basal autophagy–a homeostatic pathway which occurs in kidney epithelial cells under normal nutrient conditions– prevents ciliogenesis by sparing OFD1 (Tang et al, 2013) and digesting IFT20 (Pampliega et al, 2013), the latter being essential for both cilium formation

and length regulation. This “double lock” hints at the importance of proper cilia regulation for cell homeostasis and functions. In line with this model, our data indicate that an abnormal accumulation of IFT20 leads to increased ciliogenesis and primary cilia elongation in rat and mouse cell–based models and, notably, in kidney epithelial cells of patients with ADPKD. The correction of primary cilia length defects by loss–of–function interventions targeting IFT20 rescue epithelial differentiation and reabsorptive capacity in Cy+ kidney epithelial cells, substantiating the essential role of primary cilia homeostasis in safeguarding epithelial phenotype in specialized cells.

As target–of–rapamycin complex1 (mTORC1) signaling has been associated with ciliary size and function, we reasoned that an upregulation of proteins that are critical for ciliogenesis and cilia elongation, such as intraflagellar proteins and tubulin, might be responsible for cilia elongation in response to mTORC1 activation (Yuan et al, 2012). However, the IFT20 accumulation is still detectable in Cy+ cells under conditions in which mTOR is either silent or fully active, suggesting that the ciliary length defects are not dependent on mTORC1 activation or inactivation. Combined the accumulation of ciliary protein IFT20 and the fact that basal autophagy maintains cilia length and homeostasis by removing IFT20, these findings prompted us to examine the potential involvement of autophagy in the dysregulation of ciliogenesis and primary cilia formation. Consistent with our hypothesis, we observed that genetic blockage of basal autophagy (e.g. *Atg7* knockdown) results in accumulation of IFT20, leading to elongation of primary cilium and epithelial dedifferentiation - dysfunction as reflected by decreased endocytotic uptake capacity. These results demonstrate the importance of quality-control mechanism in maintaining primary cilia length and formation.

Similar to the changes observed in autophagy—deficient cells, there was a remarkable accumulation in *Cy+* kidney epithelial cells of p62–and ubiquitin–forming aggregates, with

ciliary protein IFT20 accumulating within autophagosomes. The accumulation of the autophagy substrate p62, which is normally degraded within autolysosomes, suggests an abnormal autophagy flux in *Cy+* and *Pdk1* depleted cells. Evidence supporting the failure to degrade autophagy cargoes in primary PT *Ctns*$^{-/-}$ cells include: abnormally elevated numbers of mature autophagosomes under-normal growth conditions; failure to clear autophagic vesicles (AVs) formed after starvation-induced autophagy, mimicking BfnA1 action; inability of BfnA1 to further induce the LC3-II protein levels. Altogether, these data indicate that the alterations of ANKS6 and PC1, causing ciliary length and endocytosis defects, delays the autophagy flux, leading to an accumulation of autophagosomes *in vitro* and *in vivo*.

The question remained how ANKS6 and PC1 impairment could impair autophagy flux and lead to defective removal of IFT20 and ciliary length defects. We postulated that defects in ANKS6 and PC1 may affect lysosome function either by controlling the delivery of newly synthesized lysosomal cathepsins from Golgi to the lysosome or by inhibiting the processing/maturation of cathepsins within endolysosome compartment. Our results support the latter hypothesis, evidencing an impairment of lysosome proteolysis (observed both *in vitro* and *in vivo*) as a result of defective cathepsin activation despite an efficient delivery of newly synthesized cathepsins from Golgi to lysosomes. Therefore, lack of autophagy completion, due to impaired lysosomal degradation capacity or through inactivation of essential genes, leads to defective clearance of ciliary proteins, leading to IFT20 accumulation which ultimately causes primary cilia length defects.

The conjugation of impaired autophagy and altered lysosomal degradative capacity is strikingly similar to the cellular changes resulting from the accumulation of monoclonal light chains (κLCs) or cystine within endolysosomes of PT cells, causing a similar epithelial

dysfunction (Festa et al, 2018; Luciani et al, 2016). Furthermore, dysfunction of endosomal pathway that results from the loss–of–function of *Clcn5*, leads to defective autophagy–mediated removal of IFT20 in lysosomes, recapitulating IFT20 accumulation and cilia elongation in kidney epithelial cells from a mouse model of Dent disease– congenital disorder causing defective receptor–mediated endocytosis and PT dysfunction. These data suggest that dysfunctional endosomal—lysosomal pathways due to congenital (Dent disease or cystinosis) or acquired (light chain disease) disorders might have similar functional consequences on epithelial phenotype, emphasizing the role of primary cilia as a crucial signaling hub to ensure cellular function and homeostasis.

These findings have a clinical relevance for biomarkers in early ADPKD. Cystogenesis in ADPKD primarily involves dedifferentiation of kidney tubular cells, with enhanced proliferation, abnormal fluid secretion and defective planar cell polarity, promoting cyst development and growth (Ong, 2017). This chain of events involves all tubular segments, including the proximal tubule (Devuyst et al, 1996; Terryn et al, 2011; Verani & Silva, 1988). Our findings substantiate evidence pointing to increased urinary excretion of PT marker damage including β2-microglobulin and β-hexosaminidase in the early phase of ADPKD (Casal et al, 2005; Meijer et al, 2010; Swedenborg et al, 1981; (Messchendorp, Meijer et al. 2018). Furthermore, *Pkd1*-null embryos exhibit an abnormal expression of megalin in PT cells and an inappropriate loss of LMW proteins in the amniotic fluid (Ahrabi et al, 2010). Altogether, these data suggest a specific and early PT defect in ADPKD.

In conclusion, our findings support a fundamental novel role of the cilia in the endocytic process These results open perspectives for autophagy-lysosomal targeted interventions to correct PT dysfunctions in PKD.

MATERIAL AND METHODS

Patient. Human kidney biopsies and urinary samples were obtained from archived samples of 19 patients with clinical diagnosis of ADPKD and a glomerular filtration rate (GFR) above 90 $ml.min^{-1}$. The use of the human samples was approved by the Ethical Review Board of the Université catholique de Louvain Medical School (Brussels, Belgium).

Animals. The experiments were performed on several animal models: male Han:SPRD heterozygous Cy/+ rats (5-9 weeks-old) *Ksp-Cre;Pkd1*$^{del2–11,lox}$ mouse (8 weeks-old), female *Ctns*$^{-/-}$ mouse (20 weeks-old), male *Clcn5*$^{Y/-}$ (8weeks-old), male *Atg7*$^{fl/fl}$ mouse(8-12 weeks-old) and C57bl/6 mouse (8 weeks-old). Age and gender-matched littermates were used as controls. All procedures were performed in accordance with the National Institutes of Health guidelines for the care and use of laboratory animals and with the approval of the Committee of the University of Zürich (Zürich, Switzerland).

Renal function parameters. The animals were trained once and kept in metabolic cages overnight. The urine was collected on ice and the diuresis was measured. After euthanasia, blood samples were obtained from the vena cava and collected in heparin coated tubes (Sarstedt, Nümbrecht, Germany). Urine and plasma parameters were analyzed using the UniCel® DxC 800 Synchron® Clinical system. Urinary LMWP were measured by western blot whereas Clara cell protein (CC16) concentrations were determined an enzyme-linked immunosorbent assay kit (Biomatik EKU03200, Wilmington, DE, USA) (Festa et al, 2018; Luciani et al, 2016).

Histological studies. After euthanasia, the kidneys were rapidly excised, rinsed in 0.1M phosphate buffer saline (PBS) solution (Thermo Fischer Scientific, MA, USA), fixed in 4% paraformaldehyde in PBS for 6 h and embedded in paraffin at 58 C°. Paraffin blocks were sectioned into consecutive 5 μm-thick slices with a Leica RM2255 rotary microtome (Thermo Fisher Scientific) on Superfrost Plus glass slides (Thermo Fisher Scientific). The sections were subsequently deparaffinized with Xylene and rehydrated with a descending ethanol percentage. Antigen retrieval was performed using the heat-induced epitope retrieval methods by incubating the slides in sodium citrate buffer (1.8% 0.1 M citric acid, 8.2% 0.1 M sodium citrate, in distillated water, pH 6.0) at 95 C° for 30 min. The slides were subsequently processed for immunofluorescence staining and confocal microscopy. (Festa et al, 2018; Luciani et al, 2016)

Primary culture. After excision, the rat or mouse kidneys were dissected in a 4°C dissection solution (DS) (HBSS with in mmol/l: 10 glucose, 5 glycine, 1 alanine, 15 HEPES, pH 7.4 and osmolality 325 mosmol/kgH_2O) which allow the separation in medullar and cortical fragments. The medullar fragments were discarded while the cortical pieces were subsequently incubated in a collagenase solution (DS with 0.1% (wt/vol) type-2 collagenase and 96 μg/ml soybean trypsin inhibitor) for 30 min at 37°C. After the incubation period, the supernatant was filtered using 250 μm and 80 μm pore size nylon sieves. The proximal tubules (PTs) were then collected on the 80 μm nylon sieve in 37°C DS and centrifuged 5 min at 300g. Finally the PTs were resuspended in the culture medium 1:1 DMEM/F12 without phenol red and supplemented with heat-inactivated FCS 1%, HEPES 15 mmol/l, L-glutamine 2 mmol/l, hydrocortisone 50 nmol/l, insulin 5 μg/ml, transferrin 5 μg/ml, selenium 50 nmol/l, sodium pyruvate 0.55 mmol/l, 100× nonessential amino acids 10 ml/l, penicillin 100 IU/ml and streptomycin 100 μg/ml buffered to pH 7.4 and osmolality of 325 mosmol/kgH_2O and seeded on the appropriate support. (Festa et al, 2018; Luciani et al, 2016)

Endocytosis assay: The endocytic uptake was monitored in mPTCs cells following incubation for 15 min at 37 °C with 100 μg ml^{-1} bovine serum albumin (BSA)–Alexa-Fluor-647 (A34785, Thermo Fisher Scientific) or with 100 μg ml^{-1} BSA–Alexa-Fluor-488 (A13100, Thermo Fisher Scientific) in complete HEPES-buffered Dulbecco's modified Eagle's medium. The cells were given an acid wash, fixed and processed for immunofluorescence analyses (Luciani et al, 2016).

Adenovirus transduction in primary PT cells: For RNA interference studies, the adenovirus constructs include scrambled short hairpin or shRNAs encoding individually rat *Ift20* or encoding mouse *Atg7*. For expression studies, adenovirus constructs include cytomegalovirus (Null) or particles individually carrying mouse GFP-tagged-*Map1lc3b*. The abovementioned adenovirus constructs were purchased from Vector Biolabs (University City Science Center, Philadelphia, USA). The primary mouse or rat PT cells were plated onto collagen-coated chamber slides or 24-well or 6-well tissue culture plates. Adenovirus transduction was performed 24 h after plating when the cells reached ~ 70–80% confluence. The cells were subsequently incubated for 16 h at 37 °C with culture medium containing the virus at the concentration (0.2125×109 PFU ml^{-1}). The cells were afterwards challenged with fresh medium every 2 days, cultured for 5 days (unless otherwise specified), and collected for analyses.

Quantitative real-time PCR: Total RNA was extracted from mouse and rat kidney tissues using Aurum Total RNA Fatty and Fibrous Tissue Kit (Bio-Rad, Hercules, CA). DNAse I treatment was performed to eliminate genomic DNA contamination. Total RNA was extracted from primary cell cultures with RNAqueous kit (Applied Biosystems, Life Technologies). One microgram of RNA was used to perform the reverse transcriptase reaction with iScript cDNA Synthesis Kit (Bio-Rad). Changes in mRNA levels of the target genes were determined by relative reverse transcriptase-quantitative PCR with a CFX96 Real-Time PCR Detection System (Bio-Rad) using iQ SYBR Green Supermix (Bio-Rad). The analyses were performed in duplicate with 100 nM of both sense and anti-sense primers in a final volume of 20 µl using iQ SYBR Green Supermix (Bio-Rad). Specific primers were designed using Primer3. PCR conditions were 95 °C for 3 min followed by 40 cycles of 15 s at 95 °C, 30 s at 60 °C. The PCR products were sequenced with the BigDye terminator kit (Perkin Elmer Applied Biosystems) using ABI3100 capillary sequencer (Perkin Elmer Applied Biosystems). The efficiency of each set of primers was determined by dilution curves. The program geNorm version 3.4 was applied to characterize the expression stability of the candidate reference genes in kidneys and six reference genes were selected to calculate the normalization factor (Vandesompele et al, 2002). The relative changes in targeted genes over Gapdh mRNAs were calculated using the $2^{-\Delta\Delta Ct}$ formula.

Lysosomal activity: The detection of lysosomal activity was performed in live rPTCs using Bodipy-FL-PepA (P12271, Thermo Fischer Scientific) or Magic Red-$(RR)_2$ substrate (MR-CtsB; 938, Immunochemistry Technologies) according to the manufacturer's specifications. The cells were pulsed with 1 µM Bodipy-FL-Pepstatin A or with 1 µM Magic Red-$(RR)_2$ in Live Cell Imaging (A14291DJ, Thermo Fischer Scientific) medium for 1 h at 37 °C followed by fixation and subsequently analyzed by confocal microscopy (Luciani et al, 2016).

Human κLCs: Human LC genes were isolated and transfected in the hybridoma cell line SP2/0 as previously described (Luciani et al, 2016). Briefly the human LCs were produced by the SP2/0 cell line, a B cell hybridoma lacking endogenous Ig and constitutively overexpressing human LCs from patients with biopsy-proven renal Fanconi syndrome (κCH). For control, a mutant version of κCH (κCHm) was generated with Ala30→Ser which causes in a low aggregation rendering κCHm non-pathogenic. For the uptake of all human κLCs, primary mPTCs were plated in culture medium, briefly rinsed, and then cultured for 4h in serum-free, HEPES-buffered DMEM/F12. The cells were then incubated with 25µg/mL of human κLCs in serum-free,

HEPES-buffered DMEM/F12 for 60 min at 4°C and chased in κLCs-free, complete medium for the indicated times at 37°C, before being processed for western blotting or immunofluorescence analyses. Each incubation was dome using a different, non-pooled monoclonal κLC.

Electron microscopy. Confluent rat proximal tubule cell monolayers were fixed with 2.5% glutaraldehyde in 0.1 M cacodylate buffer and embedded in LR-White resin (LADD Research Industries). The grids were viewed on a Philips CM100 transmission electron microscope at 80 kV. Autophagic vacuoles were identified and categorized as autophagosomes or autophagolysosomes according to standard criteria (Klionsky et al, 2012). The term autophagic vacuole was used when the differentiation between autophagosome and autophagolysosomes was not possible.

Immunofluorescence and Confocal Microscopy. Five-µm kidney sections were quenched with 50 mM NH_4Cl, blocked with 3% BSA in PBS Ca/Mg (D1283; Sigma-Aldrich) for 30 min and stained with primary antibodies diluted in blocking buffer overnight at 4°C. After two washes in 0.1% Saponin (Sigma-Aldrich) (w/v in PBS), the slides were incubated with corresponding fluorophore-conjugated secondary antibodies (Invitrogen, Thermo Fischer Scientific) diluted in blocking buffer at room temperature for 1 hour and counterstained with DAPI (D1306; Thermo Fischer Scientific). The slides were subsequently mounted in Prolong Gold Anti-fade reagent (P36930; Thermo Fisher Scientific). The slides were acquired on CLSM SP8 upright Leica confocal laser scanning microscope equipped with either a HCX PL APO Leica 40X NA 1.4 oil immersion objective or a Leica APO 63x NA 1.4 oil immersion objective at a definition of 1024x1024 pixels. After acquisition, the images were processed with Adobe Photoshop (version CS5, Adobe System Inc.) software. Quantitative image analysis was performed by selecting randomly 10 - 20 visual fields per each slide that included at least 4-10 PT sections, using the same setting parameters (i.e. pinhole, laser power, and offset gain and detector amplification below pixel saturation). Quantification was performed using the open-source cell image analysis software CellProfiler (Carpenter et al, 2006).

The cells on chambers slides were fixed for 10 min in 4% paraformaldehyde (Sigma-Aldrich,) in PBS, permeabilized and quenched with 50 mM NH_4Cl for 30 min in blocking buffer (50 mM NH4Cl, 0.1% (w/v) saponin, 3% (w/v) BSA in PBS). The cells were then incubated 2 h with the desired primary antibody, washed six times in PBS, incubated for 1 h with the Alexa-labelled

secondary antibody and mounted on Vectashield covered coverslips (Vector Laboratories, Burlingame, CA, USA) using Prolong Gold Anti-fade reagent (P36930, Thermo Fisher Scientific). Quantitative image analysis was performed by selecting randomly five visual fields pooled from biological triplicates, with each field including at least 20–25 cells, using the same setting parameters (i.e., pinhole, laser power, and offset gain and detector amplification below pixel saturation).

Primary cilia measurement. Z-stack images were acquired with Leica APO 63x NA 1.4 oil immersion objective with the lower and the upper limit of the stack comprise all the focal planes with acetylated-tubulin staining. After the Z-stack acquisition, a maximum projection image was generated and the ciliary length was measured using ImageJ/Fiji (https://imagej.nih.gov/ij/). In primary cell culture, at least 50 cilia per experimental conditions were measured before any statistical analyses. (Satir & Pampliega, 2016)

Flow stimulation. Differentiated proximal tubular cell monolayers were exposed to orbital motion by placing 6-well plates on top of a shaker table in a standard laboratory incubator set at 37 °C with a frequency of 1Hz for various amount of time. After the stimulation period, cells were either processed for western blotting of subjected to an uptake assay and further processed for immunofluorescence. (Kolb et al, 2004)

Antibodies. Unless specify otherwise, all the antibody were used at a 1:500 dilution for immunoblotting and western blot. The following antibodies were used in this study: mouse anti-rat PCNA (Dako, Glostrup, Denmark), rabbit anti-human DBP (Dako), rabbit anti-human TF (Dako), rabbit anti-Uteroglobulin (Abcam, Cambridge, UK), mouse anti-β-actin (Sigma, St. Louis, USA), rabbit anti-human AQP1 (Millipore, Billerica, USA), rabbit anti-AQP2 (Sigma) rabbit anti-Rab5 (Abcam), rabbit anti-Rab7 (Abcam), rabbit anti-SGLT2 (Abcam), rabbit anti-IFT20 (proteintech, Manchester, UK), rabbit anti-IFT88 (proteintech), mouse anti-acetylated tubulin (Abcam), mouse anti-ubiquitin (Santa Cruz Biotechnology, Texas, USA), goat anti-cathepsin-D (Santa Cruz Biotechnology), rabbit anti-ATG7 (Santa Cruz Biotechnology), rabbit anti-p62 (MBL internationlal, Woburn, MA, USA), rabbit anti-LC3 (MBL international), mouse anti-human Ki-67 (Dako). Sheep anti-megalin was kindly provided by Prof. Verroust, INSERM, Paris, France and rabbit anti-NaPi-IIa by CA Wagner, University of Zürich.

Immunoblotting. Proteins were extracted from frozen kidneys or primary PT cell cultures lysed in RIPA buffer (Sigma Life Technologies) containing protease and phosphatase inhibitors (Roche Diagnostics, Mannheim, Germany), followed by a brief sonication and centrifugation at 16'000xg for 1min at 4°C. Protein concentration was determined using the Pierce BCA protein assay (Pierce Thermo Fischer Scientific). Samples normalized and diluted in Laemmli sample buffer (Bio-Rad) containing Dithiothreitol (DTT, PanReac AppliChem, Barcelona, Spain), and proteins were separated by SDS-PAGE and subsequently blotted onto polyvinylidene difluoride membranes. Membranes were blocked for 30 min in 5% non-fat dry milk (1706404, Bio-Rad Laboratories) solution at room temperature, followed by overnight incubation of primary antibodies at 4°C. Blots were washed and incubated with peroxidase-conjugated secondary antibodies for 1h, washed again and incubated with chemiluminescent HRP substrate (Merck, Darmstadt, Germany). Immunoblots were quantified by densitometry using ImageJ software.

Immunoprecipitation: The cells were lysed in a buffer containing 25 mM Tris/HCl adjusted to pH 7.4, 150 mM NaCl, 1% NP-40, and 1 mM EDTA, 5% glycerol, protease and phosphatase inhibitors for 10 min at 4 °C. Lysates were centrifuged at 12,000 G. for 10 min and the supernatants were incubated with 1.5 µg of primary anti-megalin antibody for 16 h at 4 °C. After addition of 50 µl of protein G sepharose beads (P9424, Sigma), lysates were incubated at 4 °C for 12 h with gentle shaking. Agarose beads were washed for three times and then collected through centrifugation at 12,000 G. for 1 min. Beads were reduced by the addition of 35 µl of Laemmli sample buffer, heated at 95 °C for 5 min, and resolved on 10% SDS-polyacrylamide gel electrophoresis (PAGE) gel, and analyzed by western blotting.

Data analyses and Statistics. The quantitative data were expressed as means ± SEM. Differences between experimental groups were evaluated using one-way analysis of variance followed by Bonferroni or Dunnet's post hoc test, when appropriate. When only two groups were compared, unpaired or paired two-tailed Student's t-tests were used as appropriate. No statistical methods were used to predetermine the sample size. We estimated the sample size considering the variation and mean of the samples. Assumptions for statistical analyses were met (that is, normal distribution and equal variance). The sample size (number of cells or number of biological replicates derived from distinct mice or rats) of each experimental group is described in figure legends. The results are representative of at least three independent experiments, unless specified in the figure legends. None of the samples/animals was excluded from the experiment, and the

animals were not randomized. The investigators were not blinded to allocation during the experiments and outcome assessment. GraphPad Prism software was used for all statistical analyses. Statistical differences were considered significant at a $P < 0.05$.

REFERENCES

Ahrabi, A. K., F. Jouret, E. Marbaix, C. Delporte, S. Horie, S. Mulroy, C. Boulter, R. Sandford and O. Devuyst (2010). "Glomerular and proximal tubule cysts as early manifestations of Pkd1 deletion." Nephrol Dial Transplant **25**(4): 1067-1078.

Brown, J. H., M. T. Bihoreau, S. Hoffmann, B. Kranzlin, I. Tychinskaya, N. Obermuller, D. Podlich, S. N. Boehn, P. J. Kaisaki, N. Megel, P. Danoy, R. R. Copley, J. Broxholme, R. Witzgall, M. Lathrop, N. Gretz and D. Gauguier (2005). "Missense mutation in sterile alpha motif of novel protein SamCystin is associated with polycystic kidney disease in (cy/+) rat." J Am Soc Nephrol **16**(12): 3517-3526.

Carpenter, A. E., T. R. Jones, M. R. Lamprecht, C. Clarke, I. H. Kang, O. Friman, D. A. Guertin, J. H. Chang, R. A. Lindquist, J. Moffat, P. Golland and D. M. Sabatini (2006). "CellProfiler: image analysis software for identifying and quantifying cell phenotypes." Genome Biol **7**(10): R100.

Casal, J. A., J. Hermida, X. M. Lens and J. C. Tutor (2005). "A comparative study of three kidney biomarker tests in autosomal-dominant polycystic kidney disease." Kidney Int **68**(3): 948-954.

Christensen, E. I. and H. Birn (2002). "Megalin and cubilin: multifunctional endocytic receptors." Nat Rev Mol Cell Biol **3**(4): 256-266.

Christensen, E. I., O. Devuyst, G. Dom, R. Nielsen, P. Van der Smissen, P. Verroust, M. Leruth, W. B. Guggino and P. J. Courtoy (2003). "Loss of chloride channel ClC-5 impairs endocytosis by defective trafficking of megalin and cubilin in kidney proximal tubules." Proc Natl Acad Sci U S A **100**(14): 8472-8477.

Coon, B. G., V. Hernandez, K. Madhivanan, D. Mukherjee, C. B. Hanna, I. Barinaga-Rementeria Ramirez, M. Lowe, P. L. Beales and R. C. Aguilar (2012). "The Lowe syndrome protein OCRL1 is involved in primary cilia assembly." Hum Mol Genet **21**(8): 1835-1847.

De Matteis, M. A., L. Staiano, F. Emma and O. Devuyst (2017). "The 5-phosphatase OCRL in Lowe syndrome and Dent disease 2." Nat Rev Nephrol **13**(8): 455-470.

Devuyst, O., C. R. Burrow, E. M. Schwiebert, W. B. Guggino and P. D. Wilson (1996). "Developmental regulation of CFTR expression during human nephrogenesis." Am J Physiol **271**(3 Pt 2): F723-735.

Devuyst, O., C. R. Burrow, B. L. Smith, P. Agre, M. A. Knepper and P. D. Wilson (1996). "Expression of aquaporins-1 and -2 during nephrogenesis and in autosomal dominant polycystic kidney disease." Am J Physiol **271**(1 Pt 2): F169-183.

Devuyst, O. and A. Luciani (2015). "Chloride transporters and receptor-mediated endocytosis in the renal proximal tubule." J Physiol **593**(18): 4151-4164.

Festa, B. P., Z. Chen, M. Berquez, H. Debaix, N. Tokonami, J. A. Prange, G. V. Hoek, C. Alessio, A. Raimondi, N. Nevo, R. H. Giles, O. Devuyst and A. Luciani (2018). "Impaired autophagy bridges lysosomal storage disease and epithelial dysfunction in the kidney." Nat Commun **9**(1): 161.

Follit, J. A., R. A. Tuft, K. E. Fogarty and G. J. Pazour (2006). "The intraflagellar transport protein IFT20 is associated with the Golgi complex and is required for cilia assembly." Mol Biol Cell **17**(9): 3781-3792.

Gerhardt, C., J. M. Lier, S. Burmuhl, A. Struchtrup, K. Deutschmann, M. Vetter, T. Leu, S. Reeg, T. Grune and U. Ruther (2015). "The transition zone protein Rpgrip1l regulates proteasomal activity at the primary cilium." J Cell Biol **210**(1): 115-133.

Hoff, S., J. Halbritter, D. Epting, et al., (2013). "ANKS6 is a central component of a nephronophthisis module linking NEK8 to INVS and NPHP3." Nat Genet **45**(8): 951-956.

Kaliszewski, M., A. B. Knott and E. Bossy-Wetzel (2015). "Primary cilia and autophagic dysfunction in Huntington's disease." Cell Death Differ **22**(9): 1413-1424.

Kimura, T., Y. Takabatake, A. Takahashi, J. Y. Kaimori, I. Matsui, T. Namba, H. Kitamura, F. Niimura, T. Matsusaka, T. Soga, H. Rakugi and Y. Isaka (2011). "Autophagy protects the proximal tubule from degeneration and acute ischemic injury." J Am Soc Nephrol **22**(5): 902-913.

Klionsky, D. J., F. C. Abdalla, H. Abeliovich, et al., (2012). "Guidelines for the use and interpretation of assays for monitoring autophagy." Autophagy **8**(4): 445-544.

Kolb, R. J., P. G. Woost and U. Hopfer (2004). "Membrane trafficking of angiotensin receptor type-1 and mechanochemical signal transduction in proximal tubule cells." Hypertension **44**(3): 352-359.

Komatsu, M., S. Waguri, T. Ueno, J. Iwata, S. Murata, I. Tanida, J. Ezaki, N. Mizushima, Y. Ohsumi, Y. Uchiyama, E. Kominami, K. Tanaka and T. Chiba (2005). "Impairment of starvation-induced and constitutive autophagy in Atg7-deficient mice." J Cell Biol **169**(3): 425-434.

Lantinga-van Leeuwen, I. S., W. N. Leonhard, A. van de Wal, M. H. Breuning, S. Verbeek, E. de Heer and D. J. Peters (2006). "Transgenic mice expressing tamoxifen-inducible Cre for somatic gene modification in renal epithelial cells." Genesis **44**(5): 225-232.

Lee, J., S. Yi, Y. E. Kang, J. Y. Chang, J. T. Kim, H. J. Sul, J. O. Kim, J. M. Kim, J. Kim, A. M. Porcelli, K. S. Kim and M. Shong (2016). "Defective ciliogenesis in thyroid hurthle cell tumors is associated with increased autophagy." Oncotarget **7**(48): 79117-79130.

Liu, Y. P., I. C. Tsai, M. Morleo, E. C. Oh, C. C. Leitch, F. Massa, B. H. Lee, D. S. Parker, D. Finley, N. A. Zaghloul, B. Franco and N. Katsanis (2014). "Ciliopathy proteins regulate paracrine signaling by modulating proteasomal degradation of mediators." J Clin Invest **124**(5): 2059-2070.

Long, K. R., K. E. Shipman, Y. Rbaibi, E. V. Menshikova, V. B. Ritov, M. L. Eshbach, Y. Jiang, E. K. Jackson, C. J. Baty and O. A. Weisz (2017). "Proximal tubule apical endocytosis is modulated by fluid shear stress via an mTOR-dependent pathway." Mol Biol Cell **28**(19): 2508-2517.

Luciani, A., C. Sirac, S. Terryn, V. Javaugue, J. A. Prange, S. Bender, A. Bonaud, M. Cogne, P. Aucouturier, P. Ronco, F. Bridoux and O. Devuyst (2016). "Impaired Lysosomal Function Underlies Monoclonal Light Chain-Associated Renal Fanconi Syndrome." J Am Soc Nephrol **27**(7): 2049-2061.

Luo, N., C. C. West, C. A. Murga-Zamalloa, L. Sun, R. M. Anderson, C. D. Wells, R. N. Weinreb, J. B. Travers, H. Khanna and Y. Sun (2012). "OCRL localizes to the primary cilium: a new role for cilia in Lowe syndrome." Hum Mol Genet **21**(15): 3333-3344.

Malicki, J. J. and C. A. Johnson (2017). "The Cilium: Cellular Antenna and Central Processing Unit." Trends Cell Biol **27**(2): 126-140.

Meijer, E., W. E. Boertien, F. L. Nauta, S. J. Bakker, W. van Oeveren, M. Rook, E. J. van der Jagt, H. van Goor, D. J. Peters, G. Navis, P. E. de Jong and R. T. Gansevoort (2010). "Association of urinary biomarkers with disease severity in patients with autosomal dominant polycystic kidney disease: a cross-sectional analysis." Am J Kidney Dis **56**(5): 883-895.

Nakajima, Y., H. Kiyonari, Y. Mukumoto and T. Yokoyama (2018). "The Inv compartment of renal cilia is an intraciliary signal activating center to phosphorylate ANKS6." Kidney Int.

Nauli, S. M., F. J. Alenghat, Y. Luo, E. Williams, P. Vassilev, X. Li, A. E. Elia, W. Lu, E. M. Brown, S. J. Quinn, D. E. Ingber and J. Zhou (2003). "Polycystins 1 and 2 mediate mechanosensation in the primary cilium of kidney cells." Nat Genet **33**(2): 129-137.

Oltrabella, F., G. Pietka, I. B. Ramirez, A. Mironov, T. Starborg, I. A. Drummond, K. A. Hinchliffe and M. Lowe (2015). "The Lowe syndrome protein OCRL1 is required for endocytosis in the zebrafish pronephric tubule." PLoS Genet **11**(4): e1005058.

Ong, A. C. M. (2017). "Making sense of polycystic kidney disease." Lancet **389**(10081): 1780-1782.

Pampliega, O. and A. M. Cuervo (2016). "Autophagy and primary cilia: dual interplay." Curr Opin Cell Biol **39**: 1-7.

Pampliega, O., I. Orhon, B. Patel, S. Sridhar, A. Diaz-Carretero, I. Beau, P. Codogno, B. H. Satir, P. Satir and A. M. Cuervo (2013). "Functional interaction between autophagy and ciliogenesis." Nature **502**(7470): 194-200.

Pazour, G. J. and G. B. Witman (2003). "The vertebrate primary cilium is a sensory organelle." Curr Opin Cell Biol **15**(1): 105-110.

Piontek, K., L. F. Menezes, M. A. Garcia-Gonzalez, D. L. Huso and G. G. Germino (2007). "A critical developmental switch defines the kinetics of kidney cyst formation after loss of Pkd1." Nat Med **13**(12): 1490-1495.

Raggi, C., A. Luciani, N. Nevo, C. Antignac, S. Terryn and O. Devuyst (2014). "Dedifferentiation and aberrations of the endolysosomal compartment characterize the early stage of nephropathic cystinosis." Hum Mol Genet **23**(9): 2266-2278.

Raghavan, V., Y. Rbaibi, N. M. Pastor-Soler, M. D. Carattino and O. A. Weisz (2014). "Shear stress-dependent regulation of apical endocytosis in renal proximal tubule cells mediated by primary cilia." Proc Natl Acad Sci U S A **111**(23): 8506-8511.

Raghavan, V. and O. A. Weisz (2016). "Discerning the role of mechanosensors in regulating proximal tubule function." Am J Physiol Renal Physiol **310**(1): F1-5.

Reiter, J. F. and M. R. Leroux (2017). "Genes and molecular pathways underpinning ciliopathies." Nat Rev Mol Cell Biol **18**(9): 533-547.

Satir, B. H. and O. Pampliega (2016). "Methods to Study Interactions Between Ciliogenesis and Autophagy." Methods Mol Biol **1454**: 53-67.

Schafer, K., N. Gretz, M. Bader, I. Oberbaumer, K. U. Eckardt, W. Kriz and S. Bachmann (1994). "Characterization of the Han:SPRD rat model for hereditary polycystic kidney disease." Kidney Int **46**(1): 134-152.

Settembre, C., A. Fraldi, D. L. Medina and A. Ballabio (2013). "Signals from the lysosome: a control centre for cellular clearance and energy metabolism." Nat Rev Mol Cell Biol **14**(5): 283-296.

Swedenborg, P., B. Hultberg and H. Thysell (1981). "Urinary beta-hexosaminidase excretion in polycystic kidney disease." Acta Med Scand **210**(6): 471-473.

Tang, Z., M. G. Lin, T. R. Stowe, S. Chen, M. Zhu, T. Stearns, B. Franco and Q. Zhong (2013). "Autophagy promotes primary ciliogenesis by removing OFD1 from centriolar satellites." Nature **502**(7470): 254-257.

Terryn, S., A. Ho, R. Beauwens and O. Devuyst (2011). "Fluid transport and cystogenesis in autosomal dominant polycystic kidney disease." Biochim Biophys Acta **1812**(10): 1314-1321.

Terryn, S., F. Jouret, F. Vandenabeele, I. Smolders, M. Moreels, O. Devuyst, P. Steels and E. Van Kerkhove (2007). "A primary culture of mouse proximal tubular cells, established on collagen-coated membranes." Am J Physiol Renal Physiol **293**(2): F476-485.

Vandesompele, J., K. De Preter, F. Pattyn, B. Poppe, N. Van Roy, A. De Paepe and F. Speleman (2002). "Accurate normalization of real-time quantitative RT-PCR data by geometric averaging of multiple internal control genes." Genome Biol **3**(7): RESEARCH0034.

Verani, R. R. and F. G. Silva (1988). "Histogenesis of the renal cysts in adult (autosomal dominant) polycystic kidney disease: a histochemical study." Mod Pathol **1**(6): 457-463.

Wang, S. S., O. Devuyst, P. J. Courtoy, X. T. Wang, H. Wang, Y. Wang, R. V. Thakker, S. Guggino and W. B. Guggino (2000). "Mice lacking renal chloride channel, CLC-5, are a model for Dent's disease, a nephrolithiasis disorder associated with defective receptor-mediated endocytosis." Hum Mol Genet **9**(20): 2937-2945.

Yuan, S., J. Li, D. R. Diener, M. A. Choma, J. L. Rosenbaum and Z. Sun (2012). "Target-of-rapamycin complex 1 (Torc1) signaling modulates cilia size and function through protein synthesis regulation." Proc Natl Acad Sci U S A **109**(6): 2021-2026.

ACKNOWLEDGEMENTS

We are grateful to Fonds National de la Recherche Scientifique and the Fonds de la Recherche Scientifique Médicale (Brussels, Belgium), the Cystinosis Research Foundation (Irvine, CA, USA), the Swiss National Science Foundation (project grant 31003A-169850), the clinical research priority program (KFSP) RADIZ (Rare Disease Initiative Zurich) of the UZH,the Swiss National Centre of Competence in Research (NCCR) Kidney Control of Homeostasis *(*Kidney.CH) for support and Junior Grant (to A.L.) and the People Program (Marie Curie Actions) of the European Union's Seventh Framework Program FP7/2077-2013 under Research Executive Agency Grant Agreement 317246. We acknowledge Huguette Debaix for providing technical assistance; Prof. Andrew Hall for fruitful discussions; CA Wagner, Pierre Verroust and Renata Kozyraki for providing reagents. Imaging was performed with equipment maintained by the Center for Microscopy and Image Analysis, University of Zurich.

Table 1: Clinical and biological parameters in the HAN:SPRD rats.

	5 weeks old		9 weeks old	
Parameter	+/+	Cy/+	+/+	Cy/+
Diuresis (µL/g BW/12 h)	17.1±0.9	32±8.9	22.9±3.5	35±5.3
U Albumin(µg/mg creatinine)	0.17±0.05	0.87±0.68	2.0±0.48	77.29±35.01*
U calcium (g/mg creatinine)	2.2±0.40	1.9±0.20	1.79±0.39	2.47±0.34
U glucose (mg/mg creatinine)	0.76±0.06	0.67±0.03	0.88±0.09	0.83±0.09
BUN (mg/dL)	38.1±2.6	37.6±2.3	34±1.91	68±5.52***

Parameters represent the mean ± SEM of 5 - 8 animals per group. Statistical difference between groups were calculated with unpaired Student's t test, *P<0.05; **P<0.01; ***P<0.001
U, urine; BUN, blood urea nitrogen.

Table 2: Body weight and urine parameters in ksp-*Cre*;*Pkd1*$^{del2–11,lox}$ and control mice.

Parameter	***Pkd1* +/+**	***Pkd1*$^{del2–11,lox}$**
Body weight (g)	22.66±2.22	23.98±2.63
U volume (mL/24 h)	1.66±0.34	1.92±0.46
U CC16 (µg/mg creatinine)	4.54±1.57	27.16±6.86**
U calcium (g/mg creatinine)	1.2±0.30	1.4±0.20
U phosphate (mg/mg creatinine)	2.50±1.11	2.65±0.26
U glucose (mg/mg creatinine)	2.32±0.44	2.01±0.40
U creatinine (mg/dL)	41.05±2.07	50.51±3.64

Parameters represent the mean ± SEM of 5 animals per group. Statistical difference between groups were calculated with Mann-Whitney test, *P<0.05; **P<0.01; ***P<0.001
U, urine;

Table 3: Clinical and biological parameters of individuals with ADPKD.

ID	Gender	Age	Mutated Gene	Mutation	Mutation type	Plasma Creatinine (mg/dl)	U Creatinine (mg/dl)	Microalbumin (µg/g creat)	eGFR (ml/min)
110	F	22	*PKD1*	c.9914_9915del	frameshift	0.68	216.67	513.68	124
37	F	38	*PKD1*	c.9241T>C (p.Cys3081Arg)	missense	0.61	162.57	63.36	110
788	M	26	*PKD1*	c.8311G>A (p.Glu2771Lys)	missense	0.85	123.27	6.49	120
103	F	28	*PKD1*	c.11661 dup(p.Phe3888Leufs*73)	frameshift	0.53	124.69	8.02	137
106	F	30	*PKD1*	c.12711C>A p.(Tyr4237*)	nonsense	0.74	176.16	60.74	109
421	F	21	*PKD1*	c.8537C>A p.Thr2846Asn	missense	0.71	138.06	16.66	104
101	F	23	*PKD1*	c.7343T>C p.(Leu2448Pro)	missense	0.57	156.7	11.49	132
445	F	27	*PKD1*	c.8945dup (p.Ser2984Glufs*85)	frameshift	0.6	142.53	25.26	126
159	F	31	*PKD1*	c.6307C>T (p.Gln2103*)	nonsense	0.58	227.91	9.21	123
447	F	24	*PKD1*	c.12003+14_12003+33del	atypical splice site	0.58	27.14	18.42	129
54	F	27	*PKD1*	deletion of exon 1	large rearrangement	0.67	99.41	19.11	106
30	M	32	*PKD1*	c.2955-2958del (p.Tyr986fs)	frameshift	0.96	110.27	4.53	91
473	M	19	*PKD1*	c.5968_5969del p.(Arg1990Glufs*59)	frameshift	0.99	307.57	9.10	97
136	M	21	*PKD1*	c.11485_11487del p.Glu3829del	small IF indels	0.96	240.21	8.74	98
301	F	24	*PKD1*	c.3623T>A(p.(Val1208asp))	missense	0.66	146.68	21.82	110
993	F	33	*PKD2*	c.952dup (p.Val318Glyfs*23	frameshift	0.78	319.22	26.63	100

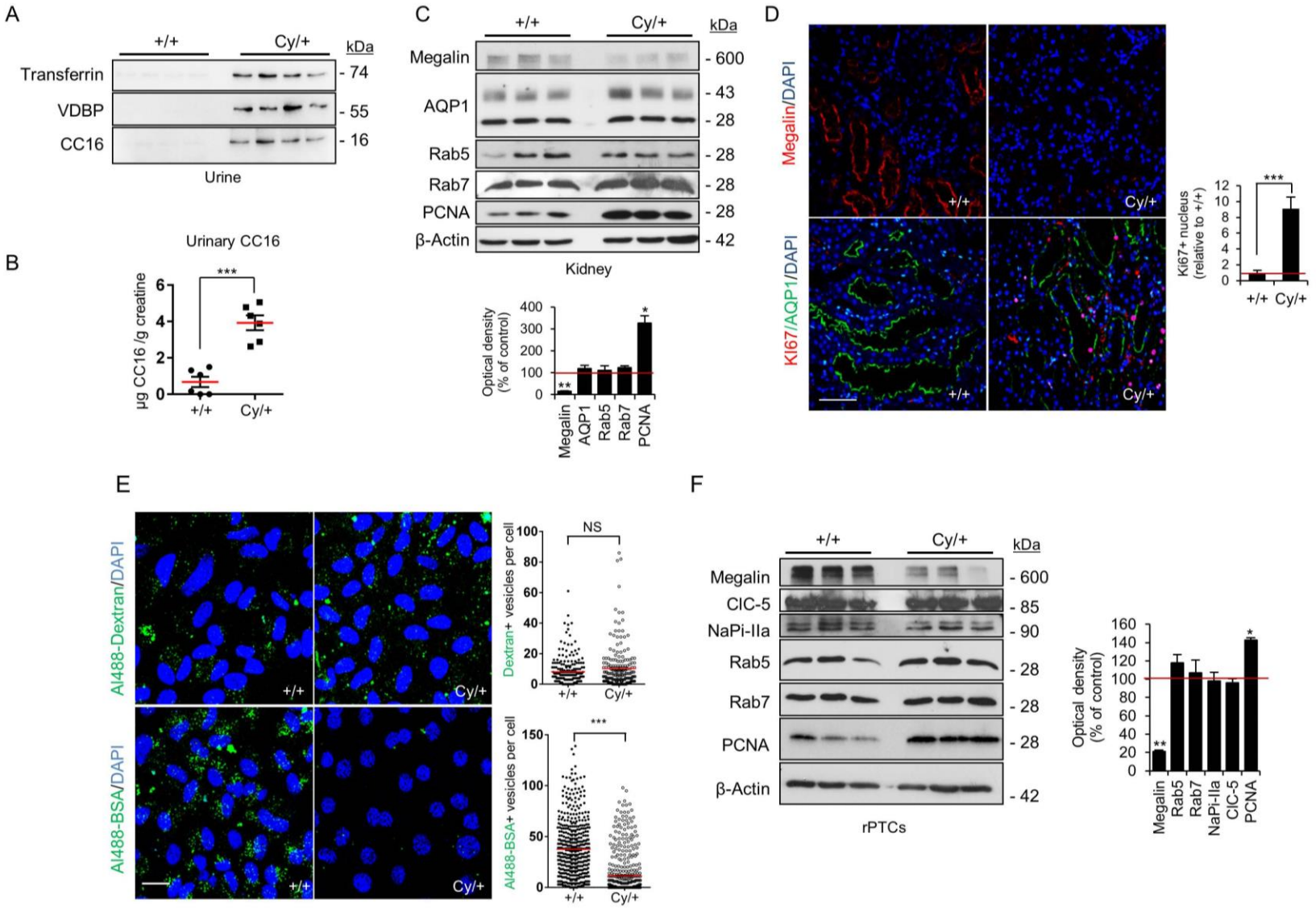

Figure 1: Defective receptor-mediated endocytosis in Han:SPRD Cy/+ rat

(A) Representative immunoblots of low molecular weight proteinuria (LMWP): transferrin, vitamin D-binding protein (VDBP) and Clara cell protein 16 (CC16) in urine samples from +/+ and Cy/+ rats (normalized to 5 µg creatinine). n = 4 rats per group (5-6 weeks old). **(B)** Urinary CC16 concentration was measured by ELISA in +/+ and Cy/+ (6-7 animals per group). Statistical differences between groups were measured with unpaired Student's t test. ***P<0.001 versus +/+. **(C)** Representative immunoblots for megalin, aquaporin-1 (AQP1), rab5, rab7, proliferative cell nuclear antigen (PCNA) and β-actin in +/+ and Cy/+ kidneys (25 µg total protein per lane, n = 5 rats per group). Unpaired Student's t test was used to assess statistical differences with *P<0.05 versus +/+, **P<0.01 versus +/+ (taken as 100%). **(D)** Immunofluorescence for megalin, AQP1 and KI67 in +/+ and Cy/+ kidneys. Nuclei were counterstained with DAPI. Quantification of KI67 positive nuclei was performed on >20 PTs per condition. Scale bar: 50 µm **(E)** Uptake of Alexa488-bovine serum albumin (BSA) and Alexa488-Dextran in rPTC derived from +/+ and Cy/+ kidneys. Quantification of BSA positive vesicles was performed on >400 cells using CellProfiler. Statistical differences were calculated with unpaired Student's t test with ***P<0.001. Scale bar: 20 µm **(F)** Representative immunoblots for megalin, SGLT2, ClC-5, NaPi-IIa, Rab5, Rab7, PCNA and β-actin. n = 4 animals per group. Unpaired Student's t test was used for statistical analyses.

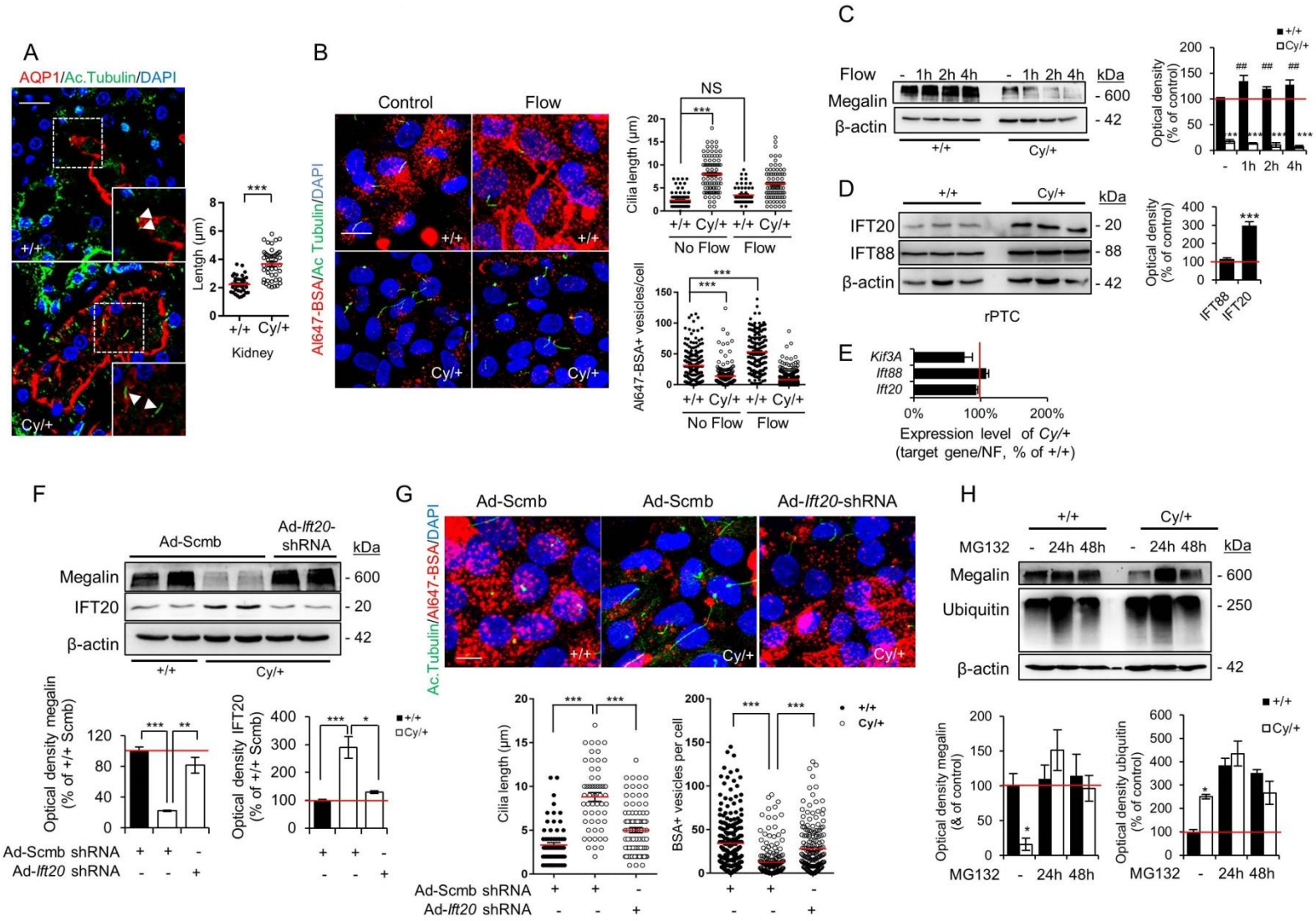

Figure 2: Defective ciliogenesis impairs megalin expression and endocytosis

(A) Representative immunofluorescence for acetylated-tubulin and AQP1 in +/+ and Cy/+ kidneys. Ciliary length was measured with ImageJ on > 100 cilia. Statistical differences were assessed with Student's t test with ***P<0.001 Scale bar: 10 µm **(B)** +/+ and Cy/+ derived rPTCs were subjected to apical fluid movement (flow, 1 Hz, 4h) followed by an endocytosis assay of Alexa647-BSA. Immunofluorescence for acetylated-tubulin on rPTC derived from +/+ and Cy/+ kidneys. Ciliary length was measured with ImageJ on 350 cilia. Quantification of BSA positive vesicles was performed on > 400 cells using CellProfiler. Statistical differences were measured using one-way analysis of variance and Turkey's range test (post-hoc) with ***P<0.001 Scale bar: 10 µm **(C)** Representative immunoblots for megalin in +/+ and Cy/+ derived rPTCs after 0, 1, 2 and 4h of apical fluid movement (flow, 1Hz). n = 3 independent experiments. Statistical differences were assessed with unpaired Student's t test with ***P<0.001 Cy/+ vs +/+ control and #p<0.001 +/+ under flow vs +/+ control **(D)** Representative immunoblots for IFT20, IFT88 and β-actin in +/+ and Cy/+ derived rPTCs (25 µg total protein per lane). n = 3 independent experiments. Statistical differences were assessed with unpaired Student's t test with ***P<0.001 **(E)** Quantitative RT-PCR to measure the mRNA expression of *Ift20*, *Ift88* and *Kif3a*. **(F)** Representative immunoblots for megalin and IFT20 in +/+ and Cy/+ derived rPTCs after treatment with Ad-IFT20-shRNA. n = 4 independent experiments. Statistical differences were assessed with unpaired Student's t test with *P<0.05, **P<0.01 and ***P<0.001 **(G)** Uptake of Alexa647-BSA in +/+ and Cy/+ rPTCs transduced with Ad-*Scmb* or Ad-*Ift20*-shRNA. Quantification of BSA positive vesicles and ciliary length measurement were performed on 200 cells per condition using cellProfiler and imageJ respectively. Scale bar: 10 µm **(H)** Representative immunoblots for megalin, ubiquitin and β-actin in +/+ and Cy/+ derived rPTCs treated or not with 5 µM of MG-132 for 24h and 48h. n = 3 independent experiments. Statistical differences were measured with Student's t test with *P<0.05.

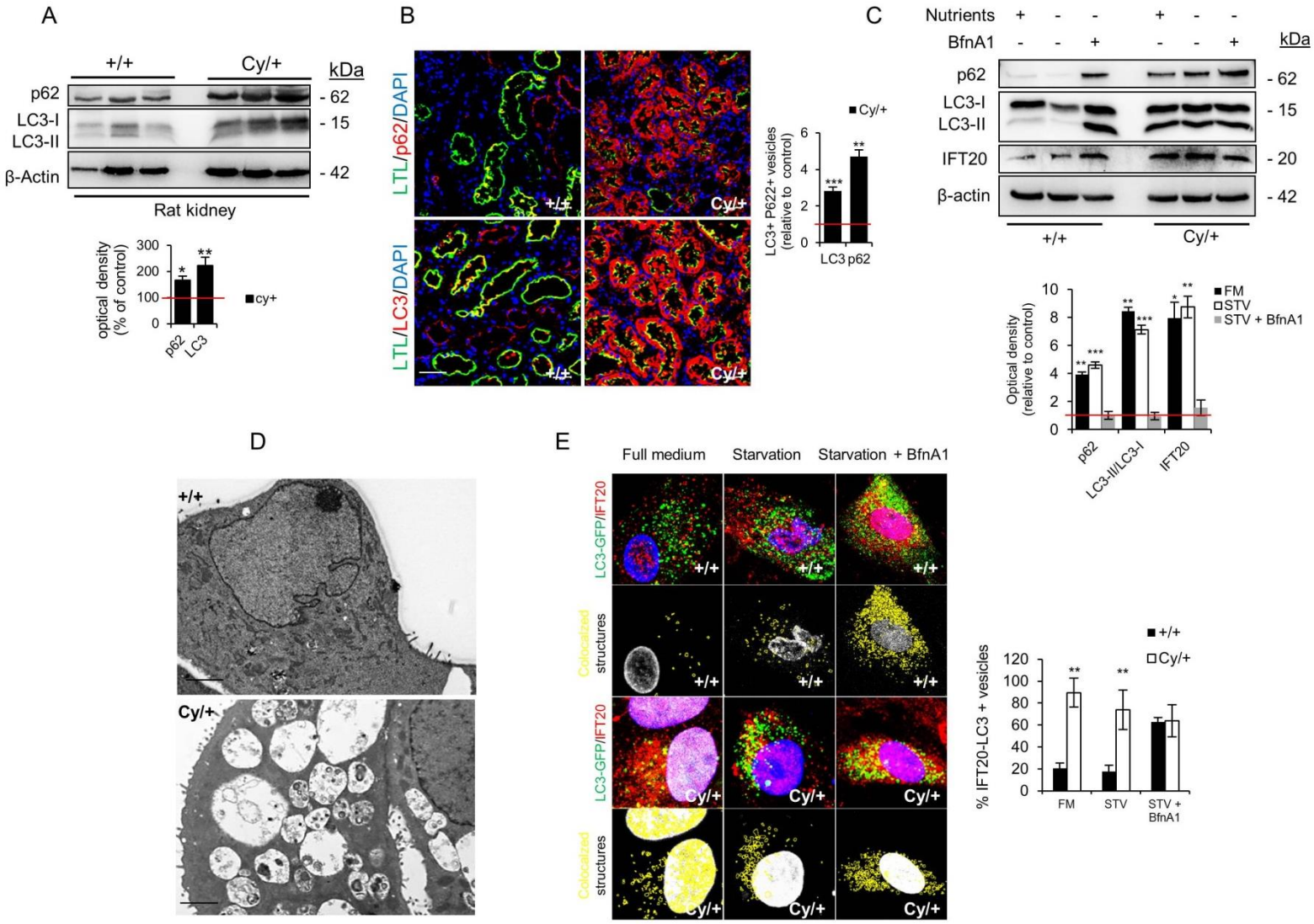

Figure 3: Defective autophagy leads to an accumulation of the ciliary protein IFT20

(A) Representative immunoblots and densitometry analyses of p62, LC3 and β-actin in +/+ and Cy/+ kidneys (25 µg total protein per lane). n = 4 pairs of 5 - 6 weeks old rats. Scale bar: 50 µm **(B)** Immunofluorescence of Lotus Tetragonolobus Lectin (LTL), p62 and LC3-positive vesicles in kidney sections of 5 weeks old Cy/+ and +/+ animals. Nuclei were counterstained with DAPI. Quantification of LC3+ and p62+ vesicles was performed on > 80 LTL positive PTs. **(C)** Representative immunoblots and densitometry analyses of p62, LC3, IFT20 and β-actin in +/+ and Cy/+ derived rPTCs cultured in nutrient-rich medium or in nutrient-depleted medium for 4 h, in presence or absence of 250 nM of BafilomycinA1. 25 µg total proteins per lane were used and the experiment was repeated 3 times. Statistical differences between experimental conditions were measured with Student's t test with **P<0.01 and ***P<0.001 versus +/+ in nutrient-rich medium. **(D)** Representative electron micrograph of +/+ and Cy/+ derived rPTCs. Scale bar = 2 µm. **(E) +/+** and Cy/+ derived rPTCs were transduced with GFP-tagged *Map1lc3b* (*Map1lc3b*/GFP, green) bearing adenoviral particles for 48 h. The cells were subsequently incubated in nutrient-rich medium or in nutrient-depleted medium for 4 h, in presence or absence of 250 nM of BafilomycinA1. The colocalization of GFP-LC3 and IFT20 was monitored by confocal microscopy, the identification and quantification of GFP-LC3 - IFT20 positive vesicles were performed on >500 autophagosomes per conditions using CellProfiler.

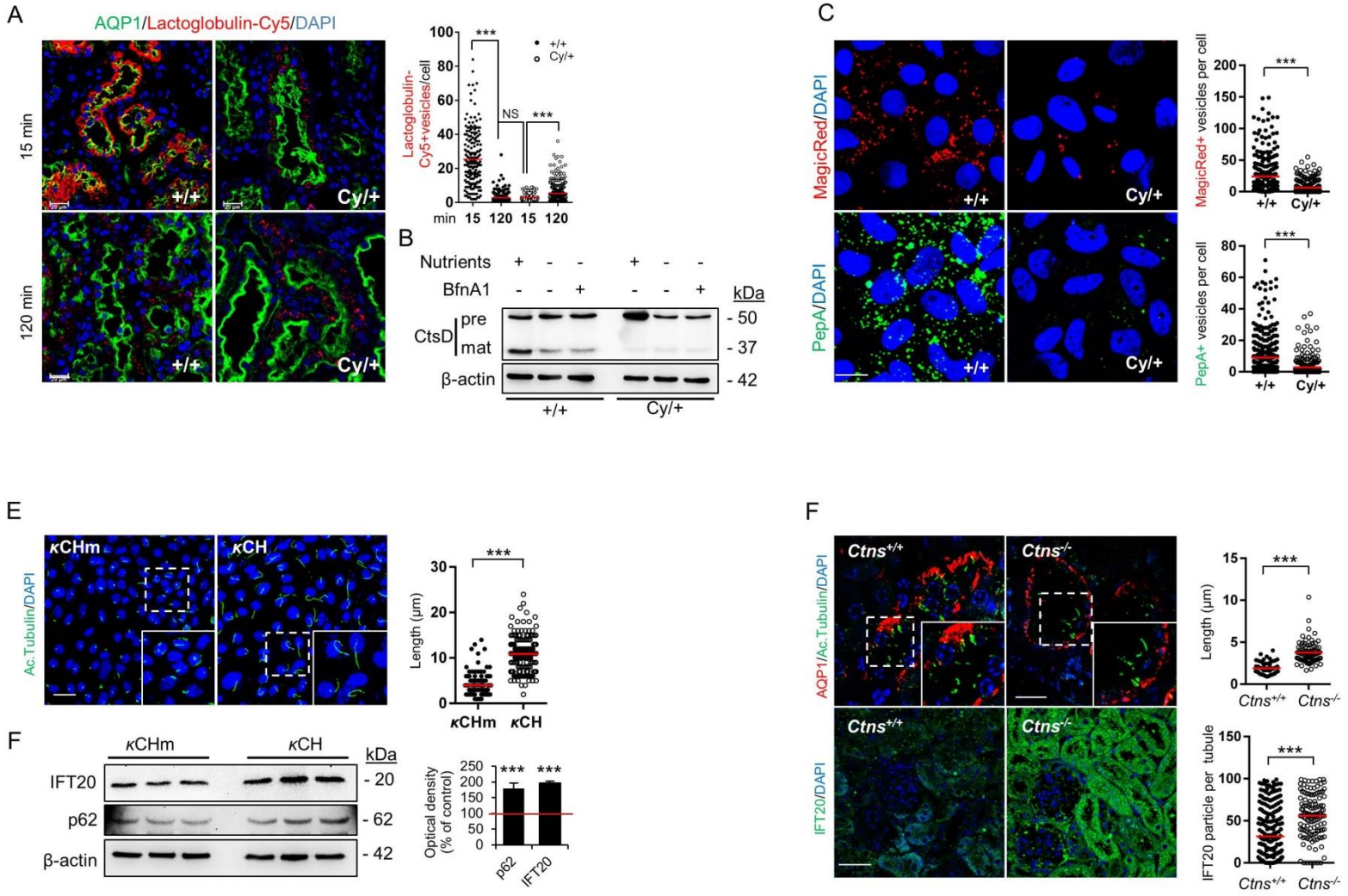

Figure 4: Lysosomal dysfunction causes defective autophagy clearance and abnormal ciliogenesis

(A) 5 weeks-old +/+ and Cy/+rats were injected with 100 µg of Lactoglobulin-Cy5 and the kidneys were harvested after 15 and 120 min and further process for immunofluorescence of AQP1 and Lactoglobulin-Cy5. Quantification of Lactoglobulin-Cy5 vesicles was performed on 20 AQP1 positive PTs per conditions. Scale bar: 20 µm **(B)** Representative immunoblots of cathepsin-D and β-actin on +/+ and Cy/+ derived rPTCs cultured in nutrient-rich medium or in nutrient-depleted medium for 4 h, in presence or absence of 250 nM of BafilomycinA1. n = 3 independent experiments **(C)** +/+ and Cy/+ derived rPTCs were incubated with 2 nM of Magic Red substrate or FL-Bodipy pepstatinA (PepA) for 1h fixed and further process for immunofluorescence. Quantification was performed on > 200 cells per conditions. Scale bar = 10 µm **(D)** Representative immunofluorescence of acetylated-tubulin of mouse primary PT cells (mPTCs) incubated for 24 h with 25 $\mu g.mL^{-1}$ of renal fanconi syndrome (RFS) associated human κ light chains (*κ*CH) or a non-pathogenic mutant version of *κ*CH (*κ*CHm). Ciliary length was measured with ImageJ on 150 cilia per conditions. Statistical differences between groups were assessed with Student's t test with ***P<0.001. **(E)** Representative immunoblots for IFT20, p62 and β-actin in mPTCs incubated for 24 h with *κ*CHm or *κ*CH. Statistical difference between groups were calculated with Student's t test with***P<0.001. Scale bar: 20 µm **(F)** Representative immunofluorescence of acetylated-tubulin, IFT20 and AQP1 in *Ctns*$^{+/+}$ and *Ctns*$^{-/-}$ kidney sections. Primary cilia length was measured on >100 cilia distributed in 40 AQP1 positive PTs. Quantification IFT20 + vesicles was performed on >20 tubules per conditions. Statistical difference between groups were calculated with Student's t test with***P<0.00. Scale bar: 50 µm

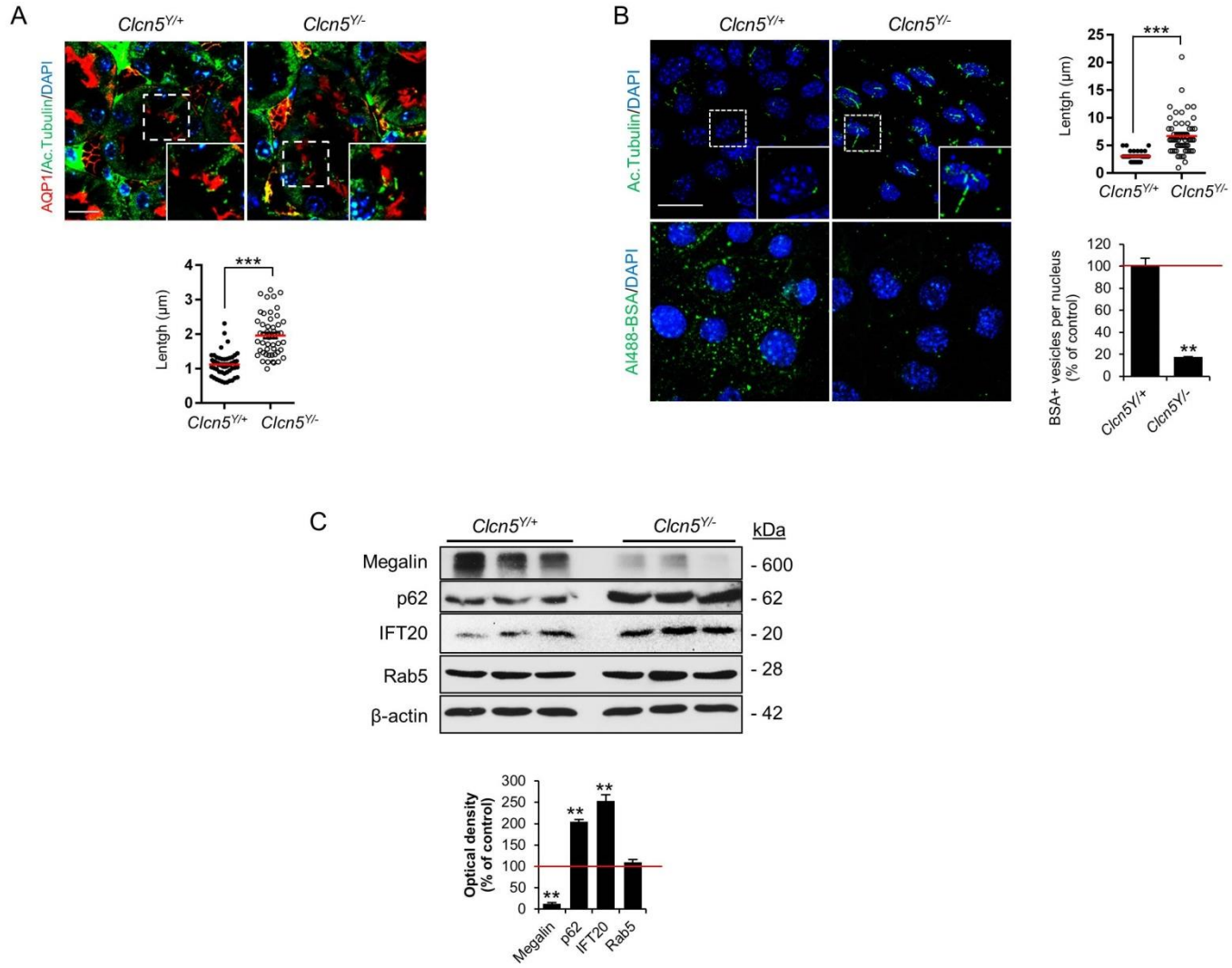

Figure 5: Dent disease mouse model exhibits impaired ciliogenesis

(A) Representative immunofluorescence of Acetylated-tubulin and AQP1 in *Clcn5*$^{Y/+}$ and *Clcn5*$^{Y/-}$ kidney sections. Primary cilia length was measured on 100 cilia distributed in 20 AQP1 positive PTs per conditions. Statistical difference between groups were calculated with Student's t test ***P<0.001. Scale bar: 10 µm **(B)** Representative immunofluorescence of acetylated-tubulin in mPTCs derived from *Clcn5*$^{Y/+}$ and *Clcn5*$^{Y/-}$ Scale bar: 10 µm **(C)** Representative immunoblots of IFT20, p62, Rab5 and β-actin in *Clcn5*$^{Y/+}$ and *Clcn5*$^{Y/-}$ derived mPTCs. Statistical difference between groups were calculated with Student's t test with *P<0.05, **P<0.01 versus *Clcn5*$^{Y/+}$ mPTCs

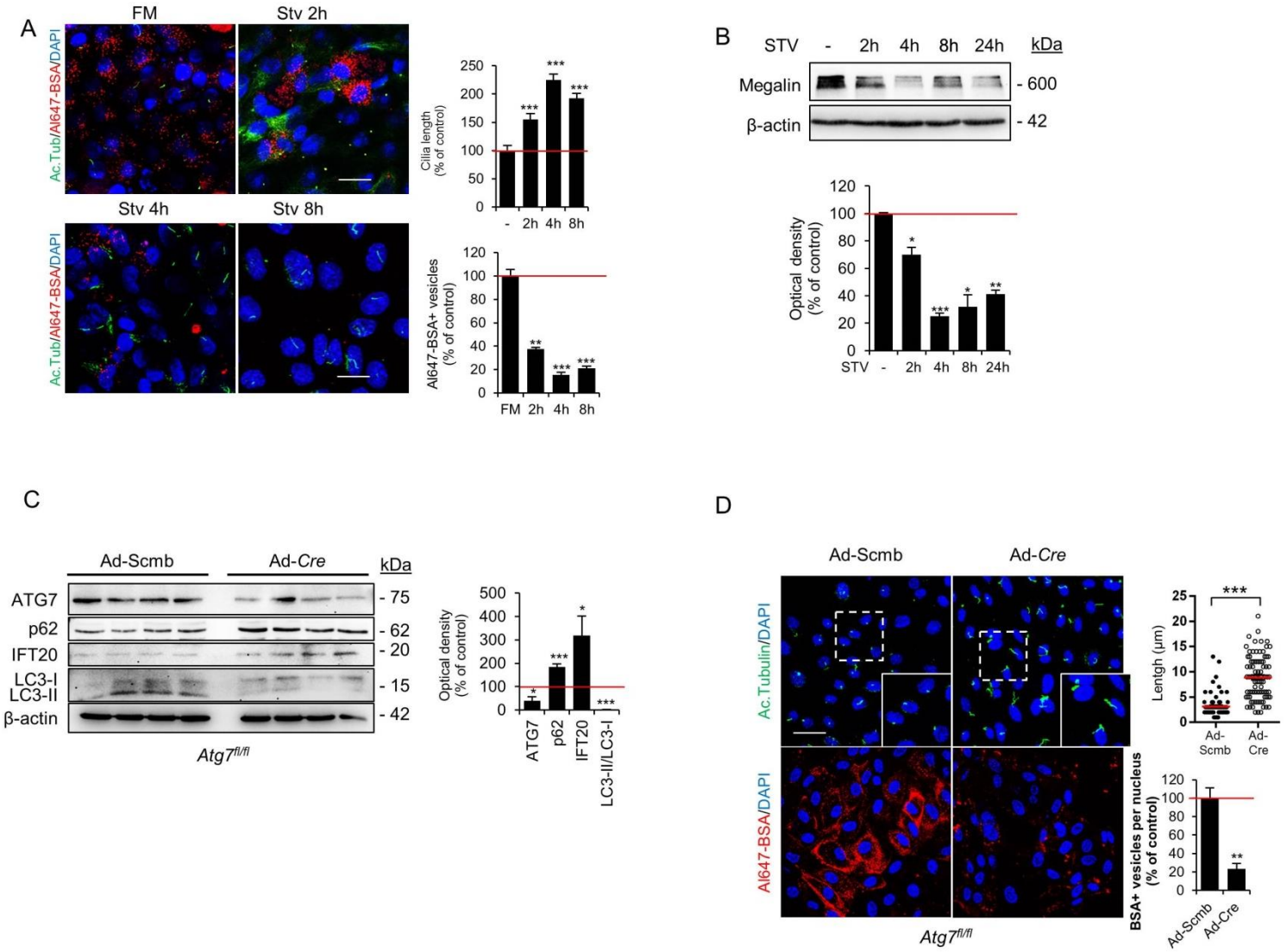

Figure 6: Autophagy regulates primary cilia length and endocytosis activity

(A) Uptake of Alexa647-bovine serum albumin (BSA) followed by an immunofluorescence of Acetylated-tubulin in mPTCs cultured in absence of nutrients for 0 (FM, full medium) 2, 4 and 8 h. >100 cells per conditions were used for quantification purposes. Statistical difference between groups were calculated with Student's t test with **P<0.01 STV versus FM and ***P<0.001 STV versus FM. Scale bar: 20 µm **(B)** Representative immunoblots of megalin and β-actin in mPTCs cultured in absence of nutrients for 0, 2, 4, 8 and 24 h. n=3 independent experiment. Statistical difference between groups were calculated with Student's t test with *P<0.05 **P<0.01 and ***P<0.001. **(C)** Representative immunoblots and densitometry for ATG7, p62, LC3 and β-actin in mPTCs derived from *Atg7*$^{fl/fl}$ mice transduced with Ad-*Cre* or Ad-Scmb. n=4 independent experiments. Statistical difference between groups were calculated with Student's t test with *P<0.05 and ***P<0.001 **(D)** Immunofluorescence for acetylated tubulin in mPTCs derived from *Atg7*$^{fl/fl}$ mice transduced with ad-Cre or Ad-Scmb. Ciliary length was measured on about 200 cells. Statistical difference between groups were calculated with Student's t test with***P<0.001. Scale bar: 20 µm

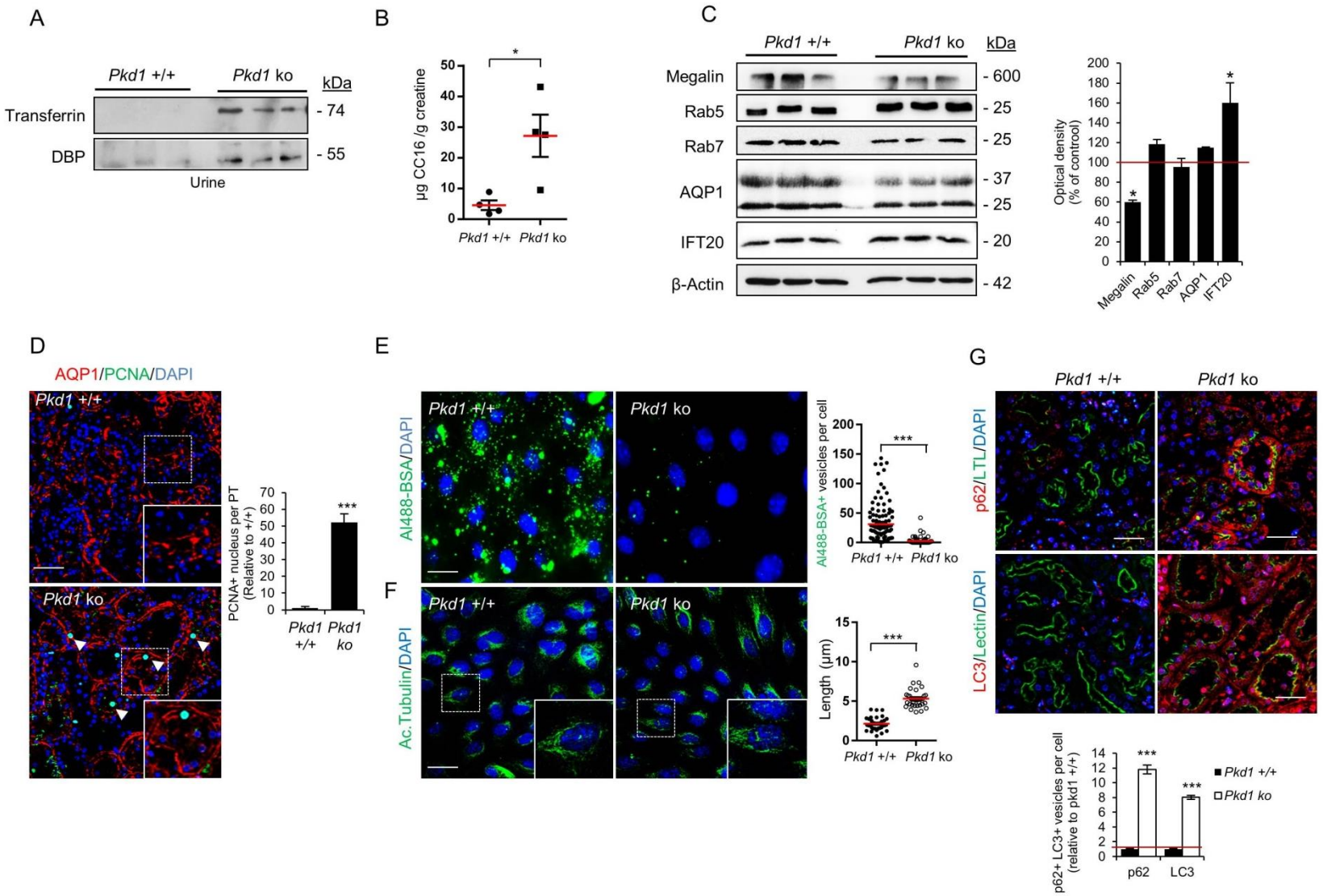

Figure 7: ksp-*Cre*;*Pkd1*$^{del2–11,lox}$ mouse model recapitulates defective autophagy and endocytosis

(A) Representative immunoblots of transferrin and vitamin D binding protein (DBP) in urine from ksp-*Cre*;*Pkd1*$^{del2–11,lox}$ mice and their control littermates (Normalized to 5 µg creatinine). n=4 animals per group **(B)** Urinary CC16 was measured by ELISA. n=4 animals per group. **(C)** Representative immunoblots for megalin, Rab5, Rab7, AQP1, IFT20 and β-actin in kidney samples from *Cre*;*Pkd1*$^{del2–11,lox}$ mice and their control littermates. 25µg of protein was loaded per lane. n = 4 animals per group. Statistical difference between groups were calculated with Student's t test with *P<0.05 **(D)** Immunofluorescence of PCNA and AQP1 in kidney sections from *Pkd1* deficient mice and control mice. Quantification was performed on 20 AQP1 positive PTs per conditions and statistical difference between groups were calculated with Student's t test with ***P<0.001. Scale bar: 50 µm **(E)** Endocytosis assay monitoring Alexa488-BSA uptake in mPTCs derived from 8 weeks-old ksp-*Cre*;*Pkd1*$^{del2–11,lox}$ mice and control mice. Quantification of BSA positive vesicles was performed on 100 cells per condition. Statistical differences were calculated with unpaired Student's t test with ***P<0.001. Scale bar: 20 µm **(F)** Immunofluorescence of Acetylated-tubulin in mPTCs from ksp-*Cre*;*Pkd1*$^{del2–11,lox}$ mice and controls. Primary cilia length was measured on > 100 cilia. **(G)** Immunofluorescence of p62 and LC3 in kidney sections from ksp-*Cre*;*Pkd1*$^{del2–11,lox}$ mice and their respective controls. Quantification of LC3+ and p62+ vesicles was performed on 20 AQP1 positive PTs per conditions and statistical difference between groups were calculated with Student's t test with ***P<0.001. Scale bar: 50 µm

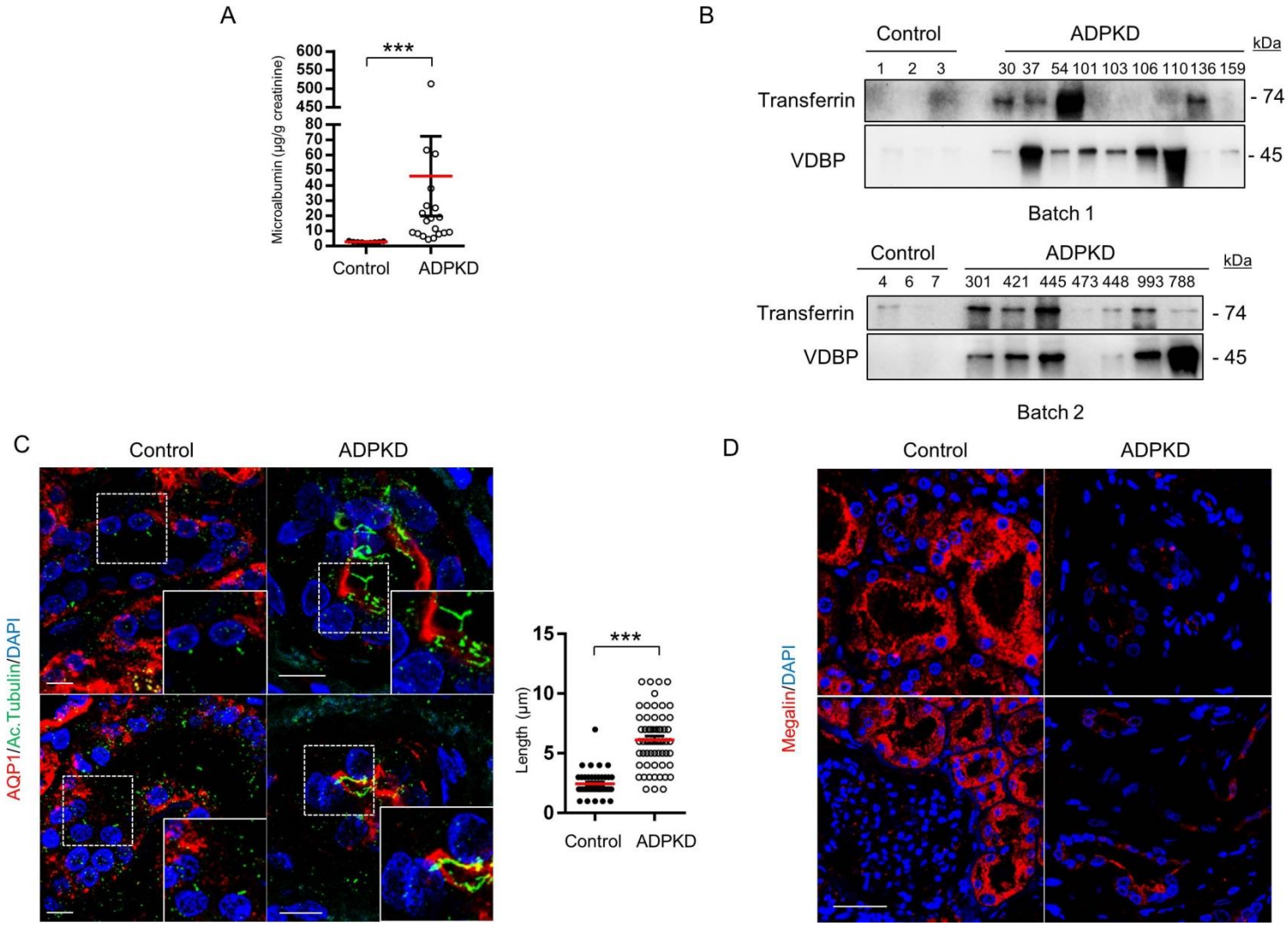

Figure 8: ADPKD patients show PT dysfunction in absence of renal failure

(A) Microalbuminuria was measured in urinary samples from 16 ADPKD patients and 9 healthy volunteers. Values were normalized to creatinine concentration. Statistical differences were assessed with Mann-whitney test with ***P<0.001. **(B)** Representative immunoblots for transferrin and vitamin D binding protein (VDBP) in urinary samples from 16 ADPKD patients and 6 healthy volunteers. Loading was normalized to creatinine concentration (20 µg per lane). **(C)** Representative immunofluorescence of Acetylated-tubulin and AQP1 in kidney sections from ADPKD patients and control. Primary cilia length was measured on 50 cilia distributed in 20 AQP1 positive PTs. Statistical difference between groups were calculated with Student's t test ***P<0.001 Scale bar: 25 µm **(D)** Representative immunofluorescence of megalin in kidney sections from ADPKD patients and control. Scale bar: 25 µm

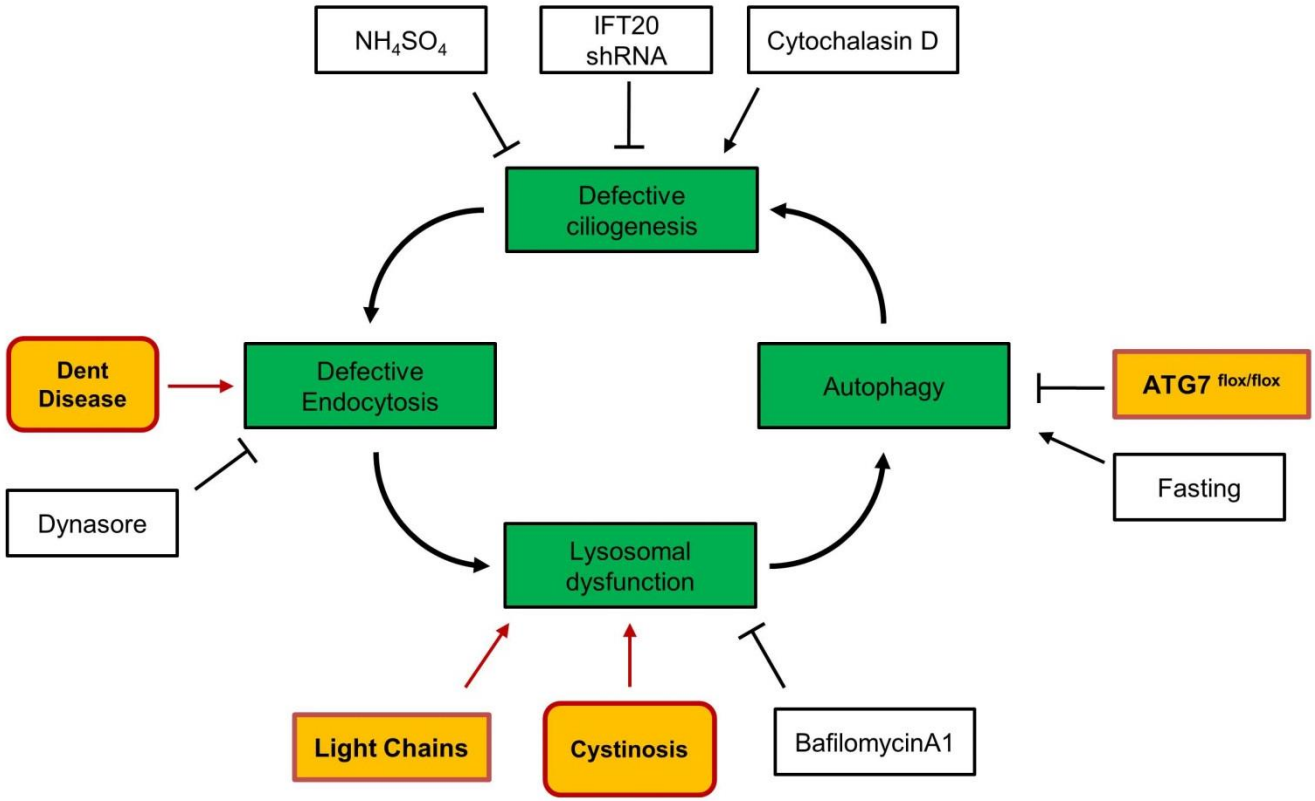

Model of interplay between ciliogenesis, receptor-mediated endocytosis and autophagy

Supplementary information

Lysosomal function links ciliogenesis and receptor mediated endocytosis

Alkaly Gassama, Nathalie Demoulin, Dorien J M Peters, Alessandro Luciani, Olivier Devuyst

S

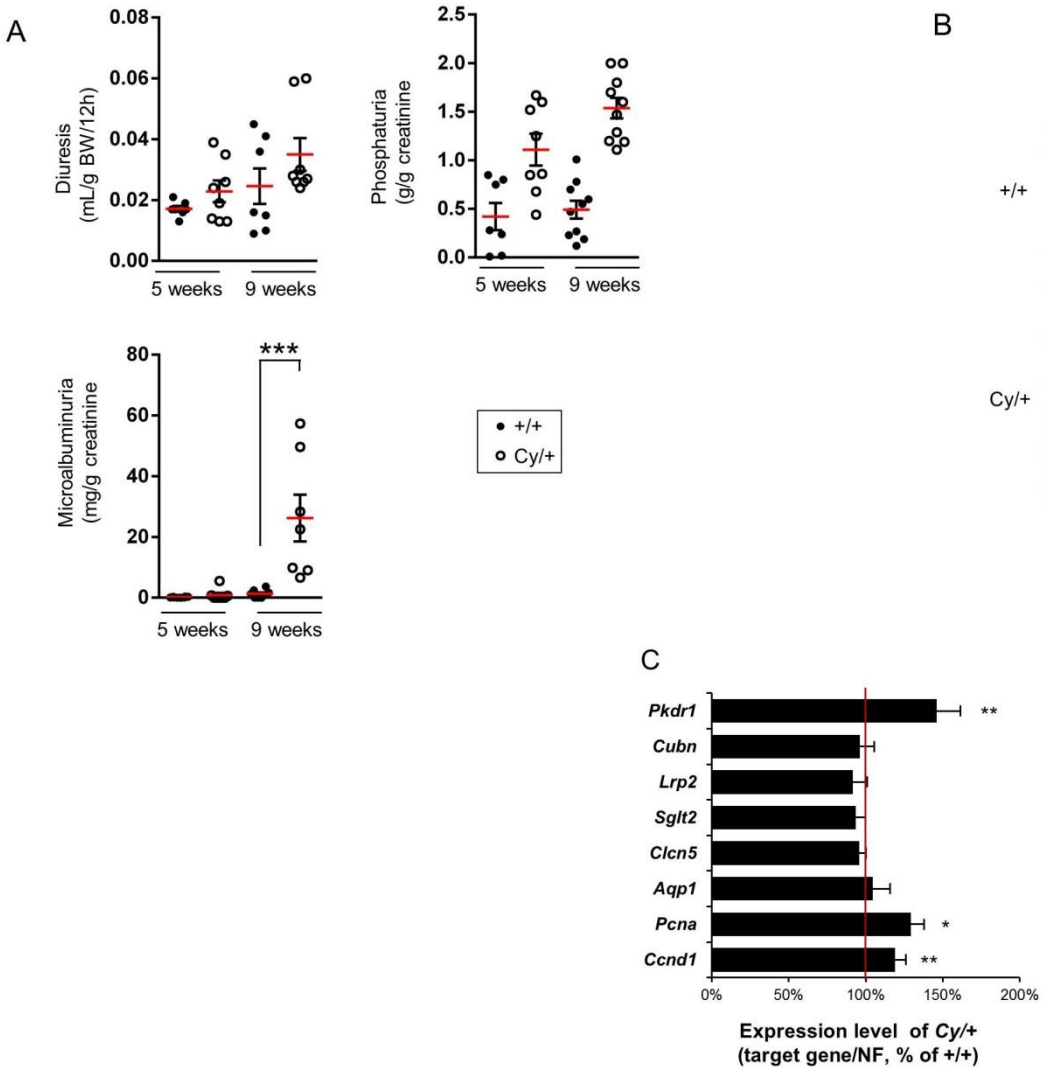

Supplementary Figure 1: Characterization of Han:SPRD Cy/+ rats kidney phenotype

(A) Urinalysis of diuresis, phosphaturia and microalbumiuria in +/+ and Cy/+ rats at 4 and 9 weeks old. Data are represented as mean +/- SEM. Statistical differences between groups were assessed with Student's t test with ***P<0.001. n=5-9 animals per group. **(B)** Representative haematoxylin and eosin staining of kidney sections from 4 and 9 weeks old +/+ and Cy/+ rats. **(C)** Quantitative RT-PCR to measure the mRNA expression of PT (*Lrp2*, *Cubn*, *Sglt2*, *Clcn5*, and *Pkdr1*) and proliferation (*Pcna* and *Ccnd1*) genes in +/+ and Cy/+ whole kidneys. n = 4 rats per group. Statistical differences between groups were assessed with Student's t test with *P<0.05, **P<0.01.

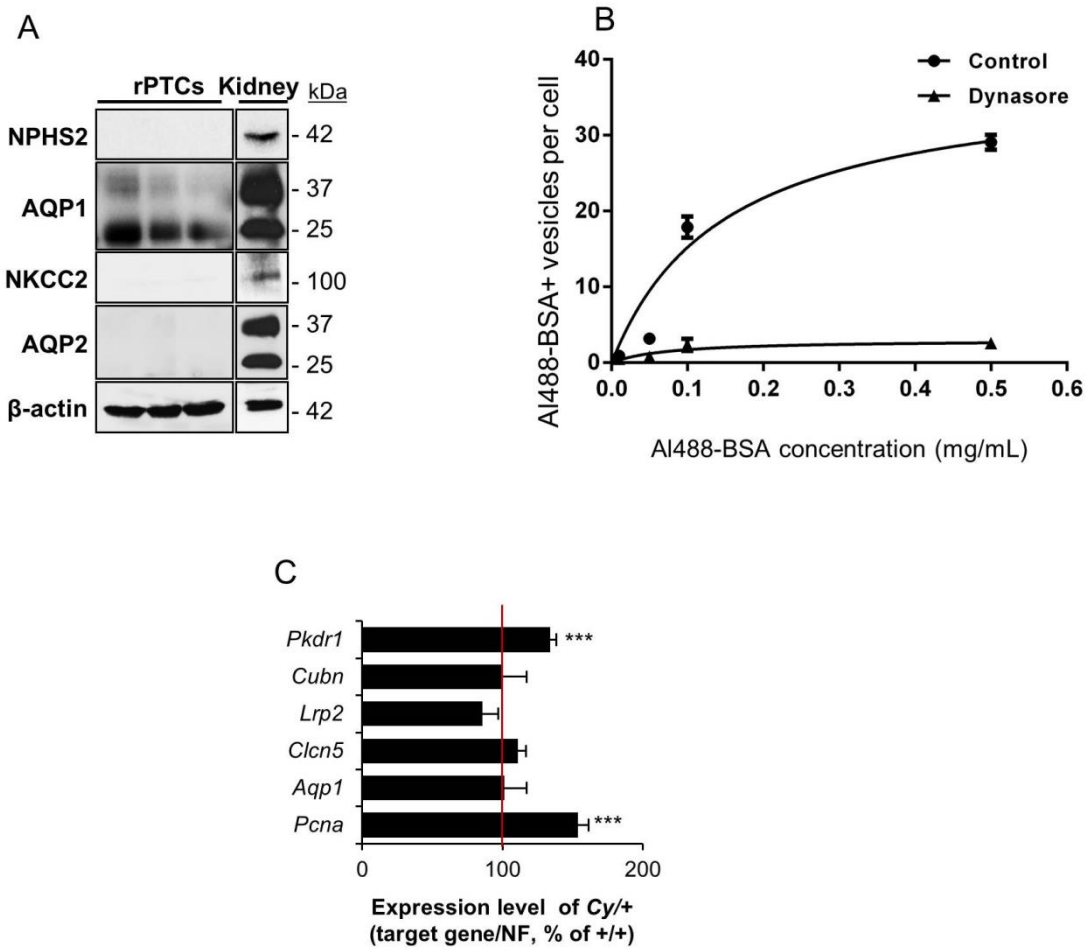

Supplementary Figure 2: Characterization of rPTCs derived from Han:SPRD Cy/+ kidneys

(A) Representative immunoblots for podocin (NPHS2), aquaporin-1 (AQP1), sodium, potassium, chloride cotransporter 2 (NKCC2), aquaporin-2 (AQP2) and β-actin in rat primary culture of proximal tubular cell (rPTCs) and in kidney. 25 µg proteins per lane were used. Experiments were performed on rPTCs derived from 3 rats. **(B)** Uptake of 0.01, 0.05, 0.1 and 0.5 mg.mL^{-1} of Alexa488-bovine serum albumin (BSA) in +/+ derived rPTCs. Additionally, rPTCs were also treated with 80 µM of dynasore, a dynamin GTPase inhibitior known to block endocytosis, at 37 °C 30 min prior to the endocytosis assay. >500 cells were used for statistical analyses. Michaleis-Menten kinetics model was used to monitor the endocytosis activity. **(C)** Quantitative RT-PCR to measure the mRNA expression of PT (*Lrp2*, *Cubn*, *Clcn5*, and *Pkdr1*) and proliferation (*Pcna* and *Ccnd1*) genes in +/+ and Cy/+ whole kidneys. n = 4 rats per group. Statistical differences between groups were assessed with Student's t test with *P<0.05, **P<0.01.

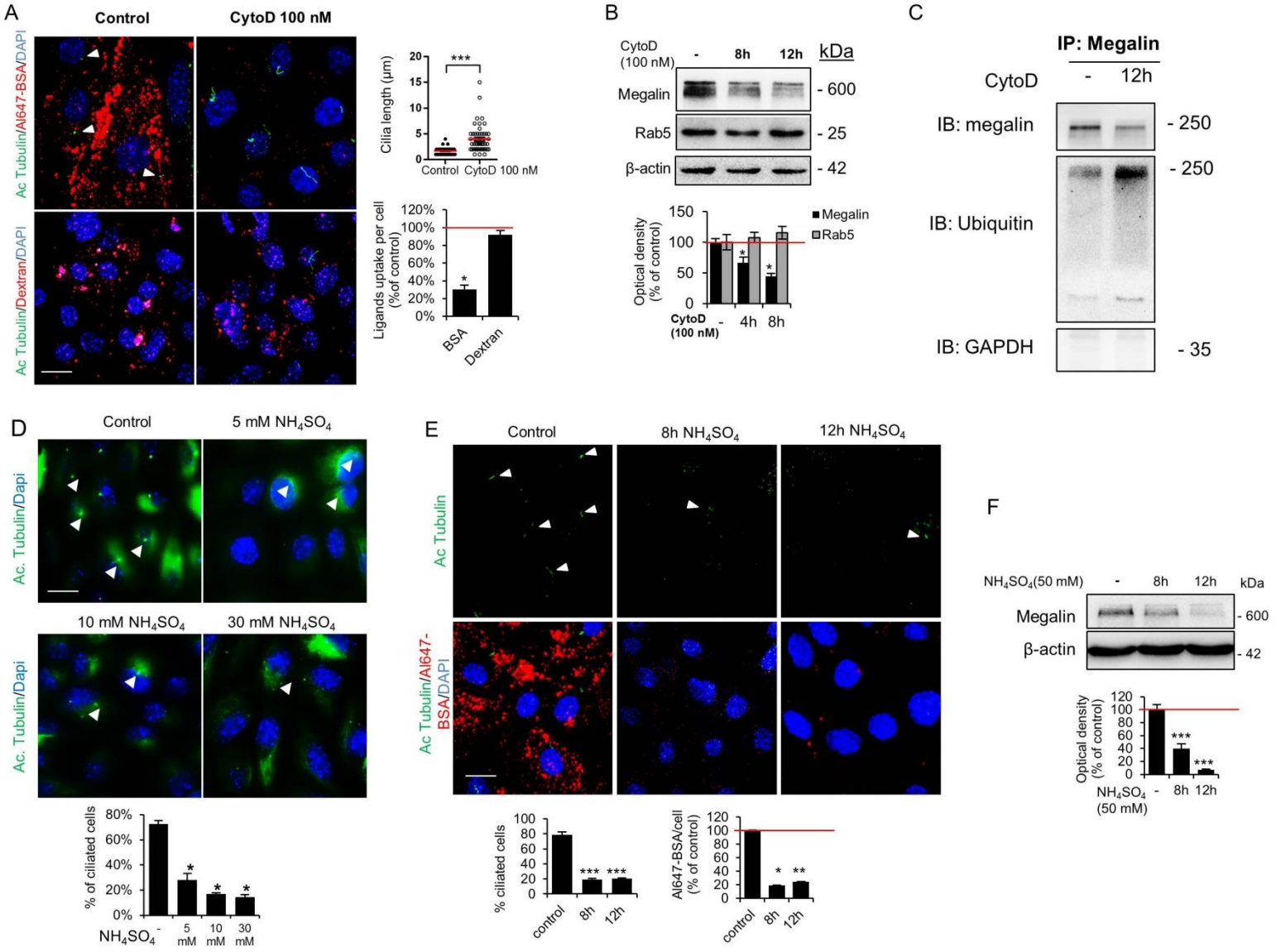

Supplementary Figure 3: Alteration of primary cilia impairs endocytosis and decrease megalin expression

(A) Uptake of Alexa647-bovine serum albumin (BSA) and Alexa647-Dextran followed by an immunofluorescence of Acetylated-tubulin in mPTCs treated or not with 100nM cytochalasin D (CytoD) for 8h. >100 cells were used per condition for quantification. Scale bar: 20 µm **(B)** Representative immunoblots of megalin and Rab5 in mPTCs after 0, 4h and 8h of CytoD treatment (25µg total protein per lane). **(C)** Immunoprecipitation of megalin from mPTCs treated or not with 100nM of cytochalasin D and immunoblotting of ubiquitin. n= 4 independent experiments **(D)** Representative immunofluorescence of Acetylated-tubulin in mPTCs treated with 0 (control), 5, 10 or 30 mM of ammonium sulfate (NH_4SO_4) for 12 h. Cilia length was measured on at least 50 cilia per conditions. Statistical differences were measured with Student's t test with *P<0.05. Scale bar: 20 µm **(E)** Uptake of Alexa647-bovine serum albumin (BSA) followed by an immunofluorescence of acetylated-tubulin in mPTCs treated with 30 mM of NH_4SO_4 for 0, 8 and 12 h. 100 cells per condition were used for quantification purposes. Statistical differences were measured with Student's t test with *P<0.05, **P<0.01 and ***P<0.001. Scale bar: 10 µm **(F)** Representative immunoblots for megalin and β-actin for mPTCs treated with 30 mM of NH_4SO_4 for 0, 8 and 12h. n = 3 independent experiments. Statistical differences were measured with Student's t test with ***P<0.001 versus control

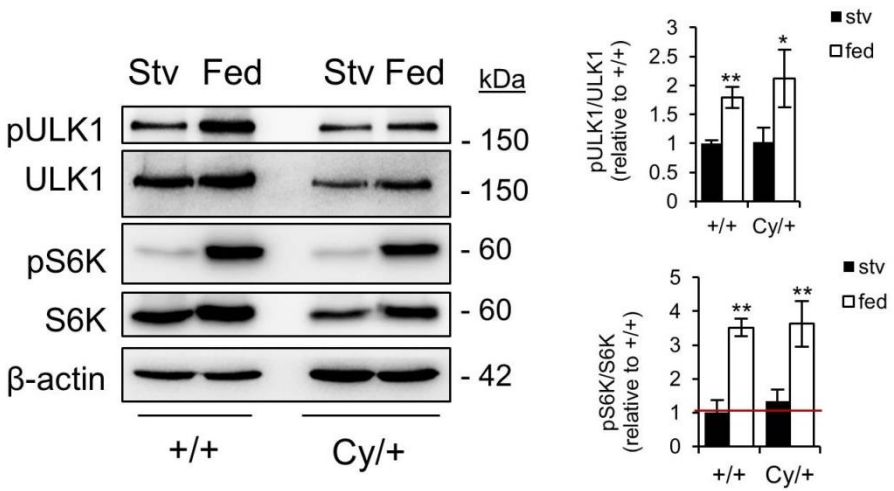

Supplementary Figure 4: mTOR activity in Cy/+ derived rPTCs

Representative immunoblots for phospho-Ulk1 (pULK1), ULK1, phosphor-S6 kinase (pS6K), S6 kinase (S6K) and β-actin in rat primary culture of proximal tubular cell (rPTCs) cultured in nutrient-rich medium (Fed) or in nutrient-depleted medium (Stv). Statistical differences were measured with Student's t test with *P<0.05 and **P<0.01 versus +/+ derived rPTCs in Stv conditions.

III-2 Bone Marrow Transplantation Improves Proximal Tubule Dysfunction in a Mouse Model of Dent Disease

Sarah S. Gabriel[1,2*], Hendrica Belge[1*], Alkaly Gassama[1*], Huguette Debaix[1], Alessandro Luciani[1], Thomas Fehr[1,2,3], Olivier Devuyst[1]

[1] Institute of Physiology, University of Zurich, Zurich, Switzerland

[2] Division of Nephrology, University Hospital Zurich, Zurich, Switzerland

[3] Department of Internal Medicine, Cantonal Hospital Graubünden, Chur, Switzerland

*SSG, HB and AG contributed equally to the study

Correspondence: Prof. Dr. Olivier Devuyst**;** Institute of physiology, University of Zurich; Winterthurerstrasse, 190, 8057 Zürich, Switzerland**;** Tel.: +41(0)44 635 50 82, E-mail: olivier.devuyst@uzh.ch

Kidney International, Volume 91, Issue 4, April 2017, Pages 776-778

DOI: https://doi.org/10.1016/j.kint.2016.11.016

ABSTRACT

Dent disease is a rare X-linked tubulopathy caused by mutations in the endosomal chloride-proton exchanger ClC-5, resulting in defective receptor-mediated endocytosis and severe proximal tubule (PT) dysfunction. Bone marrow (BM) transplantation has recently been shown to preserve kidney function in cystinosis, a lysosomal storage disease causing PT dysfunction. In this study we tested the effects of BM transplantation in *Clcn5*$^{Y/-}$ mice, a faithful model for Dent disease. Wild-type BM transplantation in *Clcn5*$^{Y/-}$ mice significantly improved PT dysfunction, with decreased low-molecular-weight proteinuria, glycosuria, calciuria and polyuria four months after transplantation, compared to *Clcn5*$^{Y/-}$ mice transplanted with ClC-5 knock-out BM. The BM-derived cells engrafted in the interstitium, surrounding PT cells which showed a rescue of the apical expression of ClC-5 and megalin receptors. The improvement of PT dysfunction correlated with *Clcn5*-gene expression in kidneys of mice transplanted with wild-type BM cells. Co-culture of *Clcn5*$^{Y/-}$ PT cells with BM-derived cells confirmed rescue of ClC-5 and megalin, and resulted in improved endocytosis. Nanotubular extensions between the engrafted BM-derived cells and PT cells were observed *in vivo* and *in vitro*. No rescue was observed when the formation of the tunneling nanotubes was prevented by actin depolymerisation or when cells were physically separated by transwell inserts. These data provide the first demonstration that BM transplantation may rescue the epithelial phenotype due to an inherited endosomal defect. Direct contacts between BM-derived cells and diseased tubular cells play a key role in the rescue mechanism.

Keywords: Low-molecular weight proteinuria; bone marrow cell; renal Fanconi syndrome; ClC-5; proximal tubule.

INTRODUCTION

The epithelial cells lining the proximal tubules (PT) of the kidney constitute a paradigm of effective communication between the external environment and the endomembrane system (1). By processing incoming substances, and recycling receptors and transporters at the apical membrane, the connecting endolysosomal system governs the terminal differentiation of PT cells and the recovery of essential substances that would be otherwise lost in the urine (2). These substances include low-molecular-weight (LMW) proteins, which are filtered and then completely reabsorbed by apical endocytosis involving the multi-ligand receptors megalin and cubilin. Following binding and internalization, ligands are delivered to endosomes and further to lysosomes for processing and degradation, so that PT cells play a pivotal role in homeostasis (3). Alterations in these transport processes can lead to a generalized PT dysfunction (renal Fanconi syndrome, RFS), characterized by urinary loss of solutes including LMW proteins, glucose and phosphate, and is often complicated by dehydration, electrolyte imbalance, rickets, and development of chronic kidney disease. Such PT dysfunction is typically encountered in congenital disorders of the endolysosomal compartment, including Dent disease and nephropathic cystinosis (4).

Dent disease (MIM #300009) is a rare, X-linked disorder characterized by LMW proteinuria, generalized PT dysfunction, kidney stones, and renal failure (5). The disease is caused by inactivating mutations of the *CLCN5* gene that encodes ClC-5, an electrogenic Cl^-/H^+ exchanger that is located in the early endosomes of PT cells (6), where it regulates vesicular Cl^- concentration potentially affecting the activity of the V-ATPase and/or vesicle recycling (7). Studies in *Clcn5*$^{Y/-}$ mice, which represent a faithful model of Dent disease, demonstrated that the functional loss of ClC-5 induced a severe loss of megalin and cubilin at the brush border membrane, with impaired endocytosis and lysosomal processing of internalized ligands in PT cells (8,9). The defective endocytosis and apical transport

processes explain why solutes are lost in the urine, often resulting in RFS. In the absence of therapy targeting the molecular defect, the current care of patients with Dent disease is solely supportive, focusing on the prevention of metabolic complications and nephrolithiasis.

Recently, bone marrow (BM) and hematopoietic stem cell (HSC) transplantation have been shown to preserve kidney function in nephropathic cystinosis, the most frequent cause of RFS in children (10,11). Cystinosis (MIM #219800) is caused by autosomal recessive mutations in the *CTNS* gene, which encodes cystinosin, a lysosomal cystine-proton cotransporter exporting cystine into the cytosol. Functional loss of cystinosin results in lysosomal accumulation of cystine crystals leading to progressive dysfunction of multiple organs including the kidney. Children with nephropathic cystinosis, the most severe and frequent form of cystinosis, develop PT dysfunction and RFS before 1 year of age, often followed by chronic kidney disease (CKD) (12). Healthy BM-derived cells decreased cystine levels in the kidneys of diseased mice and improved several serum and urinary parameters in relation to the level of engraftment (11). Subsequently, *in vitro* studies suggested that vesicular cross-correction mediated by transfer of cystinosin-bearing lysosomes could sustain the correction (13,14). Whether BM transplantation could improve the epithelial phenotype in other congenital defects of the endolysosomal pathway - in particular those that are not associated with lysosomal storage - is unknown. Furthermore, the mechanism of rescue, without evidence of target tissue differentiation and replacement of damaged cells, remains a major issue in stem cell transplantation (15).

Based on the encouraging results in cystinosis, we tested the effects of BM transplantation in the well-established *Clcn5*$^{Y/-}$ mouse model of Dent disease and used a co-culture system to analyse the potential mechanisms involved.

RESULTS

Protocol and hematopoietic chimerism

To test whether BM transplantation improves the PT dysfunction associated with Dent disease, we transplanted 10-weeks old ClC-5 knockout (KO) male (*Clcn5*$^{Y/-}$) mice with wild-type (WT) green fluorescent protein (GFP)-expressing BM cells ("treated"). As controls, *Clcn5*$^{Y/-}$ mice were transplanted with KO BM cells from *Clcn5*$^{Y/-}$ mice ("negative controls") and age- and gender-matched WT littermates (*Clcn5*$^{Y/+}$) were transplanted with WT-BM cells ("positive controls") (Fig. 1A). Urine and plasma were collected at baseline (one week prior to transplantation), and then 10 weeks and 16 weeks after transplantation. Since recipients were lethally irradiated per protocol, BM transplantation resulted in full multilineage hematopoietic chimerism in peripheral blood in all mice, as shown by a nearly 100% myeloid and B cell chimerism (Fig. 1B).

Improvement of PT dysfunction in Clcn5$^{Y/-}$ *mice transplanted with BM cells*

As previously described (9,16), *Clcn5*$^{Y/-}$ mice exhibited features of PT dysfunction including polyuria, glycosuria, hypercalciuria and LMW proteinuria (detection of 16kD Clara Cell protein, CC16), as compared to WT littermates at baseline (Table 1).

In order to assess the potential effect of BM transplantation, we analysed markers of PT dysfunction over time in treated vs. negative control *Clcn5*$^{Y/-}$ mice (Fig. 2; Table 1). Over the 16-week observation, the negative controls (*Clcn5*$^{Y/-}$ mice transplanted with KO-BM) showed a significant increase in diuresis and in urinary excretion of CC16, pointing towards progression of the disease over time. In contrast, the transplanted *Clcn5*$^{Y/-}$ mice showed no significant change in diuresis and a significant *reduction* (~30% decrease) in the urinary excretion of CC16. Similarly, glycosuria and calciuria decreased significantly in transplanted animals, while these parameters were unchanged in negative controls. These data show a

significant improvement of PT dysfunction in mice transplanted with WT BM cells compared to negative controls.

The biological effect of BM transplantation was reflected by the engraftment of BM-derived cells into *Clcn5*$^{Y/-}$ kidneys (Fig. 3). The *Clcn5*$^{Y/-}$ mice displayed a significantly higher recruitment of GFP+ BM-derived cells into the kidneys than *Clcn5*$^{Y/+}$ mice, at the mRNA and protein levels and confirmed by immunofluorescence for GFP (Figs. 3A-B).

Recovery of megalin and ClC-5 in kidneys of BM-transplanted Clcn5$^{Y/-}$ mice

Since filtered LMW proteins are reabsorbed by receptor-mediated endocytosis in PT cells, the reduced urinary loss of CC16 in transplanted mice suggests that the endocytic machinery is at least partially recovered. To test this hypothesis, we investigated the expression level of megalin in the kidneys (Fig. 4). Contrasting with the major, selective loss of megalin expression observed in control *Clcn5*$^{Y/-}$ vs. *Clcn5*$^{Y/+}$ kidneys, a strong rescue of megalin expression was detected by Western blot in *Clcn5*$^{Y/-}$ kidneys of mice transplanted with WT BM cells (Fig. 4A). The rescue of megalin was specific, since the expression of aquaporin-1 (AQP1) and the endosome catalyst Rab5 remained unchanged in all treatment groups. Of note, bone marrow transplantation had no effect on protein expression in any genotype.

The rescue of megalin was confirmed by immunofluorescence staining of kidneys in BM-transplanted mice (Fig. 4B). Whereas almost no megalin staining could be detected in *Clcn5*$^{Y/-}$ kidneys transplanted with KO BM cells, an appreciable rescue of megalin was observed in the brush border of PT cells in *Clcn5*$^{Y/-}$ kidneys transplanted with WT BM cells. In parallel, a significant rescue of ClC-5 expression was observed in *Clcn5*$^{Y/-}$ kidneys of mice transplanted with WT BM cells, as shown by immunoblot (Fig. 4A) and qPCR (Fig. 4C). The rescued ClC-5 in treated *Clcn5*$^{Y/-}$ kidneys was confirmed by immunofluorescence staining at the brush border of PT cells (Fig. 4B) and - at high magnification - in subapical vesicles reminiscing of endosomes (Suppl. Fig. 1A). The staining for ClC-5 was partially overlapping

with that of megalin in PT cells (Suppl. Fig. 2). Of note, the degree of LMW proteinuria (monitored by the urinary loss of CC16) in the treated *Clcn5*$^{Y/-}$ mice inversely correlated with the level of ClC-5 mRNA rescued in the kidneys (Fig. 4C).

Engrafted cells are mononuclear phagocytes that closely associate to PT cells

To further investigate the mechanisms driving the improvement in PT dysfunction, we analysed the location and identity of the BM-derived cells in *Clcn5* $^{Y/-}$ kidneys. Besides the fact that more BM-derived cells engrafted to the *Clcn5*$^{Y/-}$ vs. *Clcn5*$^{Y/+}$ kidneys (Fig. 3), the engrafted cells also showed a distinct distribution pattern. In *Clcn5*$^{Y/-}$ kidneys, the transplanted cells were found to be clustering around PT profiles, in close contact with PT cells, whereas in *Clcn5*$^{Y/+}$ kidneys the transplanted cells were interspersed in the interstitium without clear contact with PT sections (Fig. 5A). The different locations were confirmed by automated confocal image analysis, showing a lower average distance of GFP+ cells from PT cells in *Clcn5*$^{Y/-}$ vs. *Clcn5*$^{Y/+}$ kidneys, respectively (Fig. 5A).

The nature of the engrafted cells was then assessed (Fig. 5B). All transplanted GFP+ cells were found in the interstitium. Since we transplanted a whole BM cell suspension, i.e. a mixture of HSCs, mesenchymal stromal cells (MSCs), differentiated lymphocytes and myeloid cells as well as their immature precursors, the engrafted cells may theoretically derive from MSCs present in the suspension. Such cells do not migrate into healthy tissues, but upon irradiation injury, increased recruitment into peripheral organs has been observed (17). In case of acute injury, MSCs have been recruited to the kidneys where they may persist for a long time (18). However, with their characteristic protrusions, the GFP-expressing cells phenotypically resembled dendritic cells (DCs) or macrophages rather than MSC-derived cells, which would be spindle-shaped and compact. As DCs and macrophages further possess overlapping functions during steady state in the kidney, these cells are often referred to as "mononuclear phagocytes" (19). We confirmed this identity by staining the kidney sections

for CD45, CD11c (DC marker) and F4/80 (macrophage marker) (Fig. 5B). Co-staining of these markers with GFP allowed the conclusion that these cells originated from the hematopoietic lineage. Conversely, there was no overlap between the GFP cells and the fibroblast marker α-SMA (Fig. 5B). Furthermore, the engraftment efficiency of WT GFP+ BM cells and KO BM cells in *Clcn5*$^{Y/-}$ kidneys was similar as shown in Suppl. Fig. 3.

Rescue of receptor-mediated endocytosis in co-culture system

In order to substantiate the rescue of PT function as observed *in vivo*, we established a co-culture system based on primary cultures of PT cells (mPTCs) obtained from microdissected PT segments of *Clcn5*$^{Y/-}$ kidneys (20). These cells were then co-cultivated for 2 days with BM-derived DCs/macrophages (BM-DC/MΦ). These BM-DC/MΦ were generated by stimulating either WT (GFP+) or KO BM cells for 7 days with granulocyte-macrophage colony-stimulating factor (GM-CSF, 30ng/mL), resulting in a mixed population of adherent phagocytic cells (Fig. 6A). Fully differentiated BM-DC/MΦ expressed CD45 and F4/80 (Fig. 6B) as well as ClC-5 and megalin (Suppl. Fig. 1B). During the differentiation process of freshly isolated BM cells into BM-DC/MΦ, gradual upregulation of mRNA encoding for ClC-5 (*Clcn5*), for the macrophage/DC markers F4/80 (*Adgre1*), CD45 (*Ptprc*), CD11c (*Itgax*), and for the tunelling nanotube markers myosin Va (*Myo5a*) and Msec (*Tnfaip2*) was observed (Fig. 6C).

Immunofluorescence staining revealed that, in comparison with *Clcn5*$^{Y/-}$ mPTCs co-cultivated with KO BM-DC/MΦ, co-culture of *Clcn5*$^{Y/-}$ mPTCs with WT BM-DC/MΦ showed a rescue of megalin and ClC-5 expression, particularly evident in mPTCs close to GFP+ cells (Fig. 7A, upper panel). The recovery of megalin and ClC-5 expression was confirmed by Western blot (Fig. 7A, lower panel), with a functional counterpart based on albumin (Alexa 647-BSA) uptake by the *Clcn5*$^{Y/-}$ mPTCs (Fig. 7B). Compared to the very low level observed in *Clcn5*$^{Y/-}$

mPTCs co-cultivated with KO BM-DC/MΦ, there was a significant, ~50% rescue of albumin uptake in *Clcn5*$^{Y/-}$ mPTCs co-cultivated with WT BM-DC/MΦ, although this was still lower than the uptake by *Clcn5*$^{Y/+}$ mPTCs co-cultivated with WT BM-DC/MΦ (Fig. 7B).

Nanotubes mediate the interaction between transplanted BM-derived cells and PT cells

We finally investigated potential rescue mechanisms of PT dysfunction by the transplanted BM cells. Visualization of GFP allowed to evidence, both *in vivo* (Fig. 8A, panels a-d) and *in vitro* (Fig. 8A, panels e-g), the existence of cellular prolongations between the GFP+ BM-derived cells and PT cells from the *Clcn5*$^{Y/-}$ kidneys. These cellular prolongations resemble the tunnelling nanotubes that form intracellular bridges supporting the microtubule-mediated transfer of intracellular components, as previously described in BM transplantation experiments (14,21). Immunostaining experiments revealed that the GFP+ BM-derived cells established multiple contacts with PT cells in the *Clcn5*$^{Y/-}$ kidneys (Fig. 8A, panel b), and that the nanotubes crossed the collagen IV-positive tubular basement membrane to establish direct contact with PT cells (Fig. 8A, panels c-d). In co-culture experiments, multiple tunneling nanotubes positive for tubulin were identifed between GFP+ BM BM-DC/MΦ cells and mPTCs derived from *Clcn5*$^{Y/-}$ mice (Fig. 8A, panels e-g). A few GFP+ structures were also detected in PT cells in transplanted kidneys and in mPTCs in co-culture (Suppl. Fig. 4).

To explore the role of these nanotubular formations in the rescue mechanism, we blocked their formation by treating the mPTCs with the actin-depolymerising agent Latrunculin B (21). This treatment prevented the development of cellular prolongations (Fig. 8B), as well as the rescue of megalin and ClC-5 expression (Fig. 8C) and the recovery of endocytosis activity (Alexa 647-BSA uptake) in co-cultures of GFP+ BM-derived cells with *Clcn5*$^{Y/-}$ mPTCs (Fig. 8B). Furthermore, when the *Clcn5*$^{Y/-}$ mPTCs were separated from the GFP+ BM-derived cells by using a transwell porous insert, we could not observe any rescue of the

endocytic activity (Fig. 8D). Taken together, these data suggest that the establishment of a direct contact between transplanted BM-derived cells and diseased PT cells, via tunnelling nanotubes, plays a key role in the rescue.

DISCUSSION

The results presented here demonstrate, for the first time, that BM transplantation may rescue the epithelial phenotype caused by a genetic defect in an endosomal transporter. Transplantation of WT *Clcn5*$^{Y/+}$ BM cells to *Clcn5*$^{Y/-}$ mice significantly reduced the progression of LMW proteinuria, glycosuria, calciuria and polyuria, compared to *Clcn5*$^{Y/-}$ mice transplanted with KO *Clcn5*$^{Y/-}$ BM. The BM-derived cells differentiated into mononuclear phagocytes engrafted into the interstitium, surrounding PT cells to which they connected via nanotubular prolongations. The rescue of the epithelial phenotype is reflected by the recovery of ClC-5 and megalin expression in PT cells of *Clcn5*$^{Y/-}$ mice. Co-culture of *Clcn5*$^{Y/-}$ derived PT cells with WT BM-derived cells confirmed the recovery of ClC-5 and megalin and that of receptor-mediated endocytosis. The rescue was abolished when the formation of tunneling nanotubes was prevented *in vitro*.

Whereas the value of BM and HSC transplantation is clearly established for malignant and genetic diseases of the hematopoietic system (e.g. acute leukemia, sickle cell disease or severe combined immunodeficiency), it has also been successfully used for certain types of lysosomal storage diseases (LSDs). LSDs are a group of diseases that are characterized by enzyme deficiency in lysosomes, resulting in substrate accumulation and subsequent cellular dysfunction. Here, healthy cells derived from the transplanted hematopoietic system can engraft into various organs and through the close proximity with diseased cells, they can replace defective enzymes by secretion. In Hurler Syndrome (type 1 mucopolysaccharidosis) for example, HSC transplantation is being performed in patients for more than 30 years (22). Cystinosis is also a LSD, caused by the functional loss of the lysosomal transporter cystinosin, resulting in the accumulation of cystine crystals in multiple tissues and cell types. The seminal studies of Cherqui and colleagues have demonstrated the long-term renal protection conferred by BM and HSC transplantation in cystinosis (10,11). The main effect of

transplantation was the reduction of cystine crystals in tissues, while improvement of kidney function parameters were only modest without evidence for rescue of PT endocytic capacity (10,11). The effects were directly related to the number of phagocytic cells that engrafted in the kidneys (11).

Here, we tested the effect of BM transplantation in Dent disease, a paradigm of congenital epithelial disorder caused by the loss of a vesicular (endosomal) transporter. Dent disease is particularly suited for an intervention protocol, as the defective endocytic uptake by PT cells is readily monitored by the detection of LMW proteins in urine, the most consistent feature of the disease in man and mouse (5,6,23). Transplantation of healthy BM significantly altered the progression of PT dysfunction in *Clcn5*$^{Y/-}$ mice, as manifested most prominently in the decreased loss of CC16 in urine. This effect was related to the engraftment of BM-derived cells differentiated into monocluclear phagocytes, based on their co-expression of F4/80, CD11c and CD45. These cells are known to play a role in tissue homeostasis, e.g. by maintaining tolerance to renal antigens or by clearing apoptotic cells (19). The absence of GFP cells in PT profiles excludes the replacement of damaged tubular cells by BM-derived cells in this model.

The engraftment of BM-derived mononuclear phagocytes resulted in a partial rescue of ClC-5 and megalin expression in the *Clcn5*$^{Y/-}$ kidneys, with proper expression of the receptor and the endosomal transporter in the apical membrane and sub-apical domain of PT cells. This observation provides a mechanistic basis for the rescue of endocytosis observed in *Clcn5*$^{Y/-}$ mice. We showed previously that there is no transcriptional defect of megalin in *Clcn5*$^{Y/-}$ kidneys. Instead, the deletion of ClC-5 causes a trafficking defect reflected by the loss of megalin from the brush border (9). Thus, the transfer of a certain amount of functional ClC-5 and/or megalin (protein or mRNA) to PT cells could be sufficient to rescue megalin expression and receptor-mediated endocytosis (and potentially other apical transport systems

such as NaPi-IIa). Peritoneal macrophages are known to express ClC-5 (24), as do the differentiated BM-derived cells used here - suggesting that the transplanted BM cells express ClC-5 when acquiring their tissue-resident phenotype. This might explain the significant increase of *Clcn5* mRNA and ClC-5 protein expression in PT cells of *Clcn5*$^{Y/-}$ mice transplanted with *Clcn5*$^{Y/+}$ BM compared to controls. The possibility that low-level ClC-5 expression may rescue megalin targeting in PT cells and sustain some level of endocytic uptake is supported by the inverse correlation between rescued *Clcn5* gene expression in the *Clcn5*$^{Y/-}$ kidneys and the level of LMW proteinuria. The fact that the decrease in urinary CC16 does not exactly match the rescue of megalin and ClC-5 protein expression is not really surprising when considering the complexity of receptor-mediated endocytosis, with multiple steps including - but not limited to - those involving megalin and ClC-5. These observations made *in vivo* are supported by the *in vitro* system based on the co-culture of primary PT cells derived from *Clcn5*$^{Y/-}$ kidneys and GFP+ BM cells obtained from *Clcn5* WT and KO mice. The primary cultures of mouse PT cells (mPTCs) have been shown to retain their differentiation and the PT features observed *in vivo* (25,26), whereas prior exposure of the BM cells to GM-CSF resulted in their differentiation into functional mononuclear phagocytes expressing ClC-5 and megalin. The subsequent 2-day co-culture confirmed the rescue of megalin and ClC-5 expression, mirrored by the partial recovery of endocytosis.

What could be the mechanism driving the rescue of ClC-5 and megalin expression in the *Clcn5*$^{Y/-}$ PT cells, resulting in the improved phenotype *in vivo* and *in vitro*? The close proximity between transplanted BM-derived cells and PT cells as well as the rescue of ClC-5 and megalin expression in the latter support the hypothesis of a cell-to-cell transfer of material between the two cell types. We evidenced a higher recruitment of BM-derived cells into the *Clcn5*$^{Y/-}$ kidneys compared to the *Clcn5*$^{Y/+}$ controls, with transplanted cells surrounding PT profiles and establishing close contacts with PT cells. Chronic injury is a pre-requisite to stimulate the long-term engraftment of BM-derived cells to the kidneys (27),

suggesting that a homing factor may attract transplanted cells close to diseased PT cells. In general, intercellular communication can be achieved by paracrine and endocrine signaling, transfer of extracellular vesicles, and cell-to-cell contact mechanisms including tunneling nanotubes (28,29). The tunneling nanotubes are dynamic, F-actin based tubular connections that allow communication between relatively distant cells. They operate between various cell types, with a heterogeneous structure reflecting distinct functions. In particular, relatively thick (diameter >0.7 μM) tunneling nanotubes containing microtubules have been described in macrophages and other cell types (30), with an ability to transfer several types of cargo including vesicles derived from endosomes, plasma membrane components, as well as cytoplasmic molecules (29). Recent co-culture experiments showed that tunneling nanotubes produced by macrophages and extending into fibroblasts mediate a vesicular exchange able to correct the lysosomal defect in cystinosis (14). Such macrophage-derived tubular extensions have also been evidenced *in vivo*, penetrating the tubular basement membrane and delivering cystinosin-containing lysosomes into PT cells (14).

We observed similar nanotubular extensions between GFP+ BM-derived cells closely surrounding *Clcn5*$^{Y/-}$ PT cells *in vivo* and *in vitro*, with multiple contact points between the transplanted cells and PT cells (Fig. 8). It must be noted that the differentiated BM-derived cells expressed M-sec, a central factor in the induction of plasma membrane protrusion during tunnelling nanotube formation (31), as well as myosin Va, a motor protein that facilitates organelle transport in tunnelling nanotubes (28). Conversely, no rescue of ClC-5 and megalin, and no improvement of albumin endocytosis were observed when the cells are separated by a transwell insert system or when the formation of tunneling nanotubes is prevented by treatment with Latrunculin B - an actin-depolymerizing drug known to inhibit the development of cell-to-cell connections (30). Taken together, these results suggest that the establishment of a direct contact between transplanted mononuclear phagocytes and PT

cells, via tunnelling nanotubes, may enable the transfer of ClC-5 mRNA or protein into *Clcn5*$^{Y/-}$ PT cells, partially rescuing the PT phenotype.

In summary, these data provide the first demonstration that BM transplantation may rescue the epithelial phenotype due to an inherited endosomal defect, through direct contacts between transplanted BM-derived cells and diseased proximal tubular cells.

MATERIAL AND METHODS

Clcn5 mouse model of Dent disease. *Clcn5* mice were generated by deletion of exon VI of *Clcn5* and have been extensively characterized as a faithful model of Dent disease (9,16). ClC-5 KO males *($Clcn5^{Y/-}$)* and WT littermate controls ($Clcn5^{Y/+}$) on pure C57BL/6 background were used for experiments. BM donors expressed an enhanced GFP under the direction of the human ubiquitin C promotor (UBC-GFP), leading to ubiquitous GFP expression in all cells (The Jackson Laboratory, Bar Harbor, ME, USA). All BM donor mice were on C57BL/6 background and only males were used. Mice were bred and housed under specific pathogen-free conditions at University of Zurich, and all animal experiments were performed according to protocols approved by the local legal authority (Veterinary office, Canton of Zürich, Switzerland).

Bone marrow transplantation. The *Clcn5* littermates were lethally irradiated (900cGy) with a Cs source and reconstituted approximately 6 h later by tail vein injection of 10x 10^6 unfractionated BM cells suspended in Media 199 containing 10 mM HEPES, 10 µg/ml DNAse and 4 µg/ml Gentamycin. BM cells were either isolated from UBC-GFP or $Clcn5^{Y/-}$ donors aged 8-14 weeks. Recipients were randomly distributed among treatment groups and transplanted at the age of 10 weeks. Peripheral blood multilineage chimerism was measured by FACS at the time of harvest. Cells were stained for CD4, CD8, CD11b and B220 and acquired at FACS Canto II or LSRII Fortessa.

Urine and plasma collections. Urine samples were collected overnight in metabolic cages with *ad libitum* access to food and drinking water one week prior BM transplantation and 10 and 16 weeks after transplantation. Urinary calcium, glucose, and creatinine were measured with a Synchron CX3 Delta System (Beckman Coulter, Nyon, Switzerland) and urinary CC16 was measured by an enzyme-linked immunosorbent assay kit (Biomatik, Wilmington, DE, USA).

Kidney sampling. Mice were anesthetized using an isoflurane vaporizer and perfused through the right ventricle with a 0.9% NaCl solution containing heparin (5000 U/ml), 1% Procain-HCL (Lidocain) and 16% $CaCl_2$. Then, the left kidney was clamped and the right kidney fixed by infusion of 3% PFA dissolved in 0.1M Na-cacodylate. One half of the unfixed kidney was used for protein isolation and the other half for RT-qPCR analysis. The fixed

kidney was kept for 1h in 3% PFA on ice, then in 1% PFA overnight. After washing in PBS and soaking in 30% sucrose, the kidneys were embedded in Tissue-Tek OCT medium (VWR, Radnor, PA, USA).

Isolation and primary cultures of mouse PT cells. Primary cultures of mouse PT cells (mPTCs) were prepared from gender-matched *Clcn5*$^{Y/-}$ mice transplanted with KO-BM cells or GFP-BM cells, and from *Clcn5*$^{Y/+}$ mice transplanted with GFP+ BM cells as described previously (20,25,26). Confluent monolayers of mPTCs expanded from the tubular fragments after 6–7 days. All experiments were performed on non-passaged, confluent monolayers grown on collagen-coated filters.

Cultures of BM cells and co-culture experiments. BM cells were isolated from femurs of GFP-expressing *Clcn5*$^{Y/+}$ mice and of *Clcn5*$^{Y/-}$ mice and were differentiated in the presence of the granulocyte-macrophage colony-stimulating factor (GM-CSF, 30ng/mL) for 7 days, as previously described (32).

For contact co-culture assays, 1×10^5 mPTCs were plated with 1×10^5 GFP+ or KO BM-derived cells in 10 cm culture dishes. Cells were incubated for 2 days at 37°C, harvested using trypsin, pelleted and resuspended in PBS with 2% FBS.

For the Latrunculin B assay, 1×10^5 mPTCs were seeded with 1×10^5 GFP+ or KO BM-derived cells in 24 well-plates (Corning Life Sciences) in presence of 5 μM of Latrunculin B (Sigma, St. Louis, MO, USA) for 2 days at 37°C as previously described (33). The albumin endocytic assay was performed (see below) and the cells were further processed for immunofluorescence staining.

For the transwell co-culture assay, mPTCs were seeded onto top of collagen-coated PTFE filter membranes (0.33 cm^2, pore size 0.4 μm, Transwell-COL™, Costar™, Corning Life Sciences) and GFP+ BM-derived cells were plated on the basolateral side of collagen coated 24-well plates for 2 days at 37°C. The albumin endocytic assay was then performed on the mPTCs and the cells were processed for immunofluorescence staining.

Albumin endocytic uptake. The endocytosis assay was performed on monolayers of mPTCs as described previously (26). Briefly, monolayers of mPTCs were incubated with either 0.5 mg/mL Alexa 488- BSA or Alexa 647-BSA (both from Thermo Fischer Scientific, Watham, MA, USA) for 15 min at 37°C. After the incubation, primary cultures were washed and fixed in 4% PFA and and counterstained with 10 μM Hoechst 33342 (H1399; Thermo Fischer

Scientific). The slides were mounted in Prolong Gold Anti-fade reagent (P36930; Thermo Fisher Scientific), acquired on Leica SP5 confocal laser scanning microscope (Leica, Heerbrugg, Switzerland). Quantitative image analysis was performed by selecting randomly 2-4 fields containing ~ 50 cells, using the same setting parameters (i.e. laser power, offset gain and detector amplification below pixel saturation). The number of albumin-positive vesicles was performed using AnalySIS software (Soft Imaging Systems GmbH, Muenster, Germany).

Quantitative real-time PCR. Total RNA was extracted from kidney using the Aurum™ Total RNA Fatty and Fibrous Tissue Kit (Bio-Rad, Hercules, CA, USA) according to manufacturer's protocol. DNAse I treatment was performed to eliminate genomic DNA contamination. 1 μg of RNA was used to perform the reverse transcriptase reaction with iScript™ cDNA Synthesis Kit (Bio-Rad). Changes in target gene mRNA levels were determined by relative RT-qPCR with a CFX96™ Real-Time PCR Detection System (Bio-Rad), using iQ™ SYBR Green Supermix (Bio-Rad). RT-qPCR analyses were performed in duplicate. Specific primers were designed using Primer3 (http://simgene.com/Primer3) (Suppl. Table 1). PCR conditions were 95°C for 3 min followed by 40 cycles of 15 sec at 95°C, 30 sec at 60°C.The PCR products were sequenced with the BigDye terminator kit (Perkin Elmer Applied Biosystems, Thermo Fischer Scientific). The efficiency of each set of primers was determined by dilution curves (Suppl. Table 1). The relative changes in target over *Gapdh* mRNAs was calculated using $2^{\Delta ct}$ formula.

Antibodies. The following antibodies were used: rabbit anti-GFP (Thermo Fischer Scientific), goat anti-GFP (Sicgen Research and Development in Biotechnology, Carcavelos, Portugal), rabbit anti-AQP1 (Millipore, Temecula, California, USA), rabbit anti-Napi-IIa (gift from C.A. Wagner, University of Zurich), sheep anti-megalin (a gift from Dr. P. Verroust and Dr. R. Kozyraki, Paris), rabbit anti-ClC-5 (gift from J. Loffing, University of Zurich), rat anti-F4/80 (ABD Serotec Bio-Rad, Puchheim, Germany), hamster anti-CD11c (Bio-Rad), rat anti-CD45 (Bio-Rad), rabit anti-α-SMA (Abcam, Cambridge, UK), mouse anti-β-actin (Sigma-Aldrich), rabbit anti-Rab5 (Abcam), mouse anti-α-tubulin (Sigma-Aldrich), rabbit anti-collagen IV antibody (Abcam, Cambridge, UK). Secondary antibodies were labelled with Alexa488, Alexa633 or Dylight649.

Immunofluorescence and confocal microscopy. Six-µm mouse kidney sections were quenched with 50 mM NH_4Cl, blocked with 0.5% BSA in PBS Ca/Mg (D1283; Sigma-Aldrich) for 30 min and stained with primary antibodies diluted in blocking buffer overnight at 4°C. After two washes in 0.1% Tween 20 (v/v in PBS), the slides were incubated with corresponding fluorophore-conjugated secondary antibodies (Invitrogen, Thermo Fischer Scientific) diluted in blocking buffer at room temperature for 1 h and counterstained with 10 µM Hoechst 33342 (H1399; Thermo Fischer Scientific). The slides were mounted in Prolong Gold Anti-fade reagent (P36930; Thermo Fisher Scientific), acquired on Leica SP5 confocal laser scanning microscope. Quantitative image analysis was performed by selecting randomly ~3 visual fields per each slide that included at least 2-4 PT sections, using the same setting parameters. The number of GFP-positive cells per mm^2 was quantified by means of the Volocity software (I40250; PerkinElmer, Waltham, MA, USA) and the distance of GFP-positive cells from PT cells (megalin-positive brush border membrane) was measured using the Huygens software (Scientific Volume Imaging, Hilversum, The Netherlands).
The cells were fixed for 10 min in 4% paraformaldehyde (Sigma-Aldrich,) in PBS, permeabilized and quenched for 30 min in blocking buffer (50 mM NH4Cl, 0.1% (w/v) saponin, 3% (w/v) BSA in PBS). The cells were then incubated 2 h with the primary antibody, washed six times in PBS, incubated for 1 h with the Alexa-labelled secondary antibody and mounted on Vectashield covered coverslips (Vector Laboratories, Burlingame, CA, USA) to be acquired on Leica SP5 confocal laser scanning microscope (Leica).

Immunoblotting. Proteins were extracted from frozen kidneys lysed in RIPA buffer (Sigma) containing protease inhibitors (Roche Diagnostics, Mannheim, Germany), followed by a brief sonication and centrifugation at 16'000xg for 1min at 4°C. Protein concentration was determined using the Pierce BCA protein assay (Thermo Fischer Scientific). Immunoblotting and quantification of the signals were performed as described previously (25,26).

Statistics. The effect of BM transplantation was analyzed by comparing parameters by Kruskal Wallis, Mann Whithney or Wilcoxon signed rank tests, as indicated. Differences between unpaired groups were assessed using Mann-Whitney test, and correlation between *Clcn5* mRNA expression and urinary loss of CC16 were assessed with GraphPad Prism. $P<0.05$ was considered significant, *$P<0.05$; **$P<0.01$; ***$P<0.001$; NS, not significant.

Disclosure statement: The authors state that they do not have any interest to disclose in relation with this manuscript.

REFERENCES

1. De Matteis MA, Luini A. Mendelian disorders of membrane trafficking. New Engl J Med. 2011; **365**: 927-938.

2. Eckardt KU, Coresh J, Devuyst O, et al. Evolving importance of kidney disease: from subspecialty to global health burden. Lancet. 2013; **382**: 158-169.

3. Nielsen R, Christensen EI, Birn H. Megalin and cubulin in PT protein reabsorption: from experimental models to human disease. Kidney Int. 2016; **89**: 58-67.

4. Devuyst O, Igarashi T. Renal Fanconi Syndrome, Dent's Disease and Bartter's Syndrome. In: Thakker RV, Whyte MP, Eisman JA, Igarashi T, eds. Genetics of Bone Biology and Skeletal Disease. 2nd ed. Elsevier Inc., Amsterdam; 2015: 553-567.

5. Devuyst O, Thakker RV. Dent's disease. Orphanet J Rare Dis. 2010; **5**: 28.

6. Devuyst O, Christie PT, Courtoy PJ, et al. Intra-renal and subcellular distribution of the human chloride channel, CLC-5, reveals a pathophysiological basis for Dent's disease. Hum Mol Genet. 1999; **8**: 247-257.

7. Stauber T, Jentsch TJ. Chloride in vesicular trafficking and function. Annu Rev Physiol. 2013; **75**: 453-477.

8. Piwon N, Gunther W, Schwake M, et al. ClC-5 Cl- -channel disruption impairs endocytosis in a mouse model for Dent's disease. Nature. 2000; **408**: 369-373.

9. Christensen EI, Devuyst O, Dom G, et al. Loss of chloride channel ClC-5 impairs endocytosis by defective trafficking of megalin and cubilin in kidney proximal tubules. Proc Natl Acad Sci U S A. 2003; **100**: 8472-8477.

10. Syres K, Harrison F, Tadlock M, et al. Successful treatment of the murine model of cystinosis using bone marrow cell transplantation. Blood. 2009; **114**: 2542-2552.

11. Yeagy BA, Harrison F, Gubler MC, et al. Kidney preservation by bone marrow cell transplantation in hereditary nephropathy. Kidney Int. 2011; 79: 1198-1206.

12. Gahl WA, Thoene JG, Schneider JA. Cystinosis. N Engl J Med. 2002; **347**: 111-121.

13. Harrison F, Yeagy BA, Rocca CJ, et al. Hematopoietic stem cell gene therapy for the multisystemic lysosomal storage disorder cystinosis. Mol Ther. 2013; **21**: 433-44.

14. Naphade S, Sharma J, Gaide Chevronnay HP, et al. Lysosomal cross-correction by hematopoietic stem cell-derived macrophages via tunneling nanotubes. Stem Cells. 2015; **33**: 301-309.

15. Pinkernell K. Cellular therapies: what is still missing? Kidney Int. 2011; **79**: 1161-1163.

16. Wang SS, Devuyst O, Courtoy PJ, et al. Mice lacking renal chloride channel, CLC-5, are a model for Dent's disease, a nephrolithiasis disorder associated with defective receptor-mediated endocytosis. Hum Mol Genet. 2000; **9**: 2937-2945.

17. François S, Bensidhoum M, Mouiseddine M, et al. Local irradiation not only induces homing of human mesenchymal stem cells at exposed sites but promotes their widespread engraftment to

multiple organs: a study of their quantitative distribution after irradiation damage. Stem Cells. 2006; **24**: 1020–1029.

18. Morigi M, Imberti B, Zoja C, et al. Mesenchymal stem cells are renotropic, helping to repair the kidney and improve function in acute renal failure. J Am Soc Nephrol. 2004; **15**: 1794-1804.

19. Weisheit CK, Engel DR, Kurts C. Dendritic Cells and Macrophages: Sentinels in the Kidney. Clin J Am Soc Nephrol. 2015; **10**: 1841–1851.

20. Terryn S, Jouret F, Vandenabeele F, et al. A primary culture of mouse proximal tubular cells established on collagen-coated membranes. Am J Physiol Renal Physiol. 2007; **293**: F476-F485.

21. Rustom A, Saffrich R, Markovic I, et al. Nanotubular Highways for intercellular organelle transport. Science. 2004; **303**: 1007-1010.

22. Aldenhoven M, Wynn RF, Orchard PJ, et al. Long-term outcome of Hurler syndrome patients after hematopoietic cell transplantation: an international multicenter study. Blood. 2015; **125**: 2164-2172.

23. Bernard AM, Thielemans NO, Lauwerys RR. Urinary protein 1 or Clara cell protein: a new sensitive marker of proximal tubular dysfunction. Kidney Int. 1994; **47**: S34-37.

24. Alex P, Ye M, Zachos NC, et al. Clcn5 knockout mice exhibit novel immunomodulatory effects and are more susceptible to dextran sulfate sodium-induced colitis. J Immunol. 2010; **184**: 3988–3996.

25. Raggi C, Luciani A, Nevo N, et al. Dedifferentiation and aberrations of the endolysosomal compartment characterize the early stage of nephropathic cystinosis. Hum Mol Genet. 2014; **23**:2266-2278.

26. Luciani A, Sirac C, Terryn S, et al. Impaired lysosomal function underlies monoclonal light chain associated renal Fanconi syndrome. J Am Soc Nephrol. 2016, **27**: 2049-2061.

27. Yeagy BA, Cherqui S. Kidney repair and stem cells: a complex and controversial process. Pediatr Nephrol. 2011; **26**: 1427-1434.

28. Rustom A, Saffrich R, Markovic I, et al. Nanotubular highways for intercellular organelle transport. Science. 2004; **303**: 1007-1010.

29. Abounit S, Zurzolo C. Wiring through tunneling nanotubes-from electrical signals to organelle transfer. J Cell Sci. 2012;**125**: 1089-1098.

30. Abounit S, Delage E, Zurzolo C. Identification and characterization of tunneling nanotubes for intercellular trafficking. Curr Protoc Cell Biol. 2015; 67: 12.10.1-12.10.21.

31. Kimura S, K Hase, Ohno H. The molecular basis of induction and formation of tunnelling nanotubes. Cell Tissue Res. 2013; **352**: 67-76.

32.Madaan A, Verma R, Singh AT, Jain SK, Jaggi M. A stepwise procedure for isolation of murine bone marrow and generation of dendritic cells. J Biol Methods. 2014; **1**: e1.

33. Takahashi A, Kukita A, Li YJ, et al. Tunneling nanotube formation is essential for the regulation of osteoclastogenesis. J Cell Biochem. 2013; **114**: 1238-1247.

ACKNOWLEDGEMENTS

This work was supported by the European Community's Seventh Framework Programme (FP7/2007-2013) under grant agreement n° 305608 (EURenOmics); the Cystinosis Research Foundation (Irvine, CA, USA); the Zurich Center for Integrative Human Physiology (ZIHP); the Swiss National Science Foundation project grant 310030_146490; the KFSP RADIZ (Rare Disease Initiative Zurich) and MINZ (Molecular Imaging Zurich) from the University of Zurich, Zurich, Switzerland.

Table 1. Urine and plasma parameters at baseline and in transplanted *Clcn5*$^{Y/-}$ and *Clcn5*$^{Y/+}$ mice.

Baseline	*Clcn5*$^{Y/-}$		*Clcn5*$^{Y/+}$	P value
	(Negative controls) (n = 8-10)	(Treated) (n = 13-15)	(Positive controls) (n = 6-9)	*Clcn5*$^{Y/-}$ *vs* *Clcn5*$^{Y/+}$
Diuresis (ml/12h)	1.98 ± 0.26*	2.04 ± 0.21*	1.20 ± 0.19	<0.01
U CC16 (mg/g creat)	62.3 ± 4.3	66.7 ± 5.3	ND	ND
U glucose (mg/12h)	1.21 ± 0.15*	1.44 ± 0.14*	0.49 ± 0.06	<0.0001
U Ca^{2+} (mg/g creat)	216 ± 29*	196 ± 12*	83 ± 5	<0.0001
BUN (mg/dl)	24.5 ± 1.2	24.3 ± 1.1	25.1 ± 1.7	NS

Week 10	*Clcn5*$^{Y/-}$ + KO-BM (Negative controls)	*Clcn5*$^{Y/-}$ + GFP-BM (Treated)	*Clcn5*$^{Y/+}$ + GFP-BM (Positive controls)	P value
Diuresis (ml/12h)	4.07 ± 0.64*	4.04 ± 0.84*	1.31 ± 0.19	0.0001
U CC16 (mg/g creat)	66.6 ± 5.5	53.9 ± 6.0	ND	0.087
U glucose (mg/12h)	1.07 ± 0.18*	1.07 ± 0.16*	0.40 ± 0.08	0.0006
U Ca^{2+} (mg/g creat)	160 ± 26	132 ± 13	111 ± 36	0.13
BUN (mg/dl)	26.8 ± 1.7	25.0 ± 1.3	24.1 ± 1.2	0.54

Week 16	*Clcn5*$^{Y/-}$ + KO-BM (Negative controls)	*Clcn5*$^{Y/-}$ + GFP-BM (Treated)	*Clcn5*$^{Y/+}$ + GFP-BM (Positive controls)	P value
Diuresis (ml/12h)	6.04 ± 1.52*	3.36 ± 0.92*	1.03 ± 0.24	0.0002
U CC16 (mg/g creat)	71.2 ± 3.5	46.9 ± 5.1§	ND	0.0031
U glucose (mg/12h)	0.87 ± 0.10*	0.81 ± 0.12*	0.36 ± 0.07	0.0023
U Ca^{2+} (mg/g creat)	146 ± 21*	131 ± 10*	99 ± 31	0.0126
BUN (mg/dl)	24.6 ± 1.4	24.7 ± 0.9	23.4 ± 1.5	0.70

U, urine; CC16, Clara cell protein of 16 kDa; P, plasma; ND, not detected; NS not significant

* P<0.05 vs *Clcn5*$^{Y/+}$ + GFP-BM ; § P<0.05 vs *Clcn5*$^{Y/-}$ + KO-BM

Baseline parameters: Mann Whithney Test (*Clcn5*$^{Y/-}$ *versus Clcn5*$^{Y/+}$); Week 10 and week 16: One way anova non parametric (Kruskal Wallis Test) for all parameters except U CC16 (Mann Whithney Test)

Figure 1

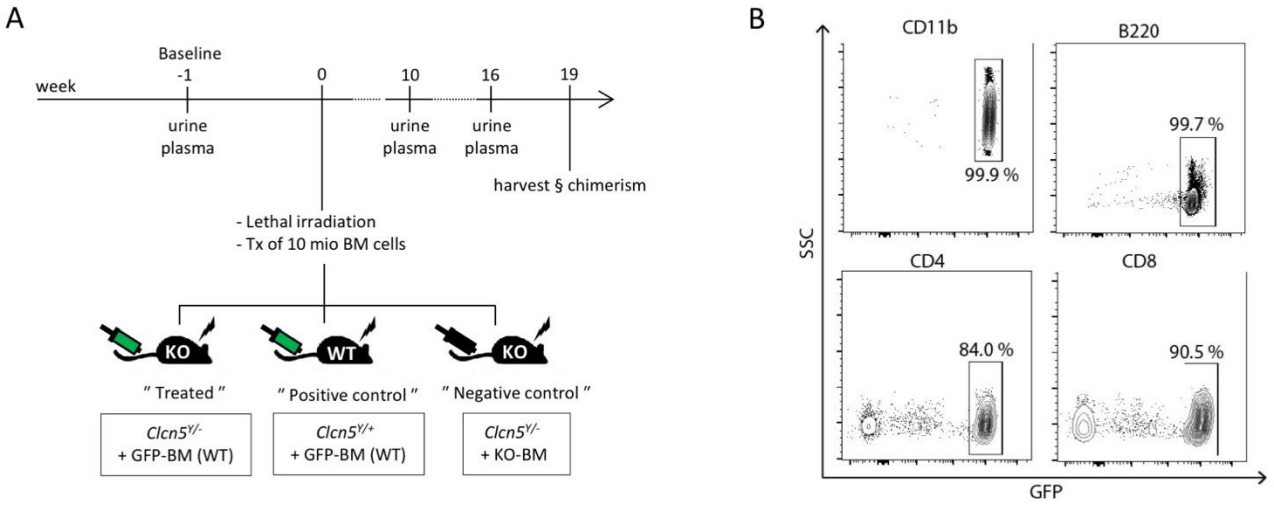

Figure 1: Study design and peripheral blood chimerism.
(A) Experimental setup of the study: *Clcn5*$^{Y/-}$ and *Clcn5*$^{Y/+}$ littermates were transplanted at the age of 10 weeks with either wild-type (WT, *Clcn5*$^{Y/+}$) GFP+ or knock-out (KO, *Clcn5*$^{Y/-}$) BM cells. Baseline blood sampling and urine collection (overnight) were performed the week before BM transplantation as well as 10 weeks and 16 weeks after BM transplantation. **(B)** Lineage-specific peripheral blood chimerism was measured by FACS analysis of GFP+ cells at time of kidney harvest. A nearly 100% myeloid and B cell chimerism was observed.

Figure 2

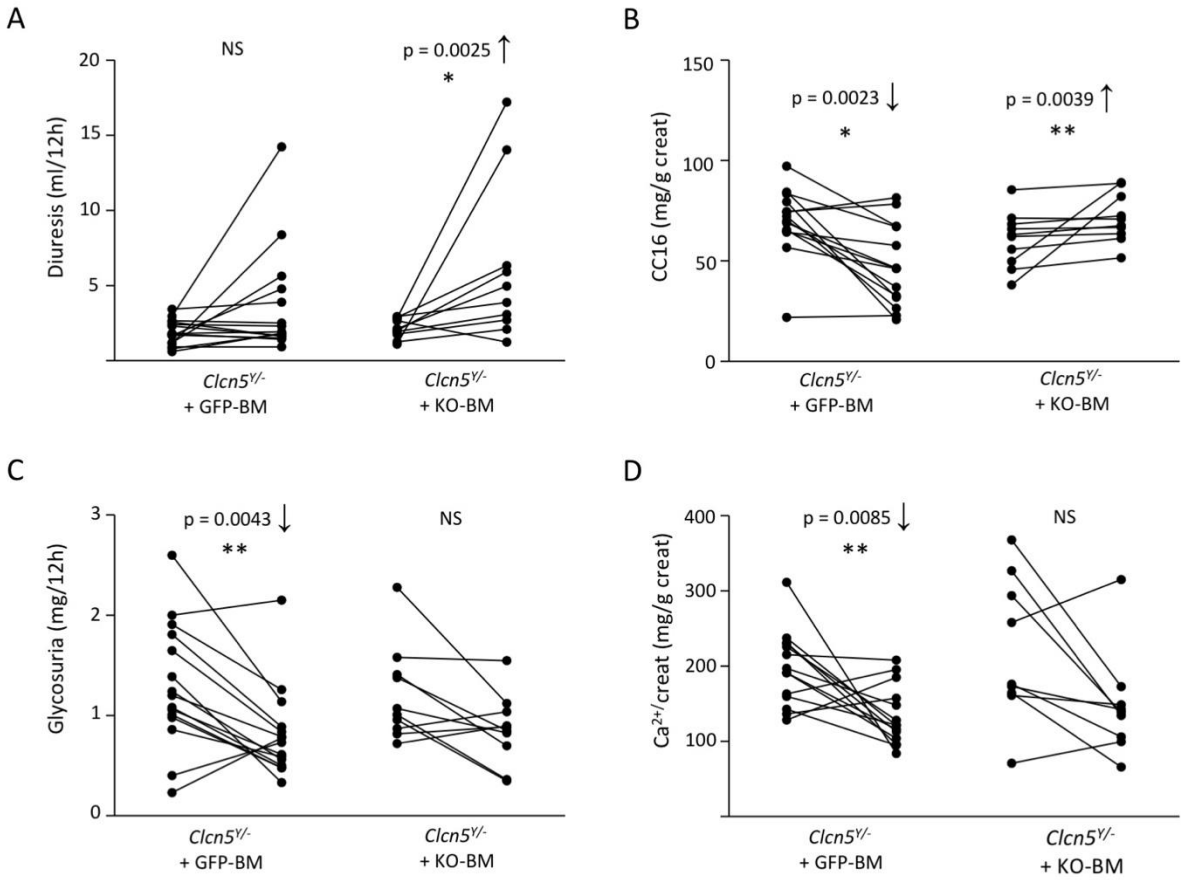

Figure 2: Evolution of urinary parameters after BM transplantation in *Clcn5*$^{Y/-}$ mice.

Evolution (baseline to week 16) of urinary parameters (diuresis, urinary excretion of the LMW protein CC16, glycosuria, calciuria) in *Clcn5*$^{Y/-}$ mice transplanted with either WT (*Clcn5*$^{Y/+}$) GFP+ or KO (*Clcn5*$^{Y/-}$) BM cells. The *Clcn5*$^{Y/-}$ mice transplanted with WT BM cells showed no significant change in diuresis and a significant reduction in the urinary excretion of CC16, glycosuria and calciuria as compared with increased or stable values in *Clcn5*$^{Y/-}$ mice transplanted with KO BM cells. Differences in urinary parameters from baseline to week 16 were assessed with Wilcoxon signed rank test. *P<0.05; **P<0.01; NS, not significant.

Figure 3

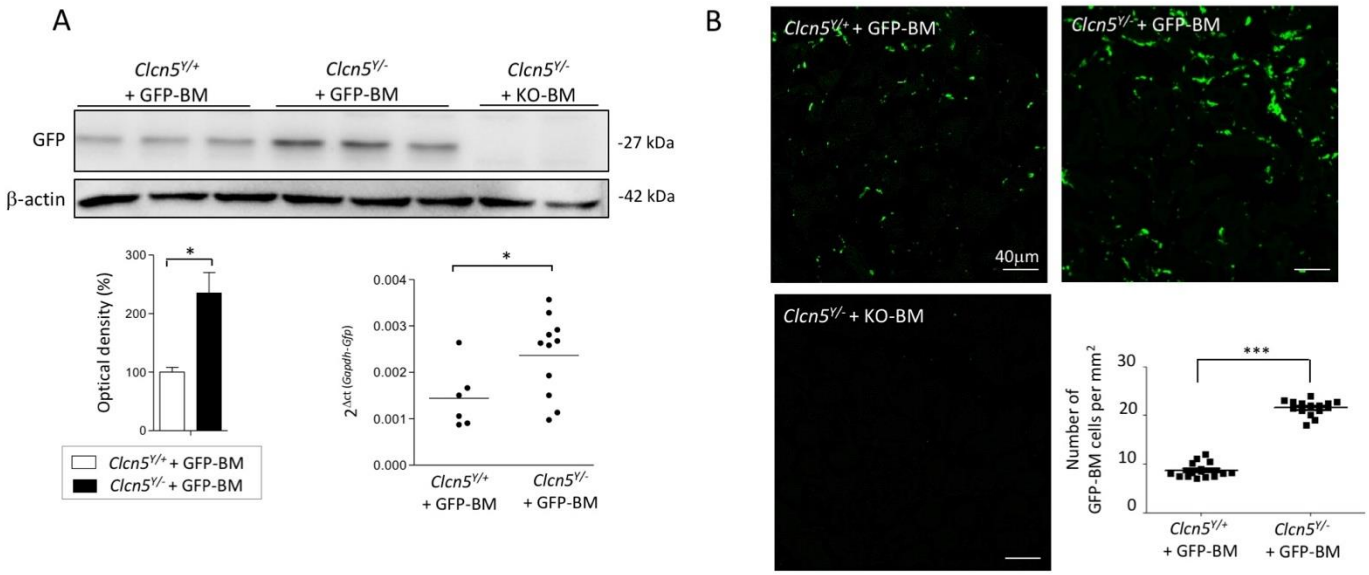

Figure 3: Engraftment of transplanted BM cells in the *Clcn5* kidneys.

(A) Western blot for GFP protein expression in kidney lysates of transplanted *ClCn5*$^{Y/+}$ and *ClCn5*$^{Y/-}$ mice. The lower panels show the densitometry of immunoblot signals and the real-time qPCR analysis of *Gfp* mRNA expression in the *Clcn5*$^{Y/+}$ and *Clcn5*$^{Y/-}$ transplanted kidneys. The engraftment of BM-derived cells is significantly higher in the *Clcn5*$^{Y/-}$ transplanted kidneys. Statistical differences were assessed using the Mann-Whitney test. *P<0.05 **(B)** Confocal microscopy images showing GFP expression in kidneys of *Clcn5*$^{Y/+}$ and *Clcn5*$^{Y/-}$ mice that were transplanted with WT, GFP+ BM cells or KO BM cells. The graph gives the quantification of GFP-BM cells per mm^2. *P<0.05; ***P<0.001.

Figure 4

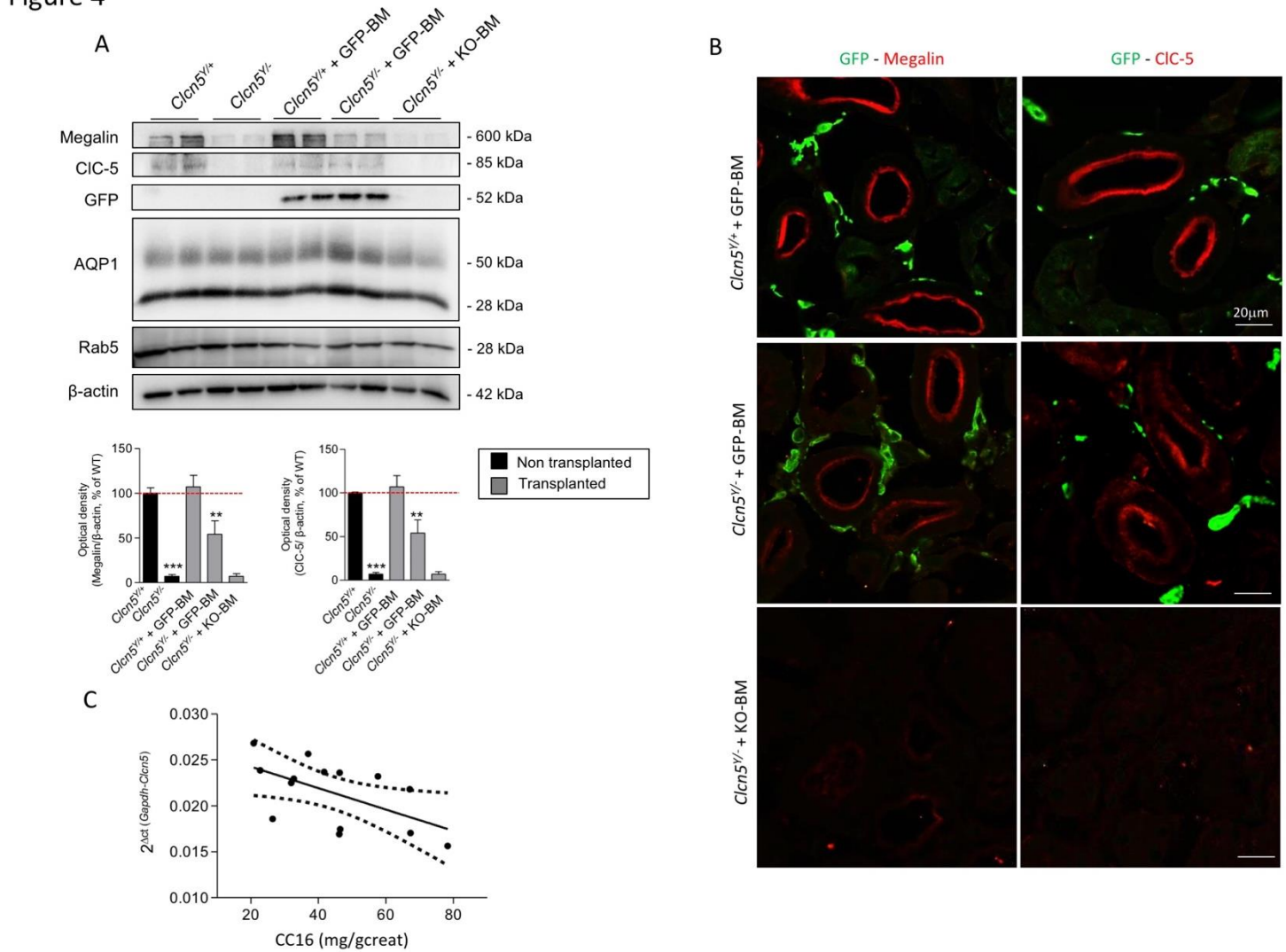

Figure 4: Recovery of megalin and ClC-5 expression in *Clcn5*$^{Y/-}$ kidneys of BM-transplanted mice.

(A) Western blot for megalin, ClC-5, GFP, AQP1 and Rab5 in kidney lysates and quantification of optical density for megalin and ClC-5 in the lower panel. Bone marrow transplantation did not induce unspecific effects on protein expression in *Clcn5*$^{Y/+}$ and *Clcn5*$^{Y/-}$ kidneys. A significant rescue of megalin and ClC-5 was detected in *Clcn5*$^{Y/-}$ kidneys of mice transplanted with WT GFP+ BM cells. n = 4 animals per conditions. ***P<0.001 *vs Clcn5*$^{Y/+}$, **P<0.01 *vs Clcn5*$^{Y/-}$ transplanted with KO-BM cells, Mann-Whitney test. **(B)** Confocal microscopy images showing staining for GFP (green), megalin (red, left panels) and ClC-5 (red, right panels) in *Clcn5*$^{Y/+}$ and *Clcn5*$^{Y/-}$ mice transplanted with WT GFP+ BM cells. Contrasting with the lack of ClC-5 and megalin staining in *Clcn5*$^{Y/-}$ kidneys of mice transplanted with KO BM cells, an appreciable rescue of megalin in the brush border and ClC-5 in the apical region was observed in *Clcn5*$^{Y/-}$ kidneys of mice transplanted with WT BM cells. **(C)** Inverse correlation between the expression of *Clcn5* mRNA in *Clcn5*$^{Y/-}$ kidneys of mice transplanted with WT BM and the levels of urinary CC16. Mann-Whitney test was used to assess difference between treatment groups, and correlation represents a linear regression-model with 95% CI. There was no *Clcn*5 mRNA signal in *ClCn5*$^{Y/-}$ kidneys of mice transplanted with KO BM.

Figure 5

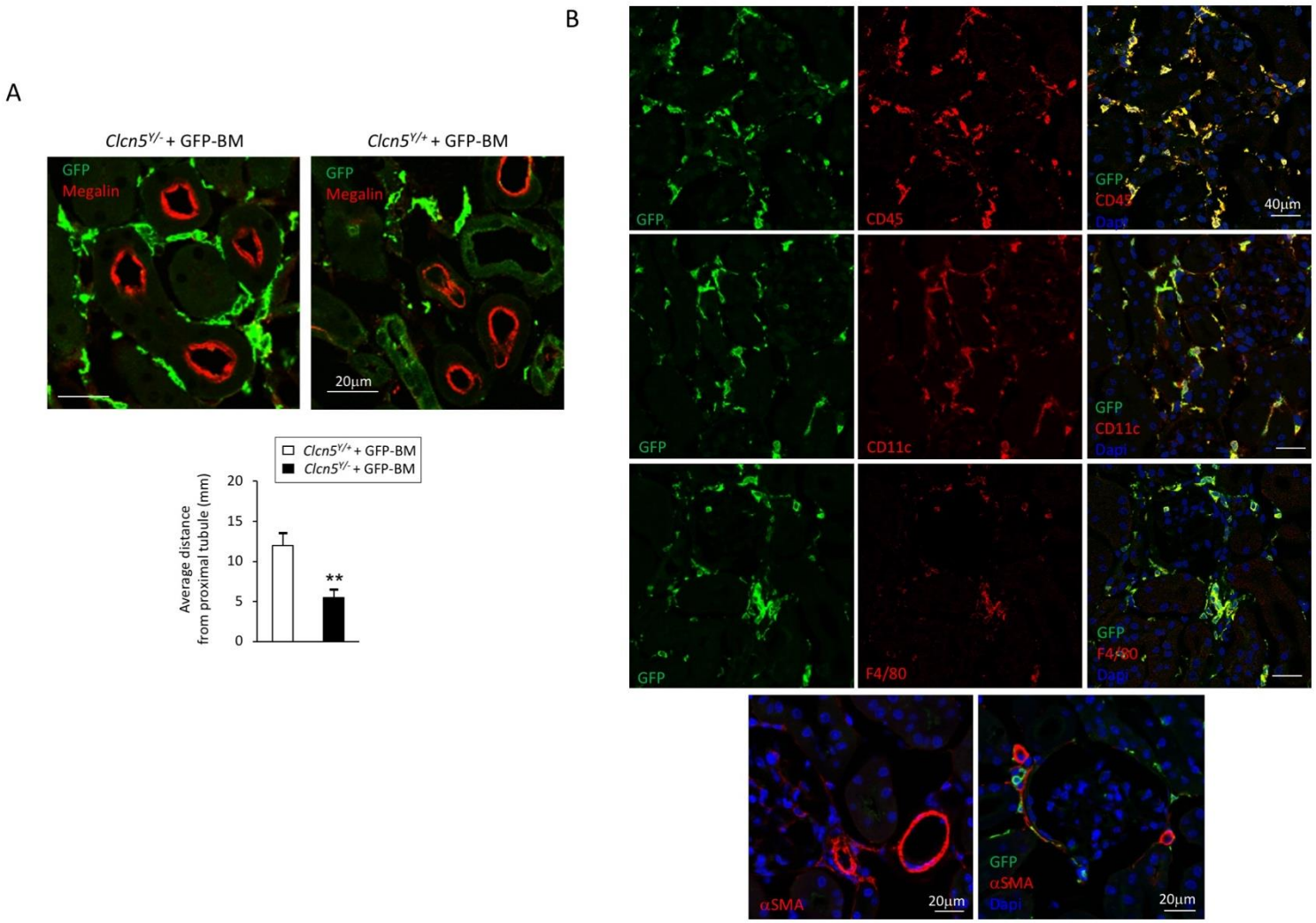

Figure 5: Characterization and distribution of BM-derived cells in *Clcn5* kidneys.

(A) Confocal microscopy images showing staining for megalin (red) and GFP (green) in kidney sections of *Clcn5*$^{Y/-}$ (left panel) and *Clcn5*$^{Y/+}$ (right panel) mice transplanted with GFP+ BM cells. Bottom panel: average distance of GFP+ BM cells in relation to (megalin-positive) PT cells in transplanted kidneys. In *Clcn5*$^{Y/-}$ kidneys, a higher number of transplanted GFP+ cells surround the PT profiles, and they are closer to PT cells, compared to the *Clcn5*$^{Y/+}$ kidneys in which less GFP+ cells are engrafted. **P<0.01, Mann-Withney test. **(B)** Staining for GFP (green), Dapi (blue), mononuclear phagocyte markers CD45, CD11c, F4/80 (red) and the fibroblast marker □-SMA in kidneys of *Clcn5*$^{Y/-}$ mice transplanted with GFP+ BM cells. The GFP+ BM-derived cells co-stain with CD45, CD11c and F4/80, identifying these cells as monoculear phagocytes There is no overlap between the GFP cells and the fibroblast marker α-SMA.

Figure 6

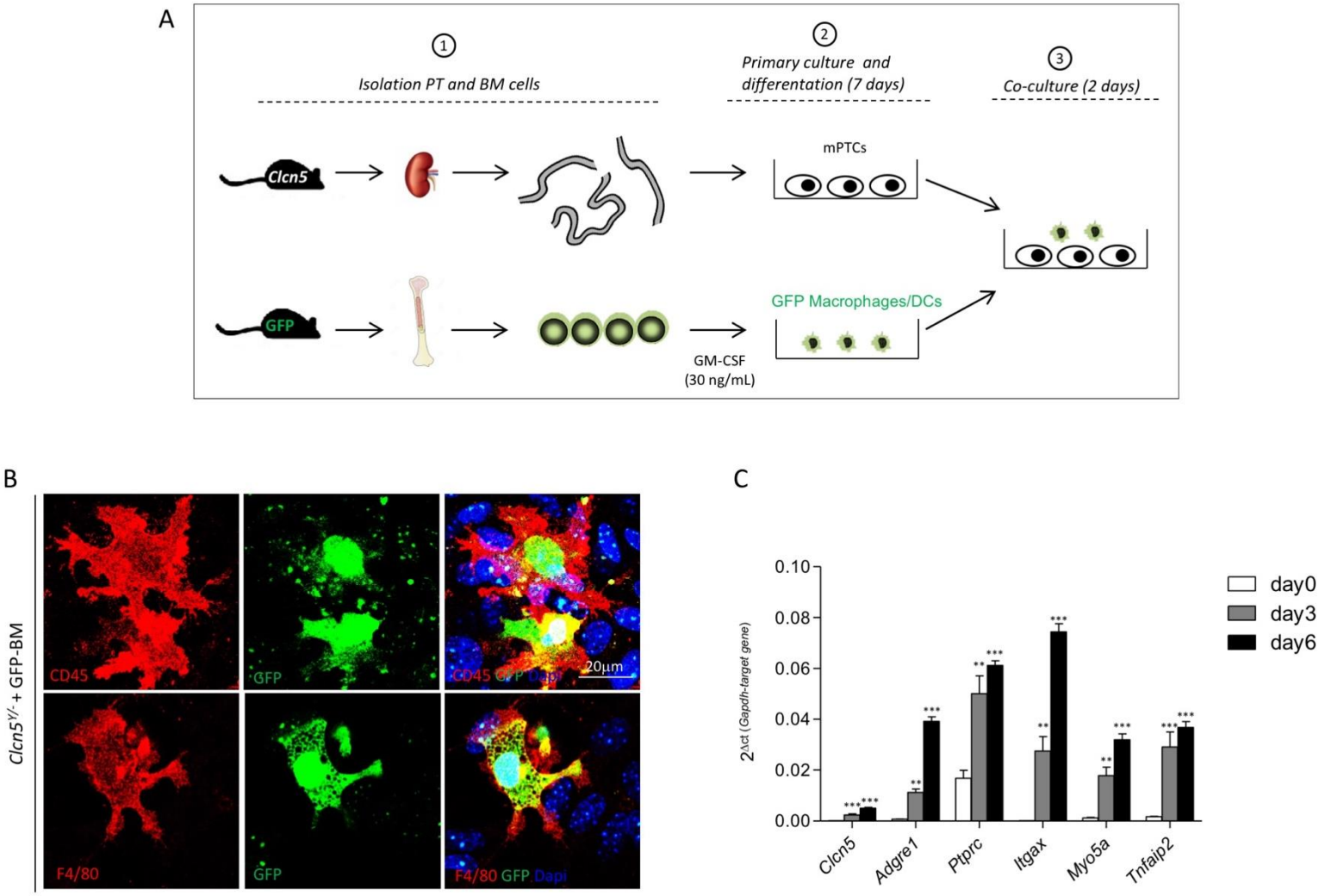

Figure 6: Setup of co-culture experiments and characterization of BM cells.

(A) Setup of co-culture experiments: primary cultures of PT cells (mPTCs) were obtained from microdissected PT segments of kidneys of *Clcn5*$^{Y/+}$ and *Clcn5*$^{Y/-}$ mice and grown for 7 days. These cells were then co-cultivated for 2 days with BM-derived DCs/macrophages (BM-DC/MΦ), that were generated by stimulating either WT (GFP+) or KO BM cells for 7 days with granulocyte-macrophage colony-stimulating factor (GM-CSF), resulting in a mixed population of adherent phagocytic cells. **(B)** Staining for GFP (green), Dapi (blue), and the mononuclear phagocyte markers CD45 (red) and F4/80 (red) in co-cultures of BM-DC/MΦ cells with mPTCs derived from *Clcn5*$^{Y/-}$ mice. **(C)** Progressive upregulation of mRNA encoding for ClC-5 (*Clcn5*), for the macrophage markers F4/80 (*Adgre1*), CD45 (*Ptprc*), CD11c (*Itgax*), and for the tunnelling nanotube markers myosin Va (*Myo5a*) and Msec (*Tnfaip2*) was observed during the differentiation process of freshly isolated BM cells into BM-DC/MΦ. **p<0.01 *vs* d0; ***p<0.001 *vs* d0, Mann-Withney test.

Figure 7

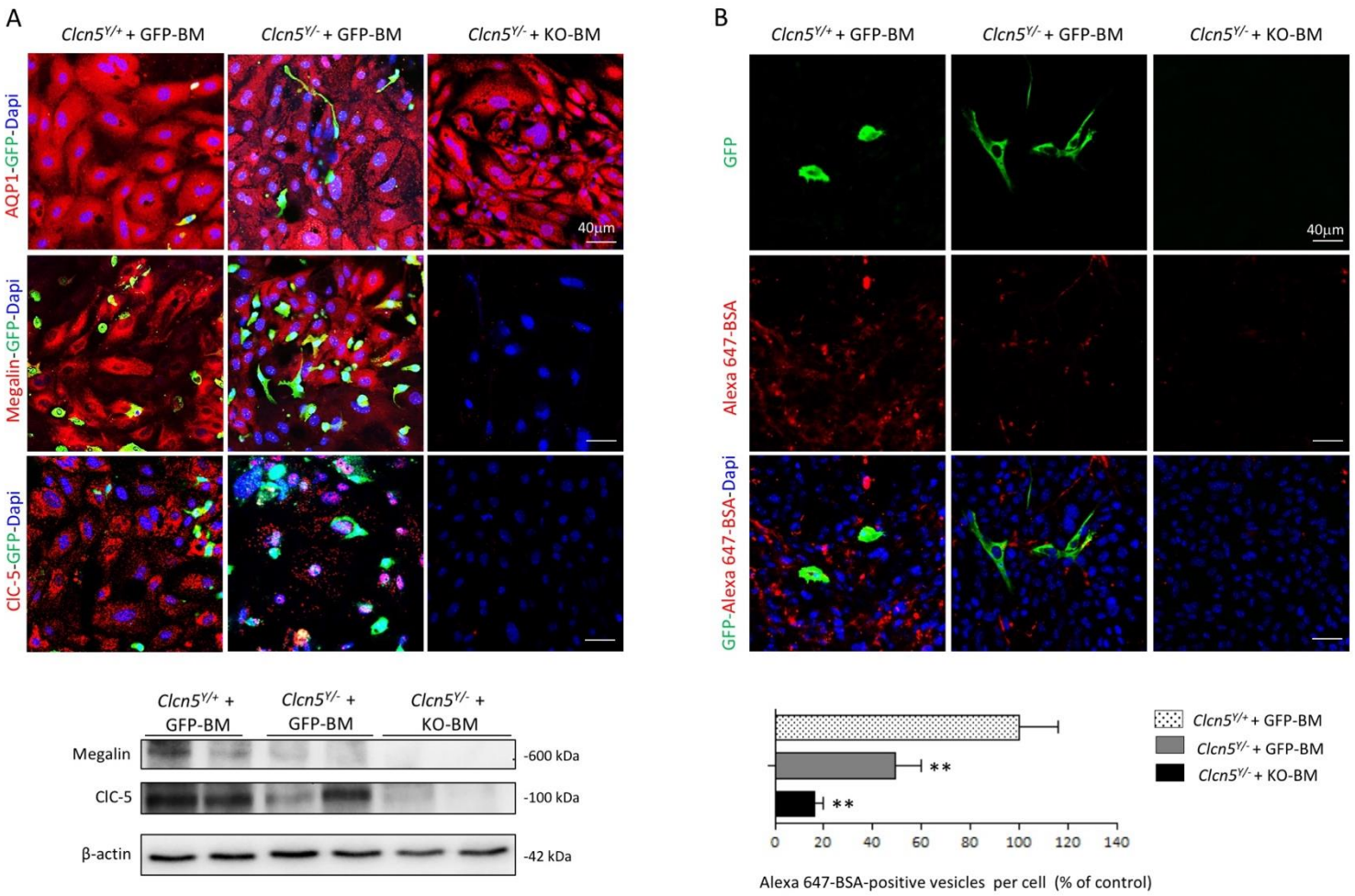

Figure 7: Co-cultures rescue megalin, ClC-5 and endocytosis in *Clcn5*$^{Y/-}$ PT cells.

(A) *Upper panel*: Staining for GFP (green), Dapi (blue), AQP1 (red), megalin (red), and ClC-5 (red) in mPTCs derived from *Clcn5*$^{Y/+}$ and *Clcn5*$^{Y/-}$ kidneys, that were co-cultured with WT GFP+ or KO BM-derived BM-DC/MΦ. Co-culture with WT GFP+ BM-derived cells rescues the expression of ClC-5 and megalin in the *Clcn5*$^{Y/-}$ mPTCs, whereas no signal is observed in *Clcn5*$^{Y/-}$ mPTCs co-cultured with KO BM-derived BM-DC/MΦ. *Lower panel*. Western blot for megalin and ClC-5 in cell lysates of mPTCs derived from *ClCn5*$^{Y/+}$ and *ClCn5*$^{Y/-}$ mice, that were co-cultured with WT GFP+ BM-derived cells from *ClCn5*$^{Y/+}$ (WT) or BM-derived cells from *Clcn5*$^{Y/-}$ (KO) mice. **(B)** *Upper panel*. Uptake of Alexa 647-conjugated BSA (red channel) in mPTCs derived from *Clcn5*$^{Y/+}$ and *Clcn5*$^{Y/-}$ kidneys, that were co-cultured with WT GFP+ BM-DC/MΦ or KO BM-DC/MΦ. A rescue of the endocytic uptake of Alexa 647-BSA is observed in *Clcn5*$^{Y/-}$ mPTCs co-cultured with WT GFP+ BM-derived cells. *Lower panel:* Quantification of Alexa 647-BSA-positive vesicles per nucleus. **P<0.01 *vs Clcn5*$^{Y/+}$.

Figure 8

A

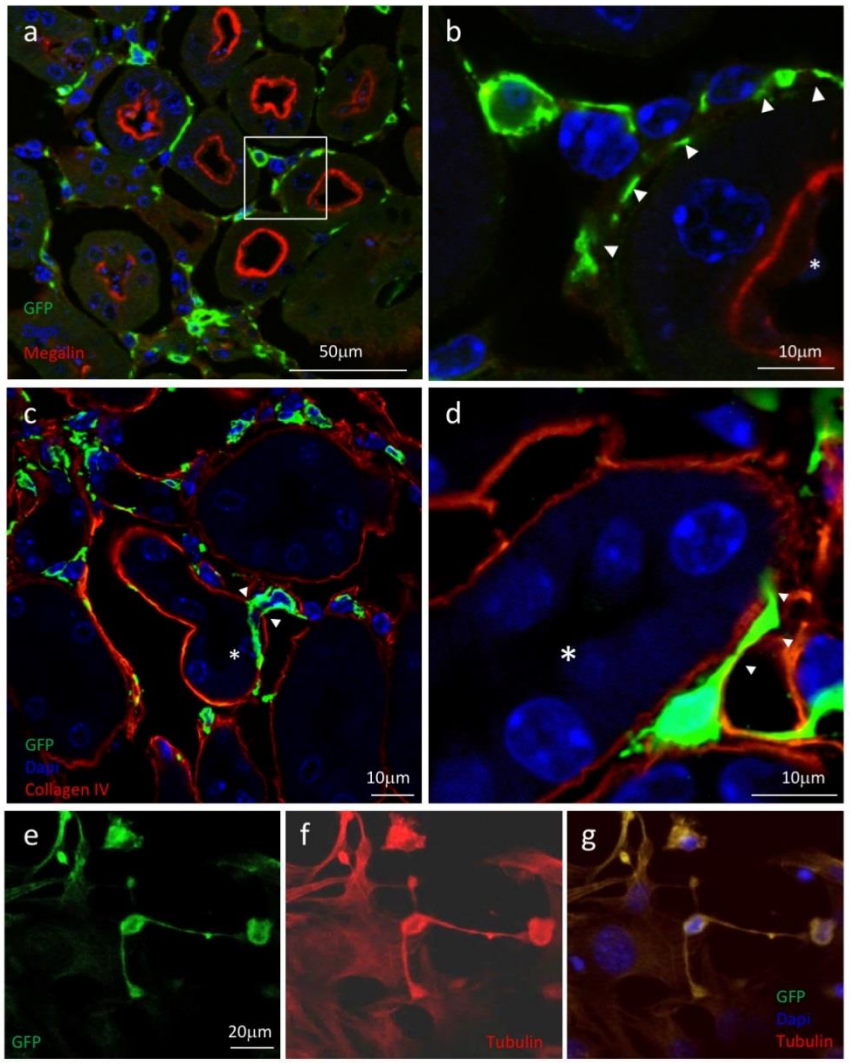

Figure 8: Nanotubes mediate interactions between BM-derived cells and PT cells.
(A) *Panels a-d:* Kidney sections of *Clcn5*$^{Y/-}$ mice transplanted with GFP+ BMcells showing staining for GFP (green), Dapi (blue) and megalin or collagen IV (red). Arrowheads indicate the nanotubular prolongations of the engrafted GFP+ cells contouring the basal membrane of a PT (panel b) and penetrating to collagen IV-positive basement membrane to establish a direct contact with PT cells (panels c and d). The asterisk indicates the lumen of the PT.
Panels e-f: Staining of GFP (green), tubulin (red) and Dapi (blue) in mPTCs derived from *Clcn5*$^{Y/-}$ mice co-cultivated with GFP+ BM BM-DC/MΦ cells. Multiple tunneling nanotubes positive for tubulin are identifed, establishing connections between BM-derived cells and mPTCs.

Figure 8 (cont.)

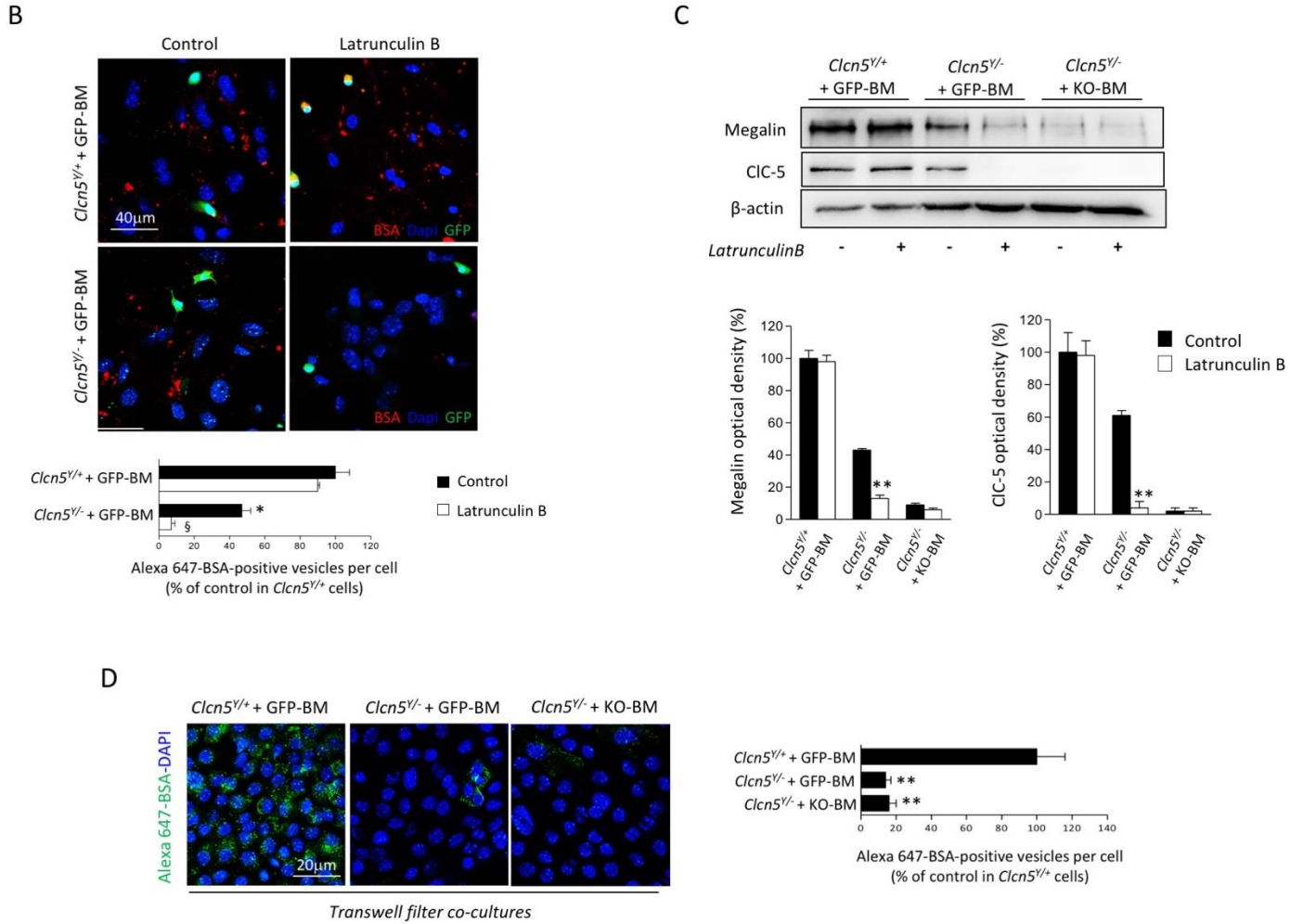

Figure 8: Nanotubes mediate interactions between BM-derived cells and PT cells.
(B) Uptake of Alexa 647-BSA (red channel) in co-cultures of mPTCs derived from *Clcn5*$^{Y/+}$ and *Clcn5*$^{Y/-}$ mice with GFP+ BM-derived cells, in presence of the actin depolymerizing agent Latrunculin B or vehicle (Control). Incubation with Latrunculin B inhibits the formation of nanotubes from the GFP+ BM-DC/MΦ, with a lack of rescue of the endocytic uptake of Alexa-BSA in *Clcn5*$^{Y/-}$ mPTCs. *P<0.05 *vs* control (*Clcn5*$^{Y/+}$+GFP-BM without Latrunculin), §P<0.05 *vs Clcn5*$^{Y/-}$+GFP-BM without Latrunculin). **(C)** Western blot for megalin and ClC-5 in lysates of mPTCs derived from *Clcn5*$^{Y/+}$ and *Clcn5*$^{Y/-}$ mice, that were co-cultured with WT GFP+ or KO BM-derived cells in the presence or not of Latrunculin B and quantification of optical densities. Treatment with Latrunculin B almost abolished the rescue of megalin and ClC-5 in co-cultures of *Clcn5*$^{Y/-}$ mPTCs and WT BM-derived cells. Representative of two experiments. **P<0.01 *vs* control. **(D)** Uptake of Alexa 647-BSA in mPTCs derived from *Clcn5*$^{Y/+}$ and *Clcn5*$^{Y/-}$ kidneys seeded onto top of collagen-coated transwell filters, with either WT or KO BM-DC/MΦ at the basolateral side. Quantification of BSA-positive vesicles per cell reveals no rescue of the endocytic uptake in *Clcn5*$^{Y/+}$ mPTCs cultured with WT BM-derived cells in the basal compartment of the transwell filters. **P<0.01 *vs Clcn5*$^{Y/+}$.

Supplementary Information

Bone Marrow Transplantation Improves Proximal Tubule Dysfunction in a Mouse Model of Dent Disease

Sarah S. Gabriel, Hendrica Belge, Alkaly Gassama, Huguette Debaix, Alessandro Luciani, Thomas Fehr, Olivier Devuyst

Suppl. Table 1: Primer sequences used in real-time qPCR analyses.

Suppl. Figure 1: Expression of ClC-5 in bone marrow-derived cells and in sub-apical vesicles of proximal tubule cells.

Suppl. Figure 2: Co-localization of megalin and ClC-5 in bone marrow-derived cells.

Suppl. Figure 3: Engraftment efficiency of bone marrow-derived cells in transplanted *Clcn5*$^{Y/+}$ and *Clcn5*$^{Y/-}$ kidneys.

Suppl. Figure 4: Detection of GFP+ structures in proximal tubule cells from transplanted *Clcn5*$^{Y/-}$ kidneys and in co-culture.

Gene	Forward primer (5'-3')	Reverse primer (5'-3')	PCR product (bp)	Efficiency
Actb	TGCCCATCTATGAGGGCTAC	CCCGTTCAGTCAGGATCTTC	102	1.03 ± 0.04
Adgre1	CTGAGGATGAATTCCCGTGT	TCCTCCACATCAGTGTTCCA	152	1.02 ± 0.02
Aqp1	CCGAGACTTAGGTGGCTCAG	CACCCAGAAAATCCAGTGGT	160	0.98 ± 0.04
Clcn5	TGGAGGAGCCAATCCCTGGTGT	AGAAAGCATCGCTCACACTG	156	0.99 ± 0.03
Gapdh	TGCACCACCAACTGCTTAGC	GGATGCAGGGATGGGGGAGA	176	1.04 ± 0.03
Gfp	CCACATGAAGCAGCAGGACTT	GGTGCGCTCCTGGAGGTA	170	1.01 ± 0.04
Hprt1	ACATTGTGGCCCTCTGTGTG	TTATGTCCCCCGTTGACTGA	162	0.99 ± 0.01
Itgax	CAAAATCTCCAACCCATGCT	CACCACCAGGGTCTTCAAGT	147	1.02 ± 0.03
Lpr2	CAGTGGATTGGGTAGCAGGA	GCTTGGGGTCAACAACGATA	150	0.99 ± 0.04
Plek	CTGGAGGAGAGAGACGCTTG	GATACAAAGCCCCCAAGTCA	136	1.01 ± 0.04
Ppiase	GTAACCCGTTGAACCCCATT	CCATCCAATCGGTAGTAGCG	151	0.98 ± 0.02
Ptprc	GGAGACCAGGAAGTCTGTGC	GTTCTGGGCTCCTTCCTCTT	149	0.97 ± 0.02
Rab5a	TGGGATACAGCTGGTCAAGA	AGGACTTGCTTGCCTTTGAA	153	1.03 ± 0.04
Slc34a1	CATCACAGAGCCCTTCACAA	TGGCCTCTACCCTGGACATA	161	1.02 ± 0.04
18S	GTAACCCGTTGAACCCCATT	CCATCCAATCGGTAGTAGCG	151	0.98 ± 0.02
36B4	CTTCATTGTGGGAGCAGACA	TTCTCCAGAGCTGGGTTGTT	150	1.02 ± 0.02

Suppl. Table 1: Primer sequences used in real-time qPCR analyses. The efficiency of each set of primers was determined by dilution curves.

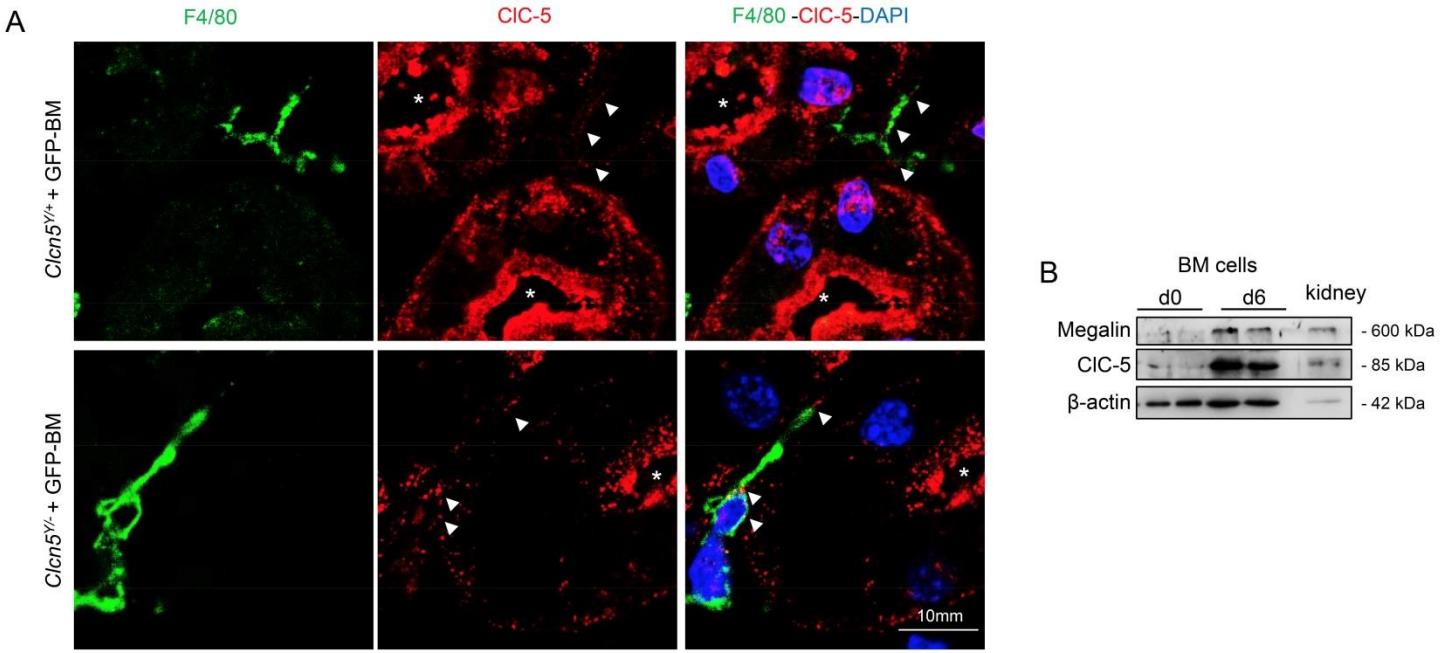

Suppl. Fig. 1: Expression of ClC-5 in bone marrow-derived cells and in sub-apical vesicles of proximal tubule cells.
(A) Confocal microscopy images showing staining for F4/80 (green), ClC-5 (red) and DAPI (blue) in the kidneys of *Clcn5* mice transplanted with wild-type GFP-labeled bone marrow (BM) cells. The ClC-5 signal was detected in BM-derived cells (arrowheads) in the kidneys of transplanted *Clcn5*$^{Y/+}$ (top panels) and *Clcn5*$^{Y/-}$ (bottom panels) mice. Note the rescue of ClC-5 expression in both the brush border and sub-apical vesicles of proximal tubule (PT) cells in the transplanted kidneys of*Clcn5*$^{Y/-}$ mice (asterisk, lumen of PT). **(B)** Representative Western blots for megalin, ClC-5 and β-actin in BM-derived dendritic cells/macrophages (BM-DC/MΦ) at d0 and at d6 of culture in medium containing GM-CSF (30ng/mL). Upon differentiation, BM-DC/MΦ express megalin and ClC-5. Kidney extracts are shown as positive controls.

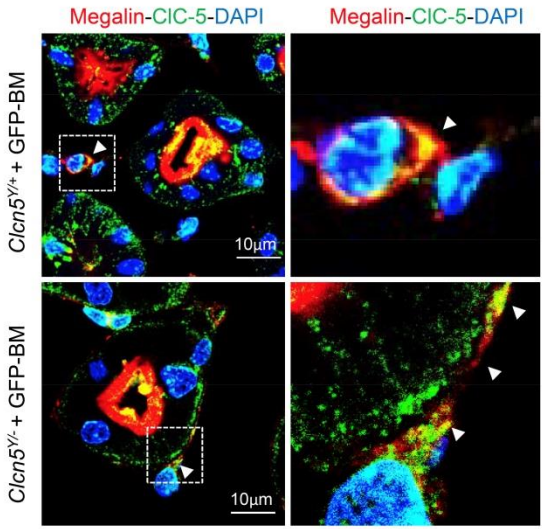

Suppl. Fig. 2: Co-localization of megalin and ClC-5 in bone marrow-derived cells.
Confocal microscopy images showing staining for megalin (red), ClC-5 (green) and DAPI (blue) in the kidneys of *Clcn5*$^{Y/+}$ (top panels) and *Clcn5*$^{Y/-}$ (bottom panels) mice transplanted with GFP-labeled bone marrow (BM) cells. Partially overlapping megalin and ClC-5 signals are detected in proximal tubule cells as well as in BM-derived cells and in the nanotubular structures (arrowheads, particularly in the transplanted kidneys from *Clcn5*$^{Y/-}$ mice).

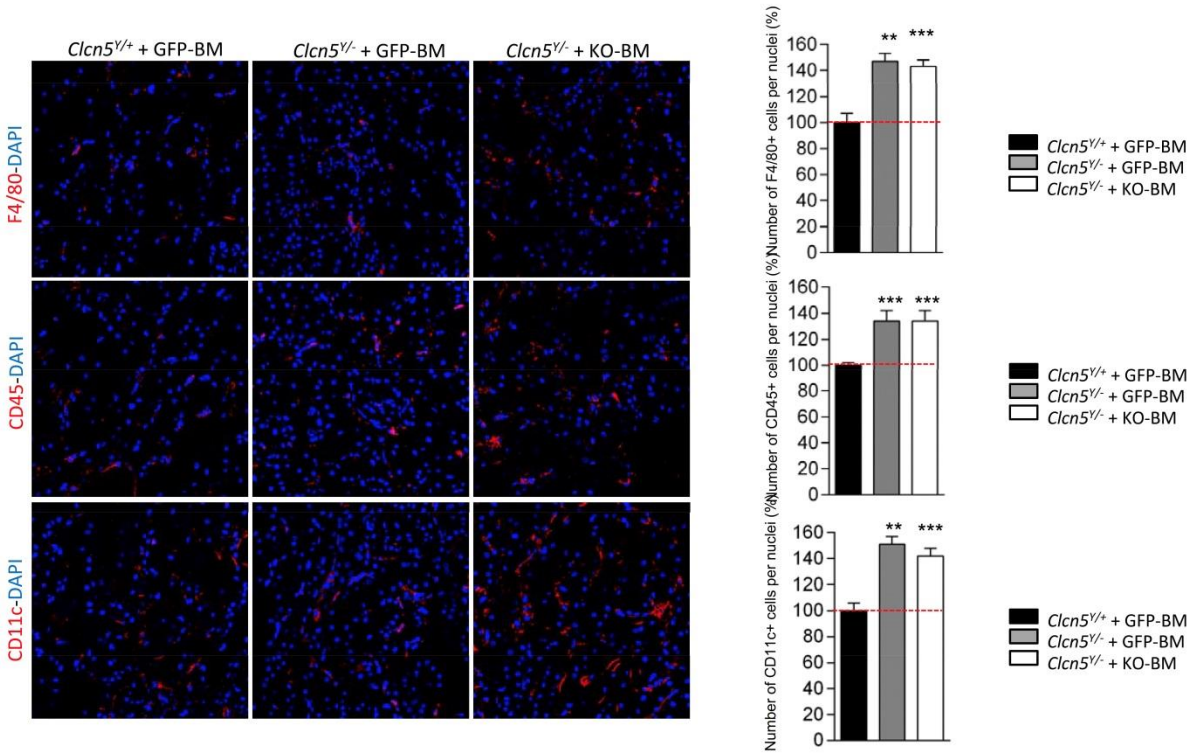

Suppl. Fig. 3: Engraftment efficiency of bone marrow-derived cells in transplanted *Clcn5*$^{Y/+}$ and *Clcn5*$^{Y/-}$ kidneys.
Confocal microscopy images showing staining for markers of dendritic cells and macrophages F4/80 (upper panels), CD45 (middle panels), CD11c (lower panels) and DAPI (blue) in the kidneys of *Clcn5*$^{Y/+}$ and *Clcn5*$^{Y/-}$ mice transplanted with wild-type (WT) GFP+ or *Clcn5*$^{Y/-}$ (KO) bone marrow (BM)-derived cells. A higher engraftment of BM-derived cells is consistently observed in the kidneys of *Clcn5*$^{Y/-}$ compared to the *Clcn5*$^{Y/+}$ mice, whereas the engraftment efficiency is similar between WT GFP+ and KO BM-derived cells in the kidneys of *Clcn5*$^{Y/-}$ mice. Quantification was performed on >200 cells per condition, distributed in 5 to 10 fields. Mann-Whitney test was used to assess the difference between groups. **P<0.01 *vs* *Clcn5*$^{Y/+}$ + GFP-BM, ***P<0.001 *vs* *Clcn5*$^{Y/+}$ + GFP-BM.

III-3 Bone marrow transplantation rescues proximal tubule function in a mouse model of Dent disease 2

Alkaly Gassama[1], Beatrice Paola Festa[1], Huguette Debaix[1], Alessandro Luciani[1], Olivier Devuyst[1]

[1] Institute of Physiology, University of Zurich, Zurich, Switzerland

Correspondence: Prof. Dr. Olivier Devuyst**;** Institute of physiology, University of Zurich; Winterthurerstrasse, 190, 8057 Zürich, Switzerland**;** Tel.: +41(0)44 635 50 82, E-mail: olivier.devuyst@uzh.ch

ABSTRACT

Dent disease 2 is a rare X-linked disease characterized by congenital cataracts, central hypotonia, intellectual disability and renal Fanconi syndrome. This disease is caused by mutations in *OCRL* which encode for an inositol polyphosphate 5-phosphatase (OCRL) that regulates intracellular trafficking by acting on phosphoinositides, constituents of cell membranes. Loss of function of *OCRL* results in defective receptor-mediated endocytosis and severe proximal tubule (PT) dysfunction. Bone marrow transplantation has recently been shown to preserve kidney function in cystinosis, a lysosomal storage disease causing proximal tubule dysfunction. Here we test the effects of bone marrow transplantation in $Ocrl^{Y/-}$ mice, faithful model for Dent disease 2. We established a co-culture system based on primary cultures of mouse proximal tubular cells which were then co-cultivated for 2 days with BM-derived DCs/macrophages. Co-culture of $Ocrl^{Y/-}$ PT cells with wild-type bone marrow–derived cells rescued megalin expression resulting in improved endocytosis. Bone marrow–derived cells established contacts with PT cells through nanotubular extensions in a dynamic manner and exchanged materials. No rescue was found when the formation of the tunneling nanotubes was prevented by actin depolymerization or when cells were physically separated by transwell inserts. In summary, bone marrow transplantation may rescue the epithelial phenotype due to an inherited endosomal defect through direct contact between transplanted BM-derived cells and diseased proximal tubular cells.

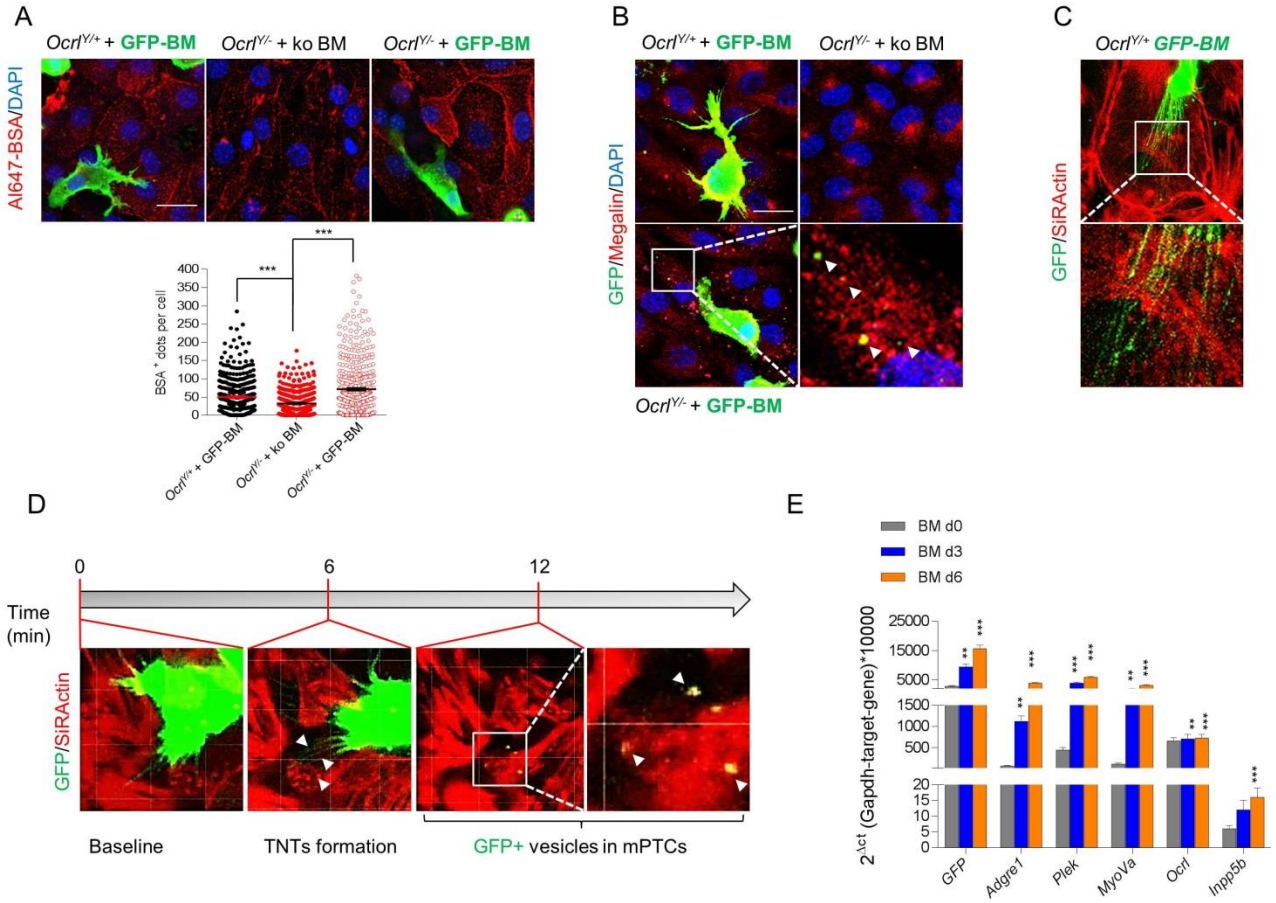

Cocultures of bone marrow (BM)-derived cells with *Ocrl*$^{Y/-}$ proximal tubule cells rescue receptor-mediated endocytosis and Megalin expression through tunneling nanotubes formation (TNTs)

mPTCs derived from *Ocrl* kidneys were cocultured with WT GFP (green) or *Ocrl*$^{Y/-}$ derived BM-DC/ MΦ. (**A**) Cocultured cells were loaded with Al647-BSA (red, 100 µg ml^{-1} for 15 min at 37 °C), fixed and analyzed by confocal microscopy. Quantification of the number of Al633-BSA+ structures (n ≈400-450 cells pooled from three mouse kidneys per condition; each point representing the number of BSA+ structures in a cell). Plotted data represent mean ± SEM. Two-tailed unpaired Student's t-test, ***P < 0.001 relative to *Ocrl*$^{Y/+}$ mPTCs. Scale bars are 10 µm. (**B**) Representative confocal micrographs of the number of Megalin+ (red) structures in cocultured cells Insets: high magnification of LRP2/ GFP+ structures. (**C-D**) Cocultured cells were loaded with Sir-Actin (red, 100nM) and immediately imaged. (**C**) Representative confocal micrographs of tunneling nanotubes structure (green, TNTs) extended from BM derived cells to proximal tubule cells. (**D**) Snapshots selected from a time-lapse video at the indicated time to visualize TNTs formation and transfer of GFP+ vesicles from BM derived cells to proximal tubule cells. Cocultured cells were imaged every 15 seconds for 45 minutes. Nuclei counterstained with DAPI (blue). (**E**) mRNA levels for *GFP* (green fluorescent protein), macrophage marker F4/80 (*Adgre1*), tunneling nanotube markers Plekstrin (Plek) and myosin Va (*MyoVa*) and *Ocrl* (Inositol Polyphosphate-5-Phosphatase) and *Inpp5b* (Inositol polyphosphate-5-phosphatase B) during the differentiation of isolated BM cells into BM-DC/MΦ were analyzed by real-time qPCR. Gene target expression normalized to *Gapdh* (n = 3 mice per group). Two-tailed unpaired Student's t-test, **P < 0.01, ***P < 0.001 relative to day 0

IV- Discussion

IV- Discussion

The epithelial cells lining the proximal tubules (PT) of the kidney ensure ~80% of the total metabolic clearance of small proteins and peptides including LMW proteins that would otherwise be lost in the urine, thus playing an important role in hormone and vitamin homeostasis (Christensen and Birn 2002). These substances are reabsorbed by receptor-mediated endocytosis triggered by their interaction with multi-ligand receptors, megalin and cubilin, followed by internalization, delivery to endosomes and further to lysosomes for processing and degradation. Genetic diseases involving the receptors (e.g. Imerslund-Gräsbeck syndrome) or the endolysosomal pathway (e.g. Dent disease or cystinosis) lead to massive urinary losses of solutes and LMW proteins, often complicated by multi-systemic complications and progression to end-organ damage (Devuyst and Luciani 2015).

The intertwining of endo-lysosomal vesicle trafficking requires a delicate spatiotemporal regulation of membrane dynamics and the capacity to adapt to changes in flow rates. It has long been hypothesized that the primary cilium, a microtubule-based organelle that is expressed on most eukaryotic cells, sense the urinary flow triggering an intracellular influx of calcium ions thus allowing the regulation of numerous cellular process (Nauli et al, 2003). Another interesting property of the cilium is its ability to adjust its morphology in response to environmental conditions, depending on the strength of the signal that they detect (Reiter and Leroux 2017). A growing number of studies show that the primary cilium regulates cell functions including endocytosis (Satir, Pedersen et al. 2010). Indeed, the ciliary pocket at the basis of the primary cilium is a privileged site of formation of clathrin-coated pits and vesicles (Molla-Herman et al 2010). Since the ciliary membrane is in continuum with the plasma membrane, this region could contribute to the endocytic activity and formation of autophagosome precursors at the apical pole of the the cells (Pampliega and Cuervo 2016). Furthermore, primary cilia have been shown to mediate the stimulation of apical endocytosis in response to flow-induced fluid shear stress in immortalized PT cells (OK, LLCPK) (Molla-Herman, Ghossoub et al. 2010, Raghavan, Rbaibi et al. 2014, Long, Shipman et al. 2017). These findings promote the hypothesis that alterations of the primary cilia could affect the regulation of apical endocytosis in PT cells (Raghavan & Weisz, 2016). On the other hand, the primary cilium function has recently been linked to

autophagy, a catabolic process that delivers cytoplasmic components and organelles to lysosomes for digestion (Settembre et al. 2013). Considering that kidney cells requires an efficient autophagy-mediated clearance system to cope with the high reabsorptive function of the PTs, this homeostatic mechanism is of particular importance and has been shown to protect against acute tubular injury (Kimura, Takabatake et al. 2011). The functional interaction between the primary cilium and autophagy is complex, reflecting mutual regulation (Pampliega and Cuervo 2016). Proper ciliogenesis and intact primary cilium function are required for autophagy activation, but autophagy also regulates primary cilia through the specific degradation of ciliary proteins, such as the intraflagellar transport system protein IFT20, that promote ciliogenesis (Pampliega, Orhon et al. 2013).

Using genetic models of PKD (*Cy/+* rat) and (*Pkd1* inducible knock-out mouse) as a hallmark of cilia dysfunction, our studies substantiate a link between primary cilium and receptor-mediated endocytosis in PTs. Indeed, we evidenced a selective LMW proteinuria at an early stage of the disease and in absence of renal failure. One major limitation to study the role of primary cilium in the kidney is the availability of appropriate cellular models. Therefore, we developed a primary proximal tubular cell culture system from rat kidneys based on our expertise and these cells recapitulate not only all the features of the epithelial cells of the PTs, but possess the ability to form cilia (Terryn, Jouret et al. 2007). Using this system, we showed that the endocytosis impairment was associated to severe morphological and functional defects of the primary cilium becoming unresponsive to flow. The inbred *Cy/+* rat is a well-established model for inherited PKD characterized by the development of cortical cysts and a slow progression to ESRD (Schafer et al, 1994). These cysts are caused missense mutation in *ANKS6* encoding for SamCystin which contains ankyrin repeats and a sterile alpha motif (SAM). *ANKS6* mutations have been identified in families affected by nephronophthisis. ANKS6 was demonstrated to mediate interaction between NEK8, INVS and NPHP3 in the Inv compartment of the primary cilium (Hoff, Halbritter et al. 2013, Nakajima, Kiyonari et al. 2018).

The endocytosis and ciliary defects reported in the *Cy/+* rats and the *Pkd1* mouse were associated with a specific marked accumulation of IFT20, a key member of intraflagellar traffic complexes ensuring the shuttle of essential ciliary proteins from the Golgi apparatus to the basal

body. Considering the fundamental role of autophagy in regulating the bioavailability of essential components of the ciliogenesis, we investigated the autophagic process and we observed an accumulation of p62 and LC3, two substrates normally degraded within the autolysosomes, suggesting an abnormal autophagic flux due to defects in the late phase of autophagy. The question arising from these findings is how primary dysfunctions of the cilium, namely ANKS6 or PC1 defects, affect the autophagic function. We hypothesized a putative role of these proteins in the delivery of cathepsins from Golgi to the lysosomes or in the maturations of these hydrolases in the lysosomal compartment. We evidenced a defective lysosomal proteolysis in *Cy/+* and *Pkd1* derived PT cells associated to a lack of active cathepsins in the lysosomes suggesting a defective maturation in spite of a normal delivery of cathepsins. Taken together, our data support the concept that the autophagy impairment, caused by a defective lysosomal function, leads to the accumulation of the ciliary protein IFT20 ultimately resulting in an increase of the ciliary length contributing to the endocytosis defects. These findings are reminiscent of the cellular changes observed in a monoclonal light chain–associated renal Fanconi Syndrome and cystinosis (Festa et al, 2018; Luciani et al, 2016). Additionally we found similar phenotypes in a pure endosomal disorder, Dent disease, where the loss-of-function of *Clcn5* results in a severe endocytic defect concomitant with an accumulation of IFT20 and an increase of the primary cilia length. Therefore dysfunctional endosomal—lysosomal pathways due to congenital (Dent disease or cystinosis) or acquired (light chain disease) disorders might have similar functional consequences on epithelial phenotype, emphasizing the fundamental role of primary cilia as a signaling hub to ensure cellular function and homeostasis.

Autosomal dominant polycystic kidney disease (ADPKD) is the most common inherited kidney disease, affecting about 1:1,000 individuals, characterized by the development of cysts resulting in the progressive enlargement of the kidneys and, ultimately, leading to end-stage renal disease (Ong et al, 2015). ADPKD is caused by mutations in *PKD1* or *PKD2* which encode proteins polycystin-1 and polycystin-2 forming a complex located on the primary cilium which allow the transduction of a flow-dependent Ca^{2+} signaling in kidney epithelial cells (Ong, 2017). The disruption of this complex impairs the balance of different cellular mechanisms, with enhanced proliferation, abnormal fluid secretion and defective PCP driving the cysts progression. Recent studies showed an association of proximal tubule markers including β2-microglobulin

with GFR decline in patients with ADPKD (Messchendorp, Meijer et al. 2018). Consistent with these results, our findings were confirmed in a cohort of ADPKD patients exhibiting a loss of LMWPs associated with an increase of ciliary length at an early stage of the disease with a normal eGFR; supporting the potential use of PT urinary biomarkers to monitor the rate of disease progression in ADPKD

In summary, this study evidence for the first time PT defects involving an impairment of the primary cilium in a PKD context before any renal failure. Our findings support a crucial role of primary cilia for PT function and raise several open questions. Indeed, while we demonstrated a direct relation between cilia integrity and PT endocytosis, the precise molecular mechanisms by which the primary cilium controls the bioavailability of megalin remain unclear. A recent study showed that LDL receptor-related protein 1 (LRP-1), which mediates ligands uptake in chondrocytes, is concentrated at the base of the cilium and that alterations of the primary cilium disrupts LRP-1 organization and impairs LRP-1 mediated endocytosis (Coveney, Collins et al. 2018). Consistent with our findings, these studies suggest a fundamental role of the cilium in regulating the distribution of endocytic receptors at the plasma membrane. However, additional mechanisms could be involved as other studies hypothesized that fluid shear stress induces cytoskeletal changes that increases the clathrin-coated invaginations size via calcium dependent mechanisms (Bhattacharyya, Jean-Alphonse et al. 2017). Additional studies will be crucial to decipher the mechanisms governing the regulation of endocytosis by the primary cilium.

Few therapeutic solutions are available to target congenital disorders of the endolysosomal pathway with the effort focusing mostly on the prevention of complications due to the proteinuria and of the development of CKD. We demonstrated for the first time that bone marrow (BM) transplantation improves the renal function in a mouse model of Dent disease (Gabriel, Belge et al. 2017). Indeed, the *Clcn5* knock out mice transplanted with wild-type BM showed a significant decrease of LMW proteinuria, glycosuria, calciuria and polyuria up to 4 months after transplantation. The BM cells differentiated in mononuclear phagocytes (presenting features of both dendritic cells and macrophages) and engrafted in the interstitium surrounding the PT cells. Although the benefit of BM transplantation has clearly been demonstrated for genetic disorders of the hematopoietic system (acute leukemia, sickle cell diseases or SCID),

BMT has also been used for enzymes replacement therapy in lysosomal storage disease such as Hurler syndrome or cystinosis (Aldenhoven, Jones et al. 2015); (Yeagy, Harrison et al. 2011). Our findings showed that the BM-derived mononuclear phagocytes induce a recovery of ClC-5 and megalin expression, providing a mechanistic basis for the endocytosis rescue. These results suggested a cell-to-cell material (mRNA and/or protein) exchange between the engrafted cells and the PT cells and prompted us to investigate more closely the interaction between them.

We developed a coculture system of BM-derived cells and PT cells and we showed that the endocytic rescue was prevented when the cells were physically separated by a transwell insert system, excluding the hypothesis of a paracrine communication as the mechanism of rescue. Another mechanism of intercellular communication is achieved by cell-to-cell contact using tunneling nanotubes (TNTs) that are F-actin based structures identified in macrophages and other cell types and allowing the transfer of several cargo types including vesicles derived from endosomes, lysosomes or cytoplasmic content (Abounit and Zurzolo 2012, Abounit, Delage et al. 2015). TNTs differs from other types of cellular protrusions such as filopodia or dendrites by establishing a continuity of the cytoplasm between the connected cells, thus allowing a direct transfer of cellular materials (Willnow 2017). We observed similar TNTs in our studies where multiple contact points between the transplanted cells and PT cells were identified both *in vivo* and *in vitro*. We confirmed the crucial role of TNTs by showing that no rescue was observed when TNTs formation was prevented with Latrunculin B which altered actin polymerization. Interestingly we observed by performing live imaging studies, that the interaction between TNTs and PTs cells is highly dynamic, with the BM-derived cells moving on the PT epithelium, rapidly establishing contact, exchanging materials and repeating this process in a relatively short time.

While our studies provide compelling arguments in favor of BMT in Dent disease, the underlying regulatory mechanisms remain puzzling. Indeed, we observed a higher engraftment of BM-derived cells in *Clcn5* knock-out mice but not in wild-type suggesting the existence of an unknown “homing” signal released by mutant cells attracting BM-derived cells to their target site in the kidney. Additionally BM-derived cells established a closer contact with PT epithelial cells through TNTs in *Clcn5* knock-out mice than in wild-type. The mechanisms governing the formation of TNTs and their guidance to a target cell remain elusive. Finally, additional studies

are needed to determine the precise contribution of the transferred material to the correction of the endocytic defect. We demonstrated that BM-derived cells provide vesicles containing megalin and ClC-5 to the defective PT epithelial cells. However the possibility of RNA exchange from the BM-derived cells and the *de novo* synthesis of functional megalin and ClC-5 in the PT cells cannot be excluded.

In spite of the open questions, our findings demonstrated the correction of an epithelial phenotype in an inherited endosomal disorder and raise the interest for additional studies regarding the benefit of bone marrow transplantation in PT disorders.

References

Abounit, S., E. Delage and C. Zurzolo (2015). "Identification and Characterization of Tunneling Nanotubes for Intercellular Trafficking." Curr Protoc Cell Biol **67**: 12 10 11-21.

Abounit, S. and C. Zurzolo (2012). "Wiring through tunneling nanotubes--from electrical signals to organelle transfer." J Cell Sci **125**(Pt 5): 1089-1098.

Absalon, S., T. Blisnick, L. Kohl, G. Toutirais, G. Dore, D. Julkowska, A. Tavenet and P. Bastin (2008). "Intraflagellar transport and functional analysis of genes required for flagellum formation in trypanosomes." Mol Biol Cell **19**(3): 929-944.

Ahrabi, A. K., F. Jouret, E. Marbaix, C. Delporte, S. Horie, S. Mulroy, C. Boulter, R. Sandford and O. Devuyst (2010). "Glomerular and proximal tubule cysts as early manifestations of Pkd1 deletion." Nephrol Dial Transplant **25**(4): 1067-1078.

Albaqumi, M., S. Srivastava, Z. Li, O. Zhdnova, H. Wulff, O. Itani, D. P. Wallace and E. Y. Skolnik (2008). "KCa3.1 potassium channels are critical for cAMP-dependent chloride secretion and cyst growth in autosomal-dominant polycystic kidney disease." Kidney Int **74**(6): 740-749.

Aldenhoven, M., S. A. Jones, D. Bonney, R. E. Borrill, M. Coussons, J. Mercer, M. B. Bierings, B. Versluys, P. M. van Hasselt, F. A. Wijburg, A. T. van der Ploeg, R. F. Wynn and J. J. Boelens (2015). "Hematopoietic cell transplantation for mucopolysaccharidosis patients is safe and effective: results after implementation of international guidelines." Biol Blood Marrow Transplant **21**(6): 1106-1109.

Amemiya, M., J. Loffing, M. Lotscher, B. Kaissling, R. J. Alpern and O. W. Moe (1995). "Expression of NHE-3 in the apical membrane of rat renal proximal tubule and thick ascending limb." Kidney Int **48**(4): 1206-1215.

Anderson, R. G. (1972). "The three-dimensional structure of the basal body from the rhesus monkey oviduct." J Cell Biol **54**(2): 246-265.

Audrezet, M. P., E. Cornec-Le Gall, J. M. Chen, S. Redon, I. Quere, J. Creff, C. Benech, S. Maestri, Y. Le Meur and C. Ferec (2012). "Autosomal dominant polycystic kidney disease: comprehensive mutation analysis of PKD1 and PKD2 in 700 unrelated patients." Hum Mutat **33**(8): 1239-1250.

Avidor-Reiss, T., A. M. Maer, E. Koundakjian, A. Polyanovsky, T. Keil, S. Subramaniam and C. S. Zuker (2004). "Decoding cilia function: defining specialized genes required for compartmentalized cilia biogenesis." Cell **117**(4): 527-539.

Behfar, M., S. Faghihi-Kashani, A. S. Hosseini, A. Ghavamzadeh and A. A. Hamidieh (2017). "Long-Term Safety of Short-Term Administration of Filgrastim (rhG-CSF) and Leukophresis Procedure in Healthy Children: Application of Peripheral Blood Stem Cell Collection in Pediatric Donors." Biol Blood Marrow Transplant.

Bhattacharyya, S., F. G. Jean-Alphonse, V. Raghavan, J. C. McGarvey, Y. Rbaibi, J. P. Vilardaga, M. D. Carattino and O. A. Weisz (2017). "Cdc42 activation couples fluid shear stress to apical endocytosis in proximal tubule cells." Physiol Rep **5**(19).

Braulke, T. and J. S. Bonifacino (2009). "Sorting of lysosomal proteins." Biochim Biophys Acta **1793**(4): 605-614.

Brown, D., T. G. Paunescu, S. Breton and V. Marshansky (2009). "Regulation of the V-ATPase in kidney epithelial cells: dual role in acid-base homeostasis and vesicle trafficking." J Exp Biol **212**(Pt 11): 1762-1772.

Camargo, S. M., D. Bockenhauer and R. Kleta (2008). "Aminoacidurias: Clinical and molecular aspects." Kidney Int **73**(8): 918-925.

Cantiello, H. F. (2004). "Regulation of calcium signaling by polycystin-2." Am J Physiol Renal Physiol **286**(6): F1012-1029.

Chen, Z., V. B. Indjeian, M. McManus, L. Wang and B. D. Dynlacht (2002). "CP110, a cell cycle-dependent CDK substrate, regulates centrosome duplication in human cells." Dev Cell **3**(3): 339-350.

Chih, B., P. Liu, Y. Chinn, C. Chalouni, L. G. Komuves, P. E. Hass, W. Sandoval and A. S. Peterson (2011). "A ciliopathy complex at the transition zone protects the cilia as a privileged membrane domain." Nat Cell Biol **14**(1): 61-72.

Christensen, E. I. and H. Birn (2002). "Megalin and cubilin: multifunctional endocytic receptors." Nat Rev Mol Cell Biol **3**(4): 256-266.

Christensen, E. I., H. Birn, T. Storm, K. Weyer and R. Nielsen (2012). "Endocytic receptors in the renal proximal tubule." Physiology (Bethesda) **27**(4): 223-236.

Christensen, E. I., O. Devuyst, G. Dom, R. Nielsen, P. Van der Smissen, P. Verroust, M. Leruth, W. B. Guggino and P. J. Courtoy (2003). "Loss of chloride channel ClC-5 impairs endocytosis by defective trafficking of megalin and cubilin in kidney proximal tubules." Proc Natl Acad Sci U S A **100**(14): 8472-8477.

Clement, C. A., K. D. Ajbro, K. Koefoed, M. L. Vestergaard, I. R. Veland, M. P. Henriques de Jesus, L. B. Pedersen, A. Benmerah, C. Y. Andersen, L. A. Larsen and S. T. Christensen (2013). "TGF-beta signaling is associated with endocytosis at the pocket region of the primary cilium." Cell Rep **3**(6): 1806-1814.

Cole, D. G., S. W. Chinn, K. P. Wedaman, K. Hall, T. Vuong and J. M. Scholey (1993). "Novel heterotrimeric kinesin-related protein purified from sea urchin eggs." Nature **366**(6452): 268-270.

Cole, D. G., D. R. Diener, A. L. Himelblau, P. L. Beech, J. C. Fuster and J. L. Rosenbaum (1998). "Chlamydomonas kinesin-II-dependent intraflagellar transport (IFT): IFT particles contain proteins required for ciliary assembly in Caenorhabditis elegans sensory neurons." J Cell Biol **141**(4): 993-1008.

Collins, B. M., A. J. McCoy, H. M. Kent, P. R. Evans and D. J. Owen (2002). "Molecular architecture and functional model of the endocytic AP2 complex." Cell **109**(4): 523-535.

Cooper, D. M., N. Mons and J. W. Karpen (1995). "Adenylyl cyclases and the interaction between calcium and cAMP signalling." Nature **374**(6521): 421-424.

Coveney, C. R., I. Collins, M. Mc Fie, A. Chanalaris, K. Yamamoto and A. K. T. Wann (2018). "Cilia protein IFT88 regulates extracellular protease activity by optimizing LRP-1-mediated endocytosis." FASEB J: fj201800334.

Craft, J. M., J. A. Harris, S. Hyman, P. Kner and K. F. Lechtreck (2015). "Tubulin transport by IFT is upregulated during ciliary growth by a cilium-autonomous mechanism." J Cell Biol **208**(2): 223-237.

Daikeler, T., A. Tichelli and J. Passweg (2012). "Complications of autologous hematopoietic stem cell transplantation for patients with autoimmune diseases." Pediatr Res **71**(4 Pt 2): 439-444.

De Duve, C. (1963). "The lysosome." Sci Am **208**: 64-72.

De Koning, J., D. W. Van Bekkum, K. A. Dicke, L. J. Dooren, J. Radl and J. J. Van Rood (1969). "Transplantation of bone-marrow cells and fetal thymus in an infant with lymphopenic immunological deficiency." Lancet **1**(7608): 1223-1227.

De Matteis, M. A., L. Staiano, F. Emma and O. Devuyst (2017). "The 5-phosphatase OCRL in Lowe syndrome and Dent disease 2." Nat Rev Nephrol **13**(8): 455-470.

de Toni, G. (1933). "Remarks on the Relations between Renal Rickets (Renal Dwarfism) and Renal Diabetes." Acta Paediatrica **16**(1): 479-485.

Deane, J. A., D. G. Cole, E. S. Seeley, D. R. Diener and J. L. Rosenbaum (2001). "Localization of intraflagellar transport protein IFT52 identifies basal body transitional fibers as the docking site for IFT particles." Curr Biol **11**(20): 1586-1590.

Debré, R., J. Marie and F. Cleret (1934). "Rachitisme tardif coexistant avec une Nephrite chronique et une Glycosurie. ." Archive de Medicine des Enfants **37**: 597-606.

DeCaen, P. G., M. Delling, T. N. Vien and D. E. Clapham (2013). "Direct recording and molecular identification of the calcium channel of primary cilia." Nature **504**(7479): 315-318.

Delling, M., A. A. Indzhykulian, X. Liu, Y. Li, T. Xie, D. P. Corey and D. E. Clapham (2016). "Primary cilia are not calcium-responsive mechanosensors." Nature **531**(7596): 656-660.

Devuyst, O., C. R. Burrow, B. L. Smith, P. Agre, M. A. Knepper and P. D. Wilson (1996). "Expression of aquaporins-1 and -2 during nephrogenesis and in autosomal dominant polycystic kidney disease." Am J Physiol **271**(1 Pt 2): F169-183.

Devuyst, O. and A. Luciani (2015). "Chloride transporters and receptor-mediated endocytosis in the renal proximal tubule." J Physiol **593**(18): 4151-4164.

Fanconi, G. (1931). "Die nicht diabetischen Glykosurien und Hyperglykaemien des aelteren Kindes." Jahrbuch fuer Kinderheilkunde **133**: 257–300.

Fass, D., S. Blacklow, P. S. Kim and J. M. Berger (1997). "Molecular basis of familial hypercholesterolaemia from structure of LDL receptor module." Nature **388**(6643): 691-693.

Ferrell, N., K. B. Ricci, J. Groszek, J. T. Marmerstein and W. H. Fissell (2012). "Albumin handling by renal tubular epithelial cells in a microfluidic bioreactor." Biotechnol Bioeng **109**(3): 797-803.

Festa, B. P., Z. Chen, M. Berquez, H. Debaix, N. Tokonami, J. A. Prange, G. V. Hoek, C. Alessio, A. Raimondi, N. Nevo, R. H. Giles, O. Devuyst and A. Luciani (2018). "Impaired autophagy bridges lysosomal storage disease and epithelial dysfunction in the kidney." Nat Commun **9**(1): 161.

Follit, J. A., R. A. Tuft, K. E. Fogarty and G. J. Pazour (2006). "The intraflagellar transport protein IFT20 is associated with the Golgi complex and is required for cilia assembly." Mol Biol Cell **17**(9): 3781-3792.

Gabriel, S. S., H. Belge, A. Gassama, H. Debaix, A. Luciani, T. Fehr and O. Devuyst (2017). "Bone marrow transplantation improves proximal tubule dysfunction in a mouse model of Dent disease." Kidney Int **91**(4): 842-855.

Gahl, W. A., J. G. Thoene and J. A. Schneider (2002). "Cystinosis." N Engl J Med **347**(2): 111-121.

Garcia-Gonzalo, F. R., K. C. Corbit, M. S. Sirerol-Piquer, G. Ramaswami, E. A. Otto, T. R. Noriega, A. D. Seol, J. F. Robinson, C. L. Bennett, D. J. Josifova, J. M. Garcia-Verdugo, N. Katsanis, F. Hildebrandt and J. F. Reiter (2011). "A transition zone complex regulates mammalian ciliogenesis and ciliary membrane composition." Nat Genet **43**(8): 776-784.

Gatti, R. A., H. J. Meuwissen, H. D. Allen, R. Hong and R. A. Good (1968). "Immunological reconstitution of sex-linked lymphopenic immunological deficiency." Lancet **2**(7583): 1366-1369.

Gilula, N. B. and P. Satir (1972). "The ciliary necklace. A ciliary membrane specialization." J Cell Biol **53**(2): 494-509.

Grantham, J. J. and V. E. Torres (2016). "The importance of total kidney volume in evaluating progression of polycystic kidney disease." Nat Rev Nephrol **12**(11): 667-677.

Haraldsson, B., J. Nystrom and W. M. Deen (2008). "Properties of the glomerular barrier and mechanisms of proteinuria." Physiol Rev **88**(2): 451-487.

Harrison, F., B. A. Yeagy, C. J. Rocca, D. B. Kohn, D. R. Salomon and S. Cherqui (2013). "Hematopoietic stem cell gene therapy for the multisystemic lysosomal storage disorder cystinosis." Mol Ther **21**(2): 433-444.

Haycraft, C. J., J. C. Schafer, Q. Zhang, P. D. Taulman and B. K. Yoder (2003). "Identification of CHE-13, a novel intraflagellar transport protein required for cilia formation." Exp Cell Res **284**(2): 251-263.

He, Q., M. Madsen, A. Kilkenney, B. Gregory, E. I. Christensen, H. Vorum, P. Hojrup, A. A. Schaffer, E. F. Kirkness, S. M. Tanner, A. de la Chapelle, U. Giger, S. K. Moestrup and J. C. Fyfe (2005). "Amnionless function is required for cubilin brush-border expression and intrinsic factor-cobalamin (vitamin B12) absorption in vivo." Blood **106**(4): 1447-1453.

Herak-Kramberger, C. M., D. Brown and I. Sabolic (1998). "Cadmium inhibits vacuolar H(+)-ATPase and endocytosis in rat kidney cortex." Kidney Int **53**(6): 1713-1726.

Hoff, S., J. Halbritter, D. Epting, et al, (2013). "ANKS6 is a central component of a nephronophthisis module linking NEK8 to INVS and NPHP3." Nat Genet **45**(8): 951-956.

Imus, P. H., A. L. Blackford, M. Bettinotti, B. Iglehart, A. Dietrich, N. Tucker, H. Symons, K. R. Cooke, L. Luznik, E. J. Fuchs, R. A. Brodsky, W. H. Matsui, C. A. Huff, D. Gladstone, R. F. Ambinder, I. M. Borrello, L. J. Swinnen, R. J. Jones and J. Bolanos-Meade (2017). "Major Histocompatibility Mismatch and Donor Choice for Second Allogeneic Bone Marrow Transplantation." Biol Blood Marrow Transplant **23**(11): 1887-1894.

Iomini, C., L. Li, J. M. Esparza and S. K. Dutcher (2009). "Retrograde intraflagellar transport mutants identify complex A proteins with multiple genetic interactions in Chlamydomonas reinhardtii." Genetics **183**(3): 885-896.

Ishikawa, H. and W. F. Marshall (2011). "Ciliogenesis: building the cell's antenna." Nat Rev Mol Cell Biol **12**(4): 222-234.

Ishikawa, H. and W. F. Marshall (2017). "Intraflagellar Transport and Ciliary Dynamics." Cold Spring Harb Perspect Biol **9**(3).

Jacobson, H. R. and J. P. Kokko (1976). "Intrinsic differences in various segments of the proximal convoluted tubule." J Clin Invest **57**(4): 818-825.

Jin, G., S. W. Lee, X. Zhang, Z. Cai, Y. Gao, P. C. Chou, A. H. Rezaeian, F. Han, C. Y. Wang, J. C. Yao, Z. Gong, C. H. Chan, C. Y. Huang, F. J. Tsai, C. H. Tsai, S. H. Tu, C. H. Wu, D. Sarbassov dos, Y. S. Ho and H. K. Lin (2015). "Skp2-Mediated RagA Ubiquitination Elicits a Negative Feedback to Prevent Amino-Acid-Dependent mTORC1 Hyperactivation by Recruiting GATOR1." Mol Cell **58**(6): 989-1000.

Jin, X., A. M. Mohieldin, B. S. Muntean, J. A. Green, J. V. Shah, K. Mykytyn and S. M. Nauli (2014). "Cilioplasm is a cellular compartment for calcium signaling in response to mechanical and chemical stimuli." Cell Mol Life Sci **71**(11): 2165-2178.

Kasper, D., R. Planells-Cases, J. C. Fuhrmann, O. Scheel, O. Zeitz, K. Ruether, A. Schmitt, M. Poet, R. Steinfeld, M. Schweizer, U. Kornak and T. J. Jentsch (2005). "Loss of the chloride channel ClC-7 leads to lysosomal storage disease and neurodegeneration." EMBO J **24**(5): 1079-1091.

Kim, S., K. Lee, J. H. Choi, N. Ringstad and B. D. Dynlacht (2015). "Nek2 activation of Kif24 ensures cilium disassembly during the cell cycle." Nat Commun **6**: 8087.

Kimura, T., Y. Takabatake, A. Takahashi, J. Y. Kaimori, I. Matsui, T. Namba, H. Kitamura, F. Niimura, T. Matsusaka, T. Soga, H. Rakugi and Y. Isaka (2011). "Autophagy protects the proximal tubule from degeneration and acute ischemic injury." J Am Soc Nephrol **22**(5): 902-913.

Kirkland, R. A., R. M. Adibhatla, J. F. Hatcher and J. L. Franklin (2002). "Loss of cardiolipin and mitochondria during programmed neuronal death: evidence of a role for lipid peroxidation and autophagy." Neuroscience **115**(2): 587-602.

Kobayashi, T. and B. D. Dynlacht (2011). "Regulating the transition from centriole to basal body." J Cell Biol **193**(3): 435-444.

Kozminski, K. G., K. A. Johnson, P. Forscher and J. L. Rosenbaum (1993). "A motility in the eukaryotic flagellum unrelated to flagellar beating." Proc Natl Acad Sci U S A **90**(12): 5519-5523.

Kristiansen, M., R. Kozyraki, C. Jacobsen, E. Nexo, P. J. Verroust and S. K. Moestrup (1999). "Molecular dissection of the intrinsic factor-vitamin B12 receptor, cubilin, discloses regions important for membrane association and ligand binding." J Biol Chem **274**(29): 20540-20544.

Krivit, W., P. Aubourg, E. Shapiro and C. Peters (1999). "Bone marrow transplantation for globoid cell leukodystrophy, adrenoleukodystrophy, metachromatic leukodystrophy, and Hurler syndrome." Curr Opin Hematol **6**(6): 377-382.

Lang, H., Y. Ebihara, R. A. Schmiedt, H. Minamiguchi, D. Zhou, N. Smythe, L. Liu, M. Ogawa and B. A. Schulte (2006). "Contribution of bone marrow hematopoietic stem cells to adult mouse inner ear: mesenchymal cells and fibrocytes." J Comp Neurol **496**(2): 187-201.

Lechtreck, K. F., E. C. Johnson, T. Sakai, D. Cochran, B. A. Ballif, J. Rush, G. J. Pazour, M. Ikebe and G. B. Witman (2009). "The Chlamydomonas reinhardtii BBSome is an IFT cargo required for export of specific signaling proteins from flagella." J Cell Biol **187**(7): 1117-1132.

Levesque, J. P., J. Hendy, Y. Takamatsu, P. J. Simmons and L. J. Bendall (2003). "Disruption of the CXCR4/CXCL12 chemotactic interaction during hematopoietic stem cell mobilization induced by GCSF or cyclophosphamide." J Clin Invest **111**(2): 187-196.

Ljungman, P., M. Bregni, M. Brune, J. Cornelissen, T. de Witte, G. Dini, H. Einsele, H. B. Gaspar, A. Gratwohl, J. Passweg, C. Peters, V. Rocha, R. Saccardi, H. Schouten, A. Sureda, A. Tichelli, A. Velardi, D. Niederwieser, B. European Group for and T. Marrow (2010). "Allogeneic and autologous transplantation for haematological diseases, solid tumours and immune disorders: current practice in Europe 2009." Bone Marrow Transplant **45**(2): 219-234.

Lloyd, S. E., S. H. Pearce, S. E. Fisher, K. Steinmeyer, B. Schwappach, S. J. Scheinman, B. Harding, A. Bolino, M. Devoto, P. Goodyer, S. P. Rigden, O. Wrong, T. J. Jentsch, I. W. Craig and R. V. Thakker (1996). "A common molecular basis for three inherited kidney stone diseases." Nature **379**(6564): 445-449.

Long, K. R., K. E. Shipman, Y. Rbaibi, E. V. Menshikova, V. B. Ritov, M. L. Eshbach, Y. Jiang, E. K. Jackson, C. J. Baty and O. A. Weisz (2017). "Proximal tubule apical endocytosis is modulated by fluid shear stress via an mTOR-dependent pathway." Mol Biol Cell **28**(19): 2508-2517.

Lorenz, E., C. Congdon and D. Uphoff (1952). "Modification of acute irradiation injury in mice and guinea-pigs by bone marrow injections." Radiology **58**(6): 863-877.

Lu, Q., C. Insinna, C. Ott, J. Stauffer, P. A. Pintado, J. Rahajeng, U. Baxa, V. Walia, A. Cuenca, Y. S. Hwang, I. O. Daar, S. Lopes, J. Lippincott-Schwartz, P. K. Jackson, S. Caplan and C. J. Westlake (2015). "Early steps in primary cilium assembly require EHD1/EHD3-dependent ciliary vesicle formation." Nat Cell Biol **17**(4): 531.

Luciani, A., C. Sirac, S. Terryn, V. Javaugue, J. A. Prange, S. Bender, A. Bonaud, M. Cogne, P. Aucouturier, P. Ronco, F. Bridoux and O. Devuyst (2016). "Impaired Lysosomal Function Underlies Monoclonal Light Chain-Associated Renal Fanconi Syndrome." J Am Soc Nephrol **27**(7): 2049-2061.

Lyons, R. A., E. Saridogan and O. Djahanbakhch (2006). "The reproductive significance of human Fallopian tube cilia." Hum Reprod Update **12**(4): 363-372.

Madsen, K. M., W. L. Clapp and J. W. Verlander (1988). "Structure and function of the inner medullary collecting duct." Kidney Int **34**(4): 441-454.

Mancardi, G., M. P. Sormani, P. A. Muraro, G. Boffa and R. Saccardi (2017). "Intense immunosuppression followed by autologous haematopoietic stem cell transplantation as a therapeutic strategy in aggressive forms of multiple sclerosis." Mult Scler: 1352458517742532.

Marion, V., C. Stoetzel, D. Schlicht, N. Messaddeq, M. Koch, E. Flori, J. M. Danse, J. L. Mandel and H. Dollfus (2009). "Transient ciliogenesis involving Bardet-Biedl syndrome proteins is a fundamental characteristic of adipogenic differentiation." Proc Natl Acad Sci U S A **106**(6): 1820-1825.

Marshansky, V. and M. Futai (2008). "The V-type H+-ATPase in vesicular trafficking: targeting, regulation and function." Curr Opin Cell Biol **20**(4): 415-426.

Maunsbach, A. B. (1966). "The influence of different fixatives and fixation methods on the ultrastructure of rat kidney proximal tubule cells. II. Effects of varying osmolality, ionic strength, buffer system and fixative concentration of glutaraldehyde solutions." J Ultrastruct Res **15**(3): 283-309.

McDowell, G. A., W. A. Gahl, L. A. Stephenson, J. A. Schneider, J. Weissenbach, M. H. Polymeropoulos, M. M. Town, W. Van't Hoff, M. Farrall and C. G. Mathew (1995). "Linkage of the gene for cystinosis to markers on the short arm of chromosome 17. The Cystinosis Collaborative Research Group." Nat Genet **10**(2): 246-248.

McGee, Z. A., A. P. Johnson and D. Taylor-Robinson (1981). "Pathogenic mechanisms of Neisseria gonorrhoeae: observations on damage to human fallopian tubes in organ culture by gonococci of colony type 1 or type 4." J Infect Dis **143**(3): 413-422.

Mehrotra, M., C. R. Williams, M. Ogawa and A. C. LaRue (2013). "Hematopoietic stem cells give rise to osteo-chondrogenic cells." Blood Cells Mol Dis **50**(1): 41-49.

Messchendorp, A. L., E. Meijer, W. E. Boertien, G. E. Engels, N. F. Casteleijn, E. M. Spithoven, M. Losekoot, J. G. M. Burgerhof, D. J. M. Peters, R. T. Gansevoort and D. Consortium (2018). "Urinary Biomarkers to Identify Autosomal Dominant Polycystic Kidney Disease Patients With a High Likelihood of Disease Progression." Kidney Int Rep **3**(2): 291-301.

Metcalf, D. (2007). "On hematopoietic stem cell fate." Immunity **26**(6): 669-673.

Mimura, I. and M. Nangaku (2010). "The suffocating kidney: tubulointerstitial hypoxia in end-stage renal disease." Nat Rev Nephrol **6**(11): 667-678.

Miyamoto, T., K. Hosoba, H. Ochiai, E. Royba, H. Izumi, T. Sakuma, T. Yamamoto, B. D. Dynlacht and S. Matsuura (2015). "The Microtubule-Depolymerizing Activity of a Mitotic Kinesin Protein KIF2A Drives Primary Cilia Disassembly Coupled with Cell Proliferation." Cell Rep.

Molla-Herman, A., R. Ghossoub, T. Blisnick, A. Meunier, C. Serres, F. Silbermann, C. Emmerson, K. Romeo, P. Bourdoncle, A. Schmitt, S. Saunier, N. Spassky, P. Bastin and A. Benmerah (2010). "The ciliary pocket: an endocytic membrane domain at the base of primary and motile cilia." J Cell Sci **123**(Pt 10): 1785-1795.

Nakajima, Y., H. Kiyonari, Y. Mukumoto and T. Yokoyama (2018). "The Inv compartment of renal cilia is an intraciliary signal activating center to phosphorylate ANKS6." Kidney Int.

Naphade, S., J. Sharma, H. P. Gaide Chevronnay, M. A. Shook, B. A. Yeagy, C. J. Rocca, S. N. Ur, A. J. Lau, P. J. Courtoy and S. Cherqui (2015). "Brief reports: Lysosomal cross-correction by hematopoietic stem cell-derived macrophages via tunneling nanotubes." Stem Cells **33**(1): 301-309.

Nauli, S. M., F. J. Alenghat, Y. Luo, E. Williams, P. Vassilev, X. Li, A. E. Elia, W. Lu, E. M. Brown, S. J. Quinn, D. E. Ingber and J. Zhou (2003). "Polycystins 1 and 2 mediate mechanosensation in the primary cilium of kidney cells." Nat Genet **33**(2): 129-137.

Neufeld, E. F. (1980). "The uptake of enzymes into lysosomes: an overview." Birth Defects Orig Artic Ser **16**(1): 77-84.

Nielsen, R., E. I. Christensen and H. Birn (2016). "Megalin and cubilin in proximal tubule protein reabsorption: from experimental models to human disease." Kidney Int **89**(1): 58-67.

Nielsen, R., P. J. Courtoy, C. Jacobsen, G. Dom, W. R. Lima, M. Jadot, T. E. Willnow, O. Devuyst and E. I. Christensen (2007). "Endocytosis provides a major alternative pathway for lysosomal biogenesis in kidney proximal tubular cells." Proc Natl Acad Sci U S A **104**(13): 5407-5412.

Nonaka, S., Y. Tanaka, Y. Okada, S. Takeda, A. Harada, Y. Kanai, M. Kido and N. Hirokawa (1998). "Randomization of left-right asymmetry due to loss of nodal cilia generating leftward flow of extraembryonic fluid in mice lacking KIF3B motor protein." Cell **95**(6): 829-837.

Novarino, G., S. Weinert, G. Rickheit and T. J. Jentsch (2010). "Endosomal chloride-proton exchange rather than chloride conductance is crucial for renal endocytosis." Science **328**(5984): 1398-1401.

O'Hagan, R., M. Silva, K. C. Q. Nguyen, W. Zhang, S. Bellotti, Y. H. Ramadan, D. H. Hall and M. M. Barr (2017). "Glutamylation Regulates Transport, Specializes Function, and Sculpts the Structure of Cilia." Curr Biol.

Ogawa, M., A. C. LaRue and M. Mehrotra (2013). "Hematopoietic stem cells are pluripotent and not just "hematopoietic"." Blood Cells Mol Dis **51**(1): 3-8.

Ou, G., O. E. Blacque, J. J. Snow, M. R. Leroux and J. M. Scholey (2005). "Functional coordination of intraflagellar transport motors." Nature **436**(7050): 583-587.

Pala, R., N. Alomari and S. M. Nauli (2017). "Primary Cilium-Dependent Signaling Mechanisms." Int J Mol Sci **18**(11).

Pampliega, O. and A. M. Cuervo (2016). "Autophagy and primary cilia: dual interplay." Curr Opin Cell Biol **39**: 1-7.

Pampliega, O., I. Orhon, B. Patel, S. Sridhar, A. Diaz-Carretero, I. Beau, P. Codogno, B. H. Satir, P. Satir and A. M. Cuervo (2013). "Functional interaction between autophagy and ciliogenesis." Nature **502**(7470): 194-200.

Passweg, J. and A. Tyndall (2007). "Autologous stem cell transplantation in autoimmune diseases." Semin Hematol **44**(4): 278-285.

Pazour, G. J., B. L. Dickert, Y. Vucica, E. S. Seeley, J. L. Rosenbaum, G. B. Witman and D. G. Cole (2000). "Chlamydomonas IFT88 and its mouse homologue, polycystic kidney disease gene tg737, are required for assembly of cilia and flagella." J Cell Biol **151**(3): 709-718.

Pazour, G. J., C. G. Wilkerson and G. B. Witman (1998). "A dynein light chain is essential for the retrograde particle movement of intraflagellar transport (IFT)." J Cell Biol **141**(4): 979-992.

Pedersen, L. B., J. B. Mogensen and S. T. Christensen (2016). "Endocytic Control of Cellular Signaling at the Primary Cilium." Trends Biochem Sci **41**(9): 784-797.

Piperno, G. and K. Mead (1997). "Transport of a novel complex in the cytoplasmic matrix of Chlamydomonas flagella." Proc Natl Acad Sci U S A **94**(9): 4457-4462.

Piwon, N., W. Gunther, M. Schwake, M. R. Bosl and T. J. Jentsch (2000). "ClC-5 Cl- -channel disruption impairs endocytosis in a mouse model for Dent's disease." Nature **408**(6810): 369-373.

Popatia, R., K. Haver and A. Casey (2014). "Primary Ciliary Dyskinesia: An Update on New Diagnostic Modalities and Review of the Literature." Pediatr Allergy Immunol Pulmonol **27**(2): 51-59.

Praetorius, H. A. and K. R. Spring (2001). "Bending the MDCK cell primary cilium increases intracellular calcium." J Membr Biol **184**(1): 71-79.

Prevo, B., J. M. Scholey and E. J. G. Peterman (2017). "Intraflagellar transport: mechanisms of motor action, cooperation, and cargo delivery." FEBS J **284**(18): 2905-2931.

Pryor, P. R., B. M. Mullock, N. A. Bright, M. R. Lindsay, S. R. Gray, S. C. Richardson, A. Stewart, D. E. James, R. C. Piper and J. P. Luzio (2004). "Combinatorial SNARE complexes with VAMP7 or VAMP8 define different late endocytic fusion events." EMBO Rep **5**(6): 590-595.

Pugacheva, E. N., S. A. Jablonski, T. R. Hartman, E. P. Henske and E. A. Golemis (2007). "HEF1-dependent Aurora A activation induces disassembly of the primary cilium." Cell **129**(7): 1351-1363.

Raggi, C., A. Luciani, N. Nevo, C. Antignac, S. Terryn and O. Devuyst (2014). "Dedifferentiation and aberrations of the endolysosomal compartment characterize the early stage of nephropathic cystinosis." Hum Mol Genet **23**(9): 2266-2278.

Raghavan, V., Y. Rbaibi, N. M. Pastor-Soler, M. D. Carattino and O. A. Weisz (2014). "Shear stress-dependent regulation of apical endocytosis in renal proximal tubule cells mediated by primary cilia." Proc Natl Acad Sci U S A **111**(23): 8506-8511.

Ratajczak, M. Z., M. Kucia, T. Jadczyk, N. J. Greco, W. Wojakowski, M. Tendera and J. Ratajczak (2012). "Pivotal role of paracrine effects in stem cell therapies in regenerative medicine: can we translate stem cell-secreted paracrine factors and microvesicles into better therapeutic strategies?" Leukemia **26**(6): 1166-1173.

Raychowdhury, R., J. L. Niles, R. T. McCluskey and J. A. Smith (1989). "Autoimmune target in Heymann nephritis is a glycoprotein with homology to the LDL receptor." Science **244**(4909): 1163-1165.

Reck, J., A. M. Schauer, K. VanderWaal Mills, R. Bower, D. Tritschler, C. A. Perrone and M. E. Porter (2016). "The role of the dynein light intermediate chain in retrograde IFT and flagellar function in Chlamydomonas." Mol Biol Cell **27**(15): 2404-2422.

Reiter, J. F., O. E. Blacque and M. R. Leroux (2012). "The base of the cilium: roles for transition fibres and the transition zone in ciliary formation, maintenance and compartmentalization." EMBO Rep **13**(7): 608-618.

Reiter, J. F. and M. R. Leroux (2017). "Genes and molecular pathways underpinning ciliopathies." Nat Rev Mol Cell Biol **18**(9): 533-547.

Rink, J., E. Ghigo, Y. Kalaidzidis and M. Zerial (2005). "Rab conversion as a mechanism of progression from early to late endosomes." Cell **122**(5): 735-749.

Rohatgi, R. and W. J. Snell (2010). "The ciliary membrane." Curr Opin Cell Biol **22**(4): 541-546.

Satir, P., L. B. Pedersen and S. T. Christensen (2010). "The primary cilium at a glance." J Cell Sci **123**(Pt 4): 499-503.

Schafer, J. C., C. J. Haycraft, J. H. Thomas, B. K. Yoder and P. Swoboda (2003). "XBX-1 encodes a dynein light intermediate chain required for retrograde intraflagellar transport and cilia assembly in Caenorhabditis elegans." Mol Biol Cell **14**(5): 2057-2070.

Scheel, O., A. A. Zdebik, S. Lourdel and T. J. Jentsch (2005). "Voltage-dependent electrogenic chloride/proton exchange by endosomal CLC proteins." Nature **436**(7049): 424-427.

Scheinman, S. J. (1998). "X-linked hypercalciuric nephrolithiasis: clinical syndromes and chloride channel mutations." Kidney Int **53**(1): 3-17.

Scherz-Shouval, R., E. Shvets, E. Fass, H. Shorer, L. Gil and Z. Elazar (2007). "Reactive oxygen species are essential for autophagy and specifically regulate the activity of Atg4." EMBO J **26**(7): 1749-1760.

Schmidt, K. N., S. Kuhns, A. Neuner, B. Hub, H. Zentgraf and G. Pereira (2012). "Cep164 mediates vesicular docking to the mother centriole during early steps of ciliogenesis." J Cell Biol **199**(7): 1083-1101.

Schroder, B. A., C. Wrocklage, A. Hasilik and P. Saftig (2010). "The proteome of lysosomes." Proteomics **10**(22): 4053-4076.

Sera, Y., A. C. LaRue, O. Moussa, M. Mehrotra, J. D. Duncan, C. R. Williams, E. Nishimoto, B. A. Schulte, P. M. Watson, D. K. Watson and M. Ogawa (2009). "Hematopoietic stem cell origin of adipocytes." Exp Hematol **37**(9): 1108-1120, 1120 e1101-1104.

Settembre, C., A. Fraldi, D. L. Medina and A. Ballabio (2013). "Signals from the lysosome: a control centre for cellular clearance and energy metabolism." Nat Rev Mol Cell Biol **14**(5): 283-296.

Snowden, J. A., J. Passweg, J. J. Moore, S. Milliken, P. Cannell, J. Van Laar, R. Verburg, J. Szer, K. Taylor, D. Joske, S. Rule, S. J. Bingham, P. Emery, R. K. Burt, R. M. Lowenthal, P. Durez, R. J. McKendry, S. Z. Pavletic, I. Espigado, E. Jantunen, A. Kashyap, M. Rabusin, P. Brooks, C. Bredeson and A. Tyndall (2004). "Autologous hemopoietic stem cell transplantation in severe rheumatoid arthritis: a report from the EBMT and ABMTR." J Rheumatol **31**(3): 482-488.

Somsel Rodman, J. and A. Wandinger-Ness (2000). "Rab GTPases coordinate endocytosis." J Cell Sci **113 Pt 2**: 183-192.

Sorokin, S. (1962). "Centrioles and the formation of rudimentary cilia by fibroblasts and smooth muscle cells." J Cell Biol **15**: 363-377.

Sorokin, S. P. (1968). "Reconstructions of centriole formation and ciliogenesis in mammalian lungs." J Cell Sci **3**(2): 207-230.

Spithoven, E. M., A. Kramer, E. Meijer, B. Orskov, C. Wanner, J. M. Abad, N. Areste, R. A. de la Torre, F. Caskey, C. Couchoud, P. Finne, J. Heaf, A. Hoitsma, J. de Meester, J. Pascual, M. Postorino, P. Ravani, O. Zurriaga, K. J. Jager, R. T. Gansevoort, E.-E. Registry, C. C. Euro and Wgikd (2014). "Renal replacement therapy for autosomal dominant polycystic kidney disease (ADPKD) in Europe: prevalence and survival--an analysis of data from the ERA-EDTA Registry." Nephrol Dial Transplant **29 Suppl 4**: iv15-25.

Takeda, T., H. Yamazaki and M. G. Farquhar (2003). "Identification of an apical sorting determinant in the cytoplasmic tail of megalin." Am J Physiol Cell Physiol **284**(5): C1105-1113.

Talbot, J. J., X. Song, X. Wang, M. M. Rinschen, N. Doerr, W. B. LaRiviere, B. Schermer, Y. P. Pei, V. E. Torres and T. Weimbs (2014). "The cleaved cytoplasmic tail of polycystin-1 regulates Src-dependent STAT3 activation." J Am Soc Nephrol **25**(8): 1737-1748.

Tang, Z., M. G. Lin, T. R. Stowe, S. Chen, M. Zhu, T. Stearns, B. Franco and Q. Zhong (2013). "Autophagy promotes primary ciliogenesis by removing OFD1 from centriolar satellites." Nature **502**(7470): 254-257.

Tanos, B. E., H. J. Yang, R. Soni, W. J. Wang, F. P. Macaluso, J. M. Asara and M. F. Tsou (2013). "Centriole distal appendages promote membrane docking, leading to cilia initiation." Genes Dev **27**(2): 163-168.

Terryn, S., F. Jouret, F. Vandenabeele, I. Smolders, M. Moreels, O. Devuyst, P. Steels and E. Van Kerkhove (2007). "A primary culture of mouse proximal tubular cells, established on collagen-coated membranes." Am J Physiol Renal Physiol **293**(2): F476-485.

Thomas, E. D., H. L. Lochte, Jr., W. C. Lu and J. W. Ferrebee (1957). "Intravenous infusion of bone marrow in patients receiving radiation and chemotherapy." N Engl J Med **257**(11): 491-496.

Till, J. E. (1961). "Radiosensitivity and chromosome numbers in strain L mouse cells in tissue culture." Radiat Res **15**: 400-409.

Torres, V. E., A. B. Chapman, O. Devuyst, R. T. Gansevoort, R. D. Perrone, G. Koch, J. Ouyang, R. D. McQuade, J. D. Blais, F. S. Czerwiec, O. Sergeyeva and R. T. Investigators (2017). "Tolvaptan in Later-Stage Autosomal Dominant Polycystic Kidney Disease." N Engl J Med **377**(20): 1930-1942.

Torres, V. E. and P. C. Harris (2009). "Autosomal dominant polycystic kidney disease: the last 3 years." Kidney Int **76**(2): 149-168.

Torres, V. E., P. C. Harris and Y. Pirson (2007). "Autosomal dominant polycystic kidney disease." Lancet **369**(9569): 1287-1301.

Tsao, C. C. and M. A. Gorovsky (2008). "Tetrahymena IFT122A is not essential for cilia assembly but plays a role in returning IFT proteins from the ciliary tip to the cell body." J Cell Sci **121**(Pt 4): 428-436.

Vij, R., R. Brown, S. Shenoy, J. S. Haug, D. Kaesberg, D. Adkins, L. T. Goodnough, H. Khoury and J. DiPersio (2000). "Allogeneic peripheral blood stem cell transplantation following CD34+ enrichment by density gradient separation." Bone Marrow Transplant **25**(12): 1223-1228.

Wang, S. S., O. Devuyst, P. J. Courtoy, X. T. Wang, H. Wang, Y. Wang, R. V. Thakker, S. Guggino and W. B. Guggino (2000). "Mice lacking renal chloride channel, CLC-5, are a model for Dent's disease, a nephrolithiasis disorder associated with defective receptor-mediated endocytosis." Hum Mol Genet **9**(20): 2937-2945.

Wang, X., C. J. Ward, P. C. Harris and V. E. Torres (2010). "Cyclic nucleotide signaling in polycystic kidney disease." Kidney Int **77**(2): 129-140.

Wang, X., H. Willenbring, Y. Akkari, Y. Torimaru, M. Foster, M. Al-Dhalimy, E. Lagasse, M. Finegold, S. Olson and M. Grompe (2003). "Cell fusion is the principal source of bone-marrow-derived hepatocytes." Nature **422**(6934): 897-901.

Waters, A. M. and P. L. Beales (2011). "Ciliopathies: an expanding disease spectrum." Pediatr Nephrol **26**(7): 1039-1056.

White, E. (2015). "The role for autophagy in cancer." J Clin Invest **125**(1): 42-46.

Willey, C. J., J. D. Blais, A. K. Hall, H. B. Krasa, A. J. Makin and F. S. Czerwiec (2017). "Prevalence of autosomal dominant polycystic kidney disease in the European Union." Nephrol Dial Transplant **32**(8): 1356-1363.

William, B. M., T. Wang, M. D. Haagenson, K. Fleischhauer, M. Verneris, K. C. Hsu, M. J. de Lima, M. Fernandez-Vina, S. R. Spellman, S. J. Lee and B. T. Hill (2017). "Impact of HLA Alleles on Outcomes of Allogeneic Transplantation for B Cell Non-Hodgkin Lymphomas: A Center for International Blood and Marrow Transplant Research Analysis." Biol Blood Marrow Transplant.

Willnow, T. E. (2017). "Nanotubes, the fast track to treatment of Dent disease?" Kidney Int **91**(4): 776-778.

Wilson, D. W., C. A. Wilcox, G. C. Flynn, E. Chen, W. J. Kuang, W. J. Henzel, M. R. Block, A. Ullrich and J. E. Rothman (1989). "A fusion protein required for vesicle-mediated transport in both mammalian cells and yeast." Nature **339**(6223): 355-359.

Wilson, P. D. (2004). "Polycystic kidney disease." N Engl J Med **350**(2): 151-164.

Wloga, D., E. Joachimiak and H. Fabczak (2017). "Tubulin Post-Translational Modifications and Microtubule Dynamics." Int J Mol Sci **18**(10).

Wolf, C. A., F. Dancea, M. Shi, V. Bade-Noskova, H. Ruterjans, D. Kerjaschki and C. Lucke (2007). "Solution structure of the twelfth cysteine-rich ligand-binding repeat in rat megalin." J Biomol NMR **37**(4): 321-328.

Xu, Q., Y. Zhang, Q. Wei, Y. Huang, Y. Li, K. Ling and J. Hu (2015). "BBS4 and BBS5 show functional redundancy in the BBSome to regulate the degradative sorting of ciliary sensory receptors." Sci Rep **5**: 11855.

Yamaguchi, T., S. Nagao, D. P. Wallace, F. A. Belibi, B. D. Cowley, J. C. Pelling and J. J. Grantham (2003). "Cyclic AMP activates B-Raf and ERK in cyst epithelial cells from autosomal-dominant polycystic kidneys." Kidney Int **63**(6): 1983-1994.

Yammani, R. R., S. Seetharam and B. Seetharam (2001). "Identification and characterization of two distinct ligand binding regions of cubilin." J Biol Chem **276**(48): 44777-44784.

Yang, Z. and D. J. Klionsky (2010). "Eaten alive: a history of macroautophagy." Nat Cell Biol **12**(9): 814-822.

Yeagy, B. A., F. Harrison, M. C. Gubler, J. A. Koziol, D. R. Salomon and S. Cherqui (2011). "Kidney preservation by bone marrow cell transplantation in hereditary nephropathy." Kidney Int **79**(11): 1198-1206.

Yoshimura, S., J. Egerer, E. Fuchs, A. K. Haas and F. A. Barr (2007). "Functional dissection of Rab GTPases involved in primary cilium formation." J Cell Biol **178**(3): 363-369.

Yu, S., K. Hackmann, J. Gao, X. He, K. Piontek, M. A. Garcia-Gonzalez, L. F. Menezes, H. Xu, G. G. Germino, J. Zuo and F. Qian (2007). "Essential role of cleavage of Polycystin-1 at G protein-coupled receptor proteolytic site for kidney tubular structure." Proc Natl Acad Sci U S A **104**(47): 18688-18693.

Zare-Shahabadi, A., E. Masliah, G. V. Johnson and N. Rezaei (2015). "Autophagy in Alzheimer's disease." Rev Neurosci **26**(4): 385-395.

Curriculum Vitae

Name **Alkaly GASSAMA**
Date of birth 02/11/1989
Nationality French
Address Zentralstrasse 53
8003 – Zürich
+41 (0)78 882 83 80
alkaly.gassama@outlook.com
Niederlassungsbewilligung C

EDUCATION

2013 - 2018	**Ph.D. in Biology** Marie-Curie Researcher (EU) **Supervisor: Prof. Dr. Olivier Devuyst**, Institute of Physiology, University of Zürich **, SWITZERLAND**
2011-2012	**M.Sc. Integrative Biology and Physiopathology *with honors*** University Pierre and Marie Curie, Paris, **FRANCE**
2010	**B.Sc. in Life Sciences *with honors*** University Pierre and Marie Curie, Paris, **FRANCE**

PROFESSIONAL EXPERIENCE

2013 – Present	**Supervision of medical students for practical courses and master thesis**, UZH (**CH**)
2013 – Present	**Proximal tubular dysfunction in Polycystic Kidney Disease,** UZH**,** (**CH**) Study how lysosomal dysfunction links abnormal ciliogenesis and defective receptor mediated endocytosis in PKD
2015 – 2016	**Pre-clinical study in Polycystic Kidney Disease,** UZH & **ROCHE**, (**CH**) Assess the potential therapeutic benefits of the inhibition of the intermediate conductance Ca^{2+}-activated K^+ channel on cysts progression in PKD animal models.
2012 (6 months)	**Pre-clinical study in Hepatocellular carcinoma INSERM**, UMR_S 938, UPMC, (**FR**) Investigate the effects of biguanide (metformin) in hepatocellular carcinoma models
2011 (4 months)	**Endothelial dysfunction in diabetes mellitus Laboratory of physiology**, University of Coimbra, (**PT**) Study of the relationship between nitric oxide (NO), metabolism and diabetes in diabetic rat models

SKILLS

Soft skills	Project management Problem solving with innovative solutions Scientific writing Teamwork Achieving deadline under pressure	
Laboratory Techniques	**Molecular Biology**	RNA and DNA isolation, Protein isolation, protein gel, electrophoresis, western blotting, PCR
	Cell Biology	Confocal microscopy, Immunohistochemistry, Immunofluorescence, Flow cytometry, Primary cell culture, ELISA
	Animal experiments	Study design, animal handling, anaesthesia, urine and blood sampling, i.p./i.v/p.o. injections, surgery, organ perfusion, FELASA category B
Languages	**French -** Native speaker **English -** Full professional proficiency (C2) **German -** Working professional proficiency (B1)	

PUBLICATIONS

Gabriel SS*, Belge H*, **Gassama A***, Debaix H, Luciani A, Fehr T and Devuyst O
Bone marrow transplantation improves proximal tubule dysfunction in a mouse model of Dent disease. Kidney Int. 2017 Apr;91(4):842-855

Gassama A, Peters DJM, Demoulin N, Luciani A and Devuyst O
Lysosomal dysfunction links defective ciliogenesis and endocytosis (MS in preparation)

Gandhi H*, **Gassama A***, Devuyst O and Simons M
The Dent's disease gene *CLCN5* is required for Insulin/mTOR-dependent Megalin expression and endocytosis (MS in preparation)

ORAL COMMUNICATION/POSTER

2017 Dec	**SGN/SSN:** 49th Annual Meeting Swiss Society of Nephrology (**Poster award**) **Fribourg**
2016 Sep	**CME-ERA/EDTA WGIKD:** Improving the care of patients with ADPKD**, Brussels**
2015 June	**TranCYST Consortium meeting, Paris**
2014 Aug	**FASEB Symposium:** Polycystic Kidney Disease: From molecular mechanisms to therapy, **Barga-Lucca**
2013 Sep	**TranCYST – ERA/EDTA WGiKD Symposium** Clinical and scientific advances in the management of patients with ADPKD, **Oxford**